UNIVERSIDADE ESTADUAL DE CAMPINAS

Instituto de Matemática, Estatística e Computação Científica

TIAGO YUZO MIYAOKA

Spatiotemporal epidemiology with optimal control and application to Zika virus

Epidemiologia espaçotemporal com controle ótimo e aplicações ao vírus Zika

Campinas

2019

Tiago Yuzo Miyaoka

Spatiotemporal epidemiology with optimal control and application to Zika virus

Epidemiologia espaçotemporal com controle ótimo e aplicações ao vírus Zika

Tese apresentada ao Instituto de Matemática, Estatística e Computação Científica da Universidade Estadual de Campinas como parte dos requisitos exigidos para a obtenção do título de Doutor em Matemática Aplicada.

Thesis presented to the Institute of Mathematics, Statistics and Scientific Computing of the University of Campinas in partial fulfillment of the requirements for the degree of Doctor in Applied Mathematics.

Orientador: João Frederico da Costa Azevedo Meyer

Este exemplar corresponde à versão final da Tese defendida pelo aluno Tiago Yuzo Miyaoka e orientada pelo Prof. Dr. João Frederico da Costa Azevedo Meyer.

Campinas

2019

Ficha catalográfica
Universidade Estadual de Campinas
Biblioteca do Instituto de Matemática, Estatística e Computação Científica
Ana Regina Machado - CRB 8/5467

M699s

Miyaoka, Tiago Yuzo, 1990-
Spatiotemporal epidemiology with optimal control and application to Zika virus / Tiago Yuzo Miyaoka. – Campinas, SP : [s.n.], 2019.

Orientador: João Frederico da Costa Azevedo Meyer.
Tese (doutorado) – Universidade Estadual de Campinas, Instituto de Matemática, Estatística e Computação Científica.

1. Epidemiologia. 2. Controle ótimo. 3. Equações diferenciais parciais. 4. Estimativa de parâmetro. 5. Zika vírus. I. Meyer, João Frederico da Costa Azevedo, 1947-. II. Universidade Estadual de Campinas. Instituto de Matemática, Estatística e Computação Científica. III. Título.

Informações para Biblioteca Digital

Título em outro idioma: Epidemiologia espaçotemporal com controle ótimo e aplicações ao vírus Zika
Palavras-chave em inglês:
Epidemiology
Optimal control
Partial differential equations
Parameter estimation
Zika virus
Área de concentração: Matemática Aplicada
Titulação: Doutor em Matemática Aplicada
Banca examinadora:
João Frederico da Costa Azevedo Meyer [Orientador]
Graciele Paraguaia Silveira
Luciana Takata Gomes
Bianca Morellli Rodolfo Calsavara
Luiz Alberto Díaz Rodrigues
Data de defesa: 08-03-2019
Programa de Pós-Graduação: Matemática Aplicada

Identificação e informações acadêmicas do(a) aluno(a)
- ORCID do autor: https://orcid.org/0000-0003-2735-3044
- Currículo Lattes do autor: http://lattes.cnpq.br/5569509996568202

Tese de Doutorado defendida em 08 de março de 2019 e aprovada

pela banca examinadora composta pelos Profs. Drs.

Prof(a). Dr(a). JOÃO FREDERICO DA COSTA AZEVEDO MEYER

Prof(a). Dr(a). GRACIELE PARAGUAIA SILVEIRA

Prof(a). Dr(a). LUCIANA TAKATA GOMES

Prof(a). Dr(a). BIANCA MORELLI RODOLFO CALSAVARA

Prof(a). Dr(a). LUIZ ALBERTO DÍAZ RODRIGUES

A Ata da Defesa, assinada pelos membros da Comissão Examinadora, consta no SIGA/Sistema de Fluxo de Dissertação/Tese e na Secretaria de Pós-Graduação do Instituto de Matemática, Estatística e Computação Científica.

Acknowledgements

I thank every single person that somehow helped me through the doctorate.

I specially thank my family, for the unconditional support.

A more than special thanks goes to Kamila, who has always been by my side, and I believe will always be.

I thank Joni and Suzanne, my mentors, for everything, from accepting me as a student to the support, and also inspiration.

I also thank the committee, for accepting the invitation and for the suggestions that made this a better work.

This study was financed in part by the Coordenação de Aperfeiçoamento de Pessoal de Nível Superior - Brasil (CAPES) - Finance Codes 001 and 88881.134100/2016-01 and in part by the Conselho Nacional de Desenvolvimento Científico e Tecnológico - Brasil (CNPq) - Finance Code 140780/2018-1.

Be curious,
and however difficult life may seem,
there is always something you can do,
and succeed at.
It matters that you don't just give up.

Stephen Hawking

Resumo

Em epidemiologia, medidas de controle podem ser propostas e implementadas de modo a reduzir infecções e custos associados a uma doença infecciosa. Neste trabalho usamos modelagem matemática, teoria de controle ótimo e simulações numéricas para descrever, simular e analisar um problema da vida real nesse sentido. Nosso objeto de estudo em particular foi o espalhamento geográfico do vírus Zika, que obteve preocupação mundial após um recente surto na América Latina que se iniciou no Brasil. Houve um alto número de doenças neurológicas, como microcefalia em recém nascidos de mães infectadas por Zika, o que nunca havia ocorrido antes. O vírus é transmitido principalmente por mosquitos *Aedes aegypti*, mas há casos confirmados de transmissão direta (sexual). Um modelo de difusão-reação foi formulado, baseado em equações diferenciais parciais, que considera movimento espaço-temporal de humanos e vetores, com transmissão local do vírus Zika. Vacinação foi introduzida como um controle variável no tempo e espaço, dando imunidade a humanos suscetíveis, com o objetivo de caracterizar uma estratégia de vacinação ótima que minimiza os custos associados a infecções e vacinas. A caracterização do controle ótimo foi obtida por meio de equações de estado e adjuntas. Soluções numéricas do modelo foram obtidas usando os métodos de elementos finitos para variáveis espaciais, e de diferenças finitas para a variável temporal. Utilizando dados para o surto inicial de Zika em 2015 do estado do Rio Grande do Norte no Brasil, alguns parâmetros do modelo foram estimados usando uma abordagem de quadrados mínimos. A metodologia de estimação de parâmetros foi testada com dados artificialmente gerados. Uma análise de sensibilidade global foi realizada de forma a encontrar os parâmetros com mais impacto no custo total e no número de infecções. Diversos cenários foram considerados e discutidos em termos do número de novas infecções e e custos, mostrando que a aplicação do controle ótimo foi bem sucedida, significantemente reduzindo estes números.

Palavras-chave: Epidemiologia. Controle ótimo. Equações diferenciais parciais. Métodos numéricos. Vírus Zika.

Abstract

In epidemiology, control measures can be proposed and implemented in order to reduce infections and associated costs of an infectious disease. In this work we used mathematical modeling, optimal control theory and numerical simulations to describe, simulate, and analyze a real life problem in this sense. Our particular subject of study was the geographical spread of the Zika virus, which has acquired worldwide concern after a recent outbreak in Latin America that started in Brazil. There was a high number of associated neurological conditions, such as microcephaly in newborns from infected mothers, which had never happened before. The virus is transmitted mainly by *Aedes aegypti* mosquitoes, but direct (sexual) transmission has been documented. We formulated a reaction diffusion model, based on partial differential equations, that considers spatiotemporal movement of humans and vectors, with local contact transmission of Zika virus. Vaccination was introduced as a space and time variable control, giving immunity to susceptible humans, with the goal of characterizing an optimal vaccination strategy that minimizes the costs associated with infections and vaccines. The optimal control characterization was obtained in terms of state and adjoint equations. Numerical solutions of the model were obtained using the finite element method for the space variables, and the finite difference method for time. Using data for the initial 2015 Zika outbreak in the state of Rio Grande do Norte in Brazil, some parameters of the model were estimated using a least squares approach. The parameter estimation methodology was tested with artificially generated data. A global sensitivity analysis was performed in order to find the parameters with most impact in the overall cost and in the number of new infections. Several scenarios were considered and discussed in terms of number of new infections and costs, showing that the optimal control application was successful, significantly reducing these quantities.

Keywords: Epidemiology. Optimal Control. Partial differential equations. Numerical methods. Zika virus.

List of Figures

Figure 1 – Flow chart showing a summary of the connections of modeling and methods considered throughout the thesis. The PDE model is defined in Chapter 2 and the optimal control system in Chapter 3. Numerical, forward-backward and predictor-corrector methods are treated in Chapter 4. The parameter estimation procedure and sensitivity analysis are contained in Chapter 5, and numerical simulations in Chapter 6. 26

Figure 2 – Flow chart for model (2.1). Squares denote humans and circles mosquitoes. S, I, R denote susceptible, infected, and immune populations, respectively. Reproduction for mosquitoes is of logistic type (not shown in figure). Parameter descriptions can be found in Table 1. 29

Figure 3 – Examples of reference elements used in the finite element method. . . . 50

Figure 4 – Spatial plots of the functions considered as exact solutions for the error analysis. 57

Figure 5 – At left: numerical errors in L^2 norm by element step sizes. At right: numerical errors in L^2 gradient norm by element step sizes. Linear regressions are shown for each case. 59

Figure 6 – Numerical errors in vector 2 norm by time step sizes. Linear regressions are shown for each case. 59

Figure 7 – Rescaled incidence in selected cities by epidemiological weeks of 2015. . 62

Figure 8 – Linear finite element mesh approximating Rio Grande do Norte state. Circles represent cities with relevant incidence data. 63

Figure 9 – Comparison between the sum in each city of data and simulated incidence. 68

Figure 10 – Comparison between the sum from data and from simulated incidence. 68

Figure 11 – Full and partial artificially generated incidence data. The latter is used in the parameter estimation tests. 70

Figure 12 – Full and partial summed artificially generated incidence data. The latter is used in the parameter estimation tests. 70

Figure 13 – Residual $\mathcal{R}$ and relative errors of estimated parameters using artificially generated data with 30%, 50%, 70%, and 100% added noise. 71

Figure 14 – Incidence in each city (blue solid lines) with estimated parameters $\beta = 6.709 \times 10^{-5}, \beta_v = 1.501 \times 10^{-2}, I_{0I} = 133, I_{0M} = 94.67, I_{0C} = 105.94$, obtained using artificially generated data with 10% added noise. The corresponding residual is $\mathcal{R} = 7.17 \times 10^{-2}$. Data with 10% added noise (red circles) and without noise (yellow dotted lines) are also shown. . . 72

Figure 15 – Summed incidence in all cities (blue solid line) with estimated parameters $\beta = 6.709 \times 10^{-5}, \beta_v = 1.501 \times 10^{-2}, I_{0I} = 133, I_{0M} = 94.67, I_{0C} = 105.94$, obtained using artificially generated data with 10% added noise. The corresponding residual is $\mathcal{R} = 7.17 \times 10^{-2}$. Summed data with 30% added noise (red circles) and without noise (yellow dotted line) are also shown. 72

Figure 16 – Incidence in each city (blue solid lines) with estimated parameters $\beta = 6.542 \times 10^{-5}, \beta_v = 1.544 \times 10^{-2}, I_{0I} = 122.62, I_{0M} = 90.45, I_{0C} = 93.30$, obtained using artificially generated data with 50% added noise. The corresponding residual is $\mathcal{R} = 1.56 \times 10^{-1}$. Data with 10% added noise (red circles) and without noise (yellow dotted lines) are also shown. . . 73

Figure 17 – Summed incidence in all cities (blue solid line) with estimated parameters $\beta = 6.542 \times 10^{-5}, \beta_v = 1.544 \times 10^{-2}, I_{0I} = 122.62, I_{0M} = 90.45, I_{0C} = 93.30$, obtained using artificially generated data with 10% added noise. The corresponding residual is $\mathcal{R} = 1.56 \times 10^{-1}$. Summed data with 50% added noise (red circles) and without noise (yellow dotted line) are also shown. 73

Figure 18 – Incidence in each city (blue solid lines) with estimated parameters $\beta = 6.807 \times 10^{-5}, \beta_v = 1.527 \times 10^{-2}, I_{0I} = 90.14, I_{0M} = 75.04, I_{0C} = 88.75$, obtained using artificially generated data with 70% added noise. The corresponding residual is $\mathcal{R} = 2.00 \times 10^{-1}$. Data with 70% added noise (red circles) and without noise (yellow dotted lines) are also shown. . . 74

Figure 19 – Summed incidence in all cities (blue solid line) with estimated parameters $\beta = 6.807 \times 10^{-5}, \beta_v = 1.527 \times 10^{-2}, I_{0I} = 90.14, I_{0M} = 75.04, I_{0C} = 88.75$, obtained using artificially generated data with 70% added noise. The corresponding residual is $\mathcal{R} = 2.00 \times 10^{-1}$. Summed data with 70% added noise (red circles) and without noise (yellow dotted line) are also shown. 74

Figure 20 – Incidence in each city (blue solid lines) with estimated parameters $\beta = 6.396 \times 10^{-5}, \beta_v = 1.561 \times 10^{-2}, I_{0I} = 133, I_{0M} = 97.28, I_{0C} = 105.30$, obtained using artificially generated data with 100% added noise. The corresponding residual is $\mathcal{R} = 3.05 \times 10^{-1}$. Data with 100% added noise (red circles) and without noise (yellow dotted lines) are also shown. . . 75

Figure 21 – Summed incidence in all cities (blue solid line) with estimated parameters $\beta = 6.396 \times 10^{-5}, \beta_v = 1.561 \times 10^{-2}, I_{0I} = 133, I_{0M} = 97.28, I_{0C} = 105.30$, obtained using artificially generated data with 100% added noise. The corresponding residual is $\mathcal{R} = 3.05 \times 10^{-1}$. Summed data with 100% added noise (red circles) and without noise (yellow dotted line) are also shown. 75

Figure 22 – Significant PRCCs over time, using incidence as output. Shaded area indicates region where PRCC is not significant. 79
Figure 23 – Scatter plots of rank-transformed data with $J(u^*)$ as output. A PRCC is considered significant if it is greater than 0.2 or if its p-value is less than 0.05. Scales in both axes result from rank transformation and linear regression. It is possible to see positive linear trends of correlation for β, β_v, κ_v, and c_1, and negative ones for δ and μ_v. 80
Figure 24 – Scatter plots of rank-transformed data with incidence as output. Results are showed for $t = 140$ days. A PRCC is considered significant if it is greater than 0.2 or if its p-value is less than 0.05. Scales in both axes result from rank transformation and linear regression. It is possible to see positive linear trends of correlation for β, β_v, κ_v, α_I and c_2, and negative ones for δ and μ_v. 81
Figure 25 – Plots of initial conditions in space ($t = 0$ days), for all scenarios. Each plot has a different scale. 84
Figure 26 – Plots of solutions in space at $t = 35$ days, scenario without control. Each plot has a different scale. 85
Figure 27 – Plots of solutions in space at $t = 52$ days, scenario without control. Each plot has a different scale. 85
Figure 28 – Plots of solutions in space at $t = 70$ days, scenario without control. Each plot has a different scale. 86
Figure 29 – Plots of solutions in space at $t = 105$ days, scenario without control. Each plot has a different scale. 86
Figure 30 – Plots of solutions in space at $t = 140$ days, scenario without control. Each plot has a different scale. 86
Figure 31 – Integrals of state solutions and optimal control over space. Scenarios without control, and with optimal control starting at $t = 35$, 52 and 70 days. 87
Figure 32 – Plots of solutions in space at $t = 35$ days, scenario with optimal control starting at $t = 35$ days. Each plot has a different scale. 88
Figure 33 – Plots of solutions in space at $t = 52$ days, scenario with optimal control starting at $t = 35$ days. Each plot has a different scale. 88
Figure 34 – Plots of solutions in space at $t = 70$ days, scenario with optimal control starting at $t = 35$ days. Each plot has a different scale. 89
Figure 35 – Plots of solutions in space at $t = 105$ days, scenario with optimal control starting at $t = 35$ days. Each plot has a different scale. 89
Figure 36 – Plots of solutions in space at $t = 140$ days, scenario with optimal control starting at $t = 35$ days. Each plot has a different scale. 89

Figure 37 – Plots of solutions in space at $t = 52$ days, scenario with optimal control starting at $t = 52$ days. Each plot has a different scale. 90
Figure 38 – Plots of solutions in space at $t = 70$ days, scenario with optimal control starting at $t = 52$ days. Each plot has a different scale. 91
Figure 39 – Plots of solutions in space at $t = 105$ days, scenario with optimal control starting at $t = 52$ days. Each plot has a different scale. 91
Figure 40 – Plots of solutions in space at $t = 140$ days, scenario with optimal control starting at $t = 52$ days. Each plot has a different scale. 91
Figure 41 – Plots of solutions in space at $t = 70$ days, scenario with optimal control starting at $t = 70$ days. Each plot has a different scale. 92
Figure 42 – Plots of solutions in space at $t = 105$ days, scenario with optimal control starting at $t = 70$ days. Each plot has a different scale. 93
Figure 43 – Plots of solutions in space at $t = 140$ days, scenario with optimal control starting at $t = 70$ days. Each plot has a different scale. 93
Figure 44 – Flow chart for model (7.1). Squares denote humans and circles mosquitoes. S, I, R denote susceptible, infected, and immune, respectively. A_v denotes mosquito immature phase. 97

List of Tables

Table 1 – Description and units of quantities from model (2.1). 29
Table 2 – Description and units of parameters for optimal control problem (3.3). . 34
Table 3 – Errors and convergence rates of the finite element method in the L^2 norm. 58
Table 4 – Errors and convergence rates of the finite element method in the L^2 gradient norm. 58
Table 5 – Errors and convergence rates of the backward Euler method in the vector 2 norm. 59
Table 6 – Number of reported Zika cases in Rio Grande do Norte state in 2015. . 61
Table 7 – Parameter values used in simulations. 65
Table 8 – Parameter bounds and estimation results. 68
Table 9 – Results of parameter estimation tests with artificially generated noisy data. 71
Table 10 – Parameter baseline values and ranges used in the PRCC analysis. 78
Table 11 – Significant PRCCs with $J(u^*)$ as output. 78
Table 12 – Insignificant PRCCs with $J(u^*)$ as output. 78
Table 13 – Optimal control results compared to the scenario without control. 84
Table 14 – Description and units of some quantities from model (7.1). The others are shown in Table (1). 96

Contents

1 INTRODUCTION 16
1.1 Background on Zika virus 19
1.2 Literature review 21
1.3 Thesis outline 24

2 MATHEMATICAL MODELING 27
2.1 Technical definitions 27
2.2 Reaction-diffusion model with vaccination 28

3 OPTIMAL CONTROL 33
3.1 Definition of the optimal control problem 33
3.2 Derivation of optimal control 35
3.2.1 Sensitivity system 35
3.2.2 Adjoint system 38
3.2.3 Optimal control characterization 39

4 NUMERICAL SOLUTIONS 41
4.1 Weak formulation 43
4.2 Galerkin method 45
4.3 Backward Euler method 48
4.4 Predictor-corrector linearization method 49
4.5 Finite element basis 50
4.6 Solutions of linear systems arising in discretization 52
4.7 Adjoint system solutions 52
4.8 Optimality system solutions: forward-backward sweep 53
4.9 Numerical error and convergence analysis 55

5 PARAMETER ESTIMATION 60
5.1 Application to 2015 Zika outbreak in Brazil 61
5.2 Parameter estimates 64
5.3 Parameter estimation using least squares 66
5.4 Tests with generated data 69
5.5 Global Sensitivity Analysis 76

6 NUMERICAL RESULTS 82
6.1 Simulation without control 84
6.2 Simulation with optimal control starting at 35 days 87

6.3 Simulation with optimal control starting at 52 days 90
6.4 Simulation with optimal control starting at 70 days 92
6.5 Simulation with optimal control starting at 105 days 93

7 CONCLUSION AND FUTURE PERSPECTIVES 94
7.1 Concluding remarks 94
7.2 Future work perspectives 96

Bibliography 100

Chapter 1
Introduction

Mathematical models have been widely used in several biological applications, such as population dynamics, neurobiology, ecology, tumor growth, cell physiology, immunology, and epidemiology. Model studies may require mathematical analysis and/or computational simulations, the latter specially in situations in which several variables are included in the model. Those analyses may result in unexpected and important properties of the phenomenon being studied, according to particular interests. In epidemiology, our main interest in this work, the purpose of the modeling is usually to describe, understand, quantify, and possibly control health care and disease conditions.

Among a variety of mathematical models, the most commonly used in epidemiology are compartmental models, based on ordinary differential equations (ODEs). This class of models considers populations in different compartments, such as susceptible, infected or infectious, exposed, recovered, immune, non linearly related to each other [53, 55]. The choice of which compartments to be used depends on the dynamics of the disease to be studied and which characteristics are important. Thus, there could be a variety of compartmental models that describe the same disease, each of them suitable to each particular approach. ODE models consider time as a continuous variable, but discrete time models could also be used, based on difference equations [9]. In this case, dynamics are also considered between compartments, with discrete time stepping. This kind of modeling could be suitable when there is some sort of generation involved with a fixed time length, such as insect reproduction period, or latent and infectious periods of a disease.

Compartmental ODE models consider only time variations, assuming that spatial variation is homogeneous. There are many kinds of models available in the literature that are used to include this additional variation. For example, patchy models use one compartmental ODE system for each spatial locus such as a city, and all ODE systems are connected through movement between the loci [7]. Another example is the use of agent based models (also called individual based models), in which movement and dynamics occur randomly, according to decision-making rules [90]. Our approach in this work considers movement through spatial diffusion of populations in a certain region, by means of systems of partial differential equations (PDEs) [21, 88]. For most ODE models, it is possible to simply include a diffusion term in each equation of the system to readily modify them to a reaction-diffusion PDE model, also defining appropriate spatial domain and boundary

conditions. Although explicit solutions of PDE models are rare, there are theoretical studies regarding existence and uniqueness of solutions and convergence of several different numerical methods [25, 36, 59].

Occasionally, it may be necessary to add a control measure in the model, either to represent the reality of the phenomenon to be modeled, as a tool in theoretical studies, or even to test hypotheses. The inclusion of this control measure could, and often does, bring associated costs (or profit) that should be taken into account. This kind of situation can be suitably modeled by the use of optimal control theory. It seeks the minimum cost (or maximum profit or advantage, if applicable) in terms of the control variable(s), balancing out the costs associated to the control and benefits, always restricted to the model. Once a well behaved objective functional to be minimized is defined, optimal control theory can be readily applied to existing ODE and PDE models. The ODE case is usually straightforward, because the solution of the optimal control problem is characterized by the well known Pontryagin's maximum principle, for systems that satisfy specific technical properties [58]. For PDE systems, however, there is no general characterization for the optimal solution and each situation must be treated separately, although the overall procedure is always similar. The characterization is obtained in terms of state and adjoint equations, using directional derivatives of the states and the objective functional with respect to the control. Optimal control may also be applied to other kinds of models, as discrete models [30], in a fairly similar way to that of differential equation models. On the other hand, there is no standard framework for solving optimal control problems in agent based models. An alternative is to approximate the model by a PDE model and then obtain the corresponding optimal control solution [4].

The modeling of a real life problem using PDEs requires the use of numerical methods in order to obtain approximated solutions, because analytical solutions are almost always impossible to be obtained. The most common numerical methods for PDEs are the finite element, finite difference, and finite volume methods. Our choice consists in the finite element for the spatial variables and the finite difference (more specifically, implicit Euler) method for time, together with a predictor-corrector linearization method [31, 32]. This combination has been showing good results in studies similar to ours [44, 91, 96, 101, 112]. The solution of the optimal control problem is obtained using a forward-backward sweep method, which is also commonly used, being the main choice in numerical simulations of optimal control [46, 58].

Another important aspect in modeling real life problems is the connection between model and data. Numerical or analytical solutions of ordinary and partial differential equations depend strongly on the model parameters. However, numerical values are not always available from literature and laboratory or field experiments [35]. It may be impossible to explicitly measure some parameters, or experiments could be too expensive. If

a set of data is available, a model can be parametrized based on it in order to represent the reality of the problem in study. This is usually done using statistical inference methods or regression methods, such as least squares, or equivalently, maximum likelihood estimation [108]. An example of a (Bayesian) inference method is the well known Markov chain Monte Carlo (MCMC), an iterative method that samples a desired probability distribution by observing a Markov chain after a usually large number of steps. Although very powerful, it may take a long time to converge, specially if each iteration is computationally time consuming [111]. On the other hand, regression methods usually do not have this kind of issue. We use a nonlinear least squares approach that relates the model output with data, minimizing their difference in terms of some model parameters.

Even when it is possible to numerically estimate parameters from the model, their values are not always exact, as uncertainties naturally arise from the measure and estimation processes. This kind of uncertainty can be evaluated through sensitivity analysis, which assesses how model's outputs are affected by variations in input parameters [103]. Methods on sensitivity analysis can be local, such as the calculus of partial derivatives of the output in respect to a parameter, or global, which take into account a whole set of possible parameter values. Usually in biological applications the model outputs have complex and non local behaviors, so global analysis are more appropriate. As an example, the statistic Pearson correlation coefficient measures linear relations between parameters and outputs, in a global manner. However, in complex models correlations are usually nonlinear and another kind of methodology should be more appropriate, as partial rank correlation coefficients [67]. We use these coefficients to study sensitivity analysis in our PDE model, after obtaining baseline values for parameters.

The main goal of this thesis is to study optimal control applied to partial differential equation models in epidemiology. We use numerical methods to obtain numerical solutions and connect the model with data. Zika virus was chosen as a real life application, because of its recent importance and public health concern. Hypothetical vaccination is considered as a control measure, in order to reduce infections in a strategy that balances cost-benefit. As a vector-borne disease, the epidemiological dynamics of Zika is similar to other diseases such as dengue, chikungunya (both transmitted by the same species of mosquitoes), malaria, yellow fever, among other important diseases. Thus, a study on mathematical models and optimal control of Zika may serve as a base reference for the others. We discuss some of Zika virus main aspects and importance in the following section.

1.1 Background on Zika virus

Zika virus (ZIKV) was first isolated from a monkey in the Zika Forest of Uganda in 1947, and later isolated from humans in Nigeria in 1954. For a long time, about 50 years, little importance was given to the virus as only few cases from Africa and Southeast Asia were reported [118]. The recent 2015-2016 outbreak that started in the northeastern region in Brazil brought more attention to Zika, as it quickly spread throughout other countries in South and Central Americas and had a large number of microcephaly among newborns allegedly linked to it. On February 2016, the World Health Organization declared Zika as a public health emergency of international concern. There were more than $580,000$ suspected and $220,000$ confirmed cases in all Americas by January 2018, with most of the cases concentrated in Brazil. Also, there were more than $3,500$ confirmed congenital syndromes in newborns associated with Zika virus in this period [89].

Zika is a flavivirus similar to dengue, and it is primarily transmitted to humans by *Aedes aegypti* and *Aedes albopictus* mosquitoes, which also transmit important diseases as dengue, chikungunya, and yellow fever in humans [64]. Zika can also be transmitted vertically (from mother to child) [12], through sexual relations [27], and through blood transfusions [81], although the main route of transmission is through the vector [3, 66]. Only about 20% of infected people develop mild symptoms such as fever, rash, conjunctivitis and joint pain, with a few documented fatalities – only 20 by January 2018 [89]. Zika virus is hard to diagnose by symptoms only because they are similar to other common diseases. Confirmed diagnosis are performed in laboratory through PCR (polymerase chain reaction) and virus isolation from blood samples. Diagnosis by serology can be difficult as the virus can cross-react with other flaviviruses such as dengue, West Nile virus and yellow fever [118]. There is no cure or specific medicine for Zika virus, but symptoms should be treated. Specialists suggest rest, hydration, and use of non-steroidal anti-inflammatory medicine to reduce fever and pain [23]. There is an increased chance of babies born from infected mothers to develop microcephaly [78] and other congenital conditions, including malformations of the head, seizures, hearing and sight abnormalities, and the virus is also linked to the development of Guillain-Barré syndrome [87]. However, precise information about the development of these conditions are still unknown [16, 74].

Microcephaly is a condition that causes a baby to be born with a smaller than normal head or causes the head to have a slow growth after birth. It is a rare condition in the absence of external factors, occurring naturally in one baby among several thousands. Diagnosis can be done early by fetal ultrasound, with a best probability of success if performed around 28 weeks. Even if fetal ultrasound does not detect microcephaly, babies should have their head circumference measured within 24 hours after birth. Microcephaly is defined by a cephalic perimeter smaller than 2 standard deviations of the same gestational

age and sex, and the severe case corresponding to less than 3 standard deviations. Besides Zika, it is mostly caused by infections during pregnancy of toxoplasmosis, rubella, syphilis, genetic abnormalities, exposure to toxic chemicals, among others [118]. There is no specific treatment, although support actions are encouraged to help the development of the baby. In Brazil, the Unified Health System (SUS - Sistema Único de Saúde) provides a stimulation program, which aims to maximize physical and neurological potential of children up to three years old [75]. Guillain-Barré syndrome (GBS) is an acute immune-mediated neurological condition that affects muscle control and nerves transmitting pain, temperature and touch sensations. It can result in weakness and loss of sensation in the legs and/or arms [118]. It is a rare condition, with approximately 1 case per 100,000 people per year, among all ages. It is potentially fatal, with some of the patients requiring ventilation and intensive care support. There is a 5% mortality rate, despite optimal care. Possible causes of GBS are infections from bacterias and viruses, such as Zika, dengue, chikungunya, HIV. Diagnosis should be done by a health-care professional with expertise in performing neruological examinations. In 2015, a total of 1708 cases were registered in Brazil, representing an increase of 19% from 2014, possibly due to the Zika outbreak [89].

The most common vector of Zika in Brazil is *Aedes aegypti* (Diptera: Culicidae), a species of mosquito native from Africa but widely spread worldwide. It thrives in tropical and subtropical regions, but can survive in temperate regions as long as there are no constant low temperatures. It is well adapted to urban areas, specially in densely populated areas. It needs clean and still water to lay eggs, which can survive for months. Once hatched, eggs turn into larvae, pupae, then adults (winged form). Female adults need blood meals in order to reproduce, and it is through these meals that diseases are transmitted. Zika or other flavivirus stay in the mosquito saliva after biting an infected human, and can be transmitted in following bites [40].

There is no specific treatment or antiviral therapies to treat Zika, but there has been great effort in the development of vaccines for the virus. The National Institute of Allergy and Infectious Diseases (NIAID) in the USA started a clinical trial of a Zika vaccine in humans in August 2016, with a second phase launched in March 2017 [86]. Tests are being performed in hospitals around the world, including Brazil, United States, Puerto Rico, Peru, and Mexico. The trial aims to further evaluate the vaccine's safety and ability to stimulate an immune response in participants, also assessing the optimal dose. It will also attempt to determine if the vaccine can effectively prevent disease caused by Zika infection. [85]. Although the vaccine is still not publicly available, it is important to consider the impact and efficacy of a possible vaccination program, accounting for the costs involved, such as production, application, and logistic costs.

1.2 Literature review

Many models have been developed in order to study the spread, impact, and control of infectious and vector borne diseases, including Zika virus. Most of the works uses systems of ordinary differential equations (ODEs), but there is also interest in including spatial dependence in the models, by the use of partial differential equations (PDEs) and other techniques, considering the spread of the disease. In this section we review some important literature in vector-borne diseases, Zika virus, and application of optimal control and numerical methods that are related to our study.

Gao et al. [41] developed an ODE model considering vector and sexual transmission with several compartments for infected humans, analyzed the endemic equilibrium stability, estimated the basic reproduction number with data from Brazil, Colombia and El Salvador, and performed a global stability analysis. Similar models were developed with estimations of the basic reproduction number for Colombia, El Salvador and Suriname [106], and for Barranquilla, Colombia [113]. Agusto et al. [2] studied an ODE model with separate compartments for female and male humans, with different transmission rates. They explored endemic equilibrium stability and numerical simulations for their model. Saad-Roy et al. [102] also studied an ODE model with sexual transmission, but with migrated infections between two regions. They also estimated the number of Zika infections based on the number of microcephaly cases. Manore et al. [65] used an ODE model with field data to assess conditions in which Zika and chikungunya from travelers could spread in eastern USA. They conclude that spatial mosquito data, biting behavior and seasonality are important factors that should be taken into account to better understand transmission risk. The introduction of transgenosis mosquitoes carrying the *Wolbachia* bacteria was studied by Wang et al. [116] in order to control the Zika virus using Brazil data for the year of 2016, and by Zheng et al. [122] in a more general sense, analyzing the vertical transmission of the bacteria in mosquitoes population, both being ODE models. Bonyah et al. [14] considered the use of bednets, treatment, and insecticide spray as control measures, comparing the results with constant and time dependent optimal controls in an ODE system.

A spatial agent based model was studied by Matheson et al. [68] in order to model the spread of Zika at the 2016 Olympics. They varied some parameters (bite rates, population sizes) and discussed the consequent outcomes, using some data from Rio de Janeiro city. Zhang et al. [121] used a spatiotemporal stochastic model based on compartments to study Zika in the American continent. They estimated the introduction of Zika in America between August 2013 and April 2014, and simulated infections in several countries based on mosquito, temperature, population and mobility data. Zinszer et al. [123] modeled spatial and temporal data in order to reconstruct the introduction

of Zika in Brazil, in a very simple modeling using only interpolation of data. A different modeling was used by Gardner et al. [42] to infer risks of Zika infection in the Americas. Their model is based on optimization to estimate the parameters, and uses a data driven stochastic-dynamic epidemic model for evaluation. They find that local vector control is more important than travel restrictions in reducing risks of Zika infections. Roques and Bonnefon [99] proposed a hybrid two and one dimensional PDE model to study the spread of *Aedes albopictus* mosquitoes in France, considering the effect of corridors (highways) that facilitates movement of mosquitoes.

Fitzgibbon et al. [38] considered a reaction-diffusion PDE model with compartments for susceptible vectors, and infected humans and vectors, including seasonality through the mosquito breeding rate. It is assumed that the susceptible human population does not change in time. They applied their model to the 2015–2016 Zika outbreak in Rio de Janeiro municipality, using data for the total number of infections in the city. De Araujo et al. [28] studied existence and uniqueness of weak solutions of a reaction-diffusion PDE model for the spatial spread of dengue, with an example of optimal control applied to reduction of mosquitoes. In their model, the mosquito population is divided into winged and aquatic forms (eggs, larvae and pupae), and the human population into susceptible, infected and immune. A PDE model coupled with a system based on fuzzy rules was used by Silveira and Barros [107] to study the risk of dengue spread. A Markov chain method was used to model the stochastic dependence of rainfall in the model, and numerical simulations were carried out for the city of Campinas, Brazil. Ramírez Bernate [96] studied the effects of larvicides and insecticides and the introduction of sterile *Aedes aegypti* mosquitoes using reaction-diffusion PDEs. Their approach for numerical solutions is very similar to the one we use in the present work.

Other works have been successfully applying the same methodology (finite element and difference and predictor-corrector methods) than ours to numerical PDE solutions, in several applications. As some examples, we can cite [91], in a pollutant dispersal model with fuzzy parameters in a water reservoir in the central-eastern area of São Paulo state, Brazil. Gomes [44] applied a model coupled with fuzzy parameters to dengue in the south district of Campinas, Brazil. Rubianes Silva [101] modeled competition of aquatic macrophytes in the presence of pollution, and also the introduction of herbivore fish to control the growth of macrophyte. A benthic sediments model was used in [112] to study climate effect changes in an Antarctic cove. All these models are based on reaction-diffusion or reaction-advection-diffusion equations, and their numerical solutions were capable of provide important conclusions in real life problems.

Some research considered applications of vaccination to control and possibly reduce infections, particularly in vector-borne diseases. Valega-Mackenzie and Ríos-Soto [114] analyzed an ODE model for Zika virus with constant vaccination rate, studying its

role in the impact of direct and vector transmissions. An ODE vector-borne model with vaccination was studied in [95], considering waning protective immunity, incomplete vaccine-induced protection and adverse events, with an application to yellow fever. Rodrigues et al. [98] investigated the usefulness of a hypothetical dengue vaccine, with constant and optimal controls in ODEs, different efficacies and different ways of distribution. A general arboviral disease model was studied in [1], with analysis of bifurcation of endemic equilibriums and application of optimal control of vaccination, treatment and individual protection, and adult vectors, eggs and larvae elimination in an ODE model. They showed the existence of up to two endemic equilibrium points, and how optimal controls would affect them, using numerical simulations. Optimal vaccine strategies for rabies in raccoons are analyzed in an ODE metapopulation model in [7], and in a PDE model in [84]. Both models consider spatial and temporal SIR dynamics of raccoons and vaccines, with the latter distributed by food baits. Although it is not a vector-borne disease, the techniques used in those papers are similar to our approach.

We can cite other control and optimal control models that have been successfully applied to real life problems. Kelly Jr et al. [54] studied a metapopulation model for the effect of human and cholera pathogen movement in Haiti, considering optimal vaccination strategies. Stephenson et al. [110] also considered optimal vaccination, but applied to an ODE model of a particular bacteria infection in hospitals. Levy et al. [60] studied the dynamics of Ebola in the presence of public health education in Sudan. Outside epidemiology, Edholm et al. [34] studied optimal introduction of biological control agents working as biopesticides of invasive insect species in a discrete model. Heines et al. [49] assessed the economic tradeoffs between prevention and suppression of forest fires, using ODE models.

Among the already mentioned works, some of them use a least squares or maximum likelihood approach in order to estimate parameters from real data [38, 41, 60, 113]. The methodology in these works is similar to the one we propose. Considering a residual that measures the difference between data and output from the model, numerically calculated, an optimization procedure is performed in order to find the parameters that gives the least squared residual. Some other works rely on statistical inference methods [99, 106, 111, 116, 121], or even particularly designed methods [42]. Other works in the sense of parameter estimation for ODEs can be cited, as [120], in which time dependent entomological parameters are estimated using dengue data. Ramsay et al. [97] used a smoothing treatment of data and included penalty in the optimization procedure. Xue et al. [119] uses B-splines interpolation for time dependent parameters. For PDEs, we can cite [79], that compares a standard nonlinear approach to linear least squares in the case that the solution is explicitly obtained. Anguelov et al. [5] use least squares with finite element method in a trap-insect model. Carvalho et al. [22] considered different methods for the optimization procedure in parameter estimation of PDE models, and discussed

associated difficulties.

A study on global sensitivity analysis is well depicted in [67], in which the authors apply partial rank correlation coefficients (PRCCs) and extended Fourier amplitude sensitivity test (eFAST) to ODE and agent based models in immunology. PRCCs are an extension of the well known Pearson correlation coefficients, and thus are a sampling based method, while eFAST is variance based. The authors show that PRCCs are appropriate when relationships between input and output are monotonic and nonlinear, while eFAST can be applied when they are non-monotonic. The aforementioned works [41, 60, 65, 116] also use PRCCs to assess sensitivity, identifying which parameters have the most impact in the basic reproduction number and infections. On the other hand, Heines et al. [49] use PRCCs analysis to find the parameters with most impact in the optimal functional, which in that case represents an expected value for a forest in the presence of fire, in an ODE model.

In the present work, we propose a spatiotemporal PDE model for the Zika virus spread between humans and mosquitoes. A reaction-diffusion system is proposed to model the spatial movement of the populations (diffusion) and their dynamics (reaction). We consider susceptible, infected, and immune/recovered compartments for humans, and susceptible and infected for mosquitoes. Hypothetical vaccination is considered as a time and space varying control, converting susceptible humans into immune. The main goal is to obtain the most cost-effective vaccination strategy and simulate it in realistic scenarios. Using numerical solutions of PDEs, the optimality system (state and adjoint systems with optimal control characterization) is applied to data for the initial 2015 Zika outbreak in the state of Rio Grande do Norte, in the northeastern region of Brazil. Some parameters of the model are estimated from incidence data in a least squares approach, and different scenarios are evaluated in terms of the number of new infections and costs. The simulations show that the application of the optimal vaccine strategy is successful, reducing both infections and the overall associated cost. A global sensitivity analysis using PRCCs is carried out in order to find the parameters with most impact in the overall cost and in the total number of new infections. To the best of our knowledge, this work is the first to study vaccination and optimal control in a reaction-diffusion model for Zika virus. Furthermore, in optimal control applied to PDE models, regardless of the application, the strong connection between model and data is novel, as well as the sensitivity analysis performed, which considers the impact of parameters in the optimal functional cost.

1.3 Thesis outline

The remainder of this thesis is organized as follows: in Chapter 2 we present the mathematical modeling of Zika virus dynamics with vaccination, developing a reaction-

diffusion vector-borne partial differential equation model. We consider the transmission of the virus between humans and mosquitoes, and immunization through vaccination.

The optimal control problem is defined in Chapter 3. The control variable is the vaccination rate u, that varies in space and time. The overall cost to be minimized consists of costs from infections, vaccine applications and vaccine production and logistic costs. The characterization of the optimal solution is carried out in terms of sensitivity and adjoint equations, in the proper weak sense. Rigorous proofs are not our main focus, therefore are omitted but properly referenced to the available literature.

Chapter 4 is about the methods used to obtain numerical solutions of the optimal problem. Finite element and finite difference methods are used for the PDE approximated solutions, coupled with a predictor-corrector iteration for nonlinearities, and a forward-backward sweep is used for the optimal system solution. A clear but not detailed explanation of the methods is given, so that the reader can understand and possibly apply them to other problems of their interest. A numerical error and convergence analysis is performed in order to show the accuracy of the methods.

In Chapter 5 the parameter estimation procedure is presented and used to connect the model to data from the 2015 Zika outbreak in the Rio Grande do Norte state in Brazil. Some parameter values are estimated from data in a least squares approach and others from available literature. The methodology is tested using artificially generated data with added noise. More precisely, random normally distributed noise is considered, adding deviation to the baseline values. Maximum variation from generated data is considered as up to 100%, providing reliable results in all cases. Furthermore, a sensitivity analysis on parameters is performed considering the overall cost and number of new cases as output.

Numerical results are discussed in Chapter 6. Several scenarios are considered, first without control, then with constant and optimal controls, also varying the starting time of intervention. All scenarios are evaluated in terms of quantities of interest: number of new infections, overall cost and number of vaccinated people. Spatial and time plots are presented, the latter obtained by integrating solutions in space.

Lastly, Chapter 7 concludes this work, pointing out important features and commenting all results obtained. Some future work perspectives are also commented, the most important being the extension of the model in order to include multiple control variables, such as human and mosquito contact reduction and insecticides. Another modification is the inclusion of an immature phase for mosquitoes and larva/egg removal as control. Our work is readily adaptable for these inclusions, with all necessary mathematical and computational tools already presented.

A flow chart with of all the methods used throughout this work is shown below in Figure 1. It shows the connection of the modeling and each of the methods, all of them

together resulting in the numerical simulations, which are used for the qualitative and quantitative analysis of the problem of interest.

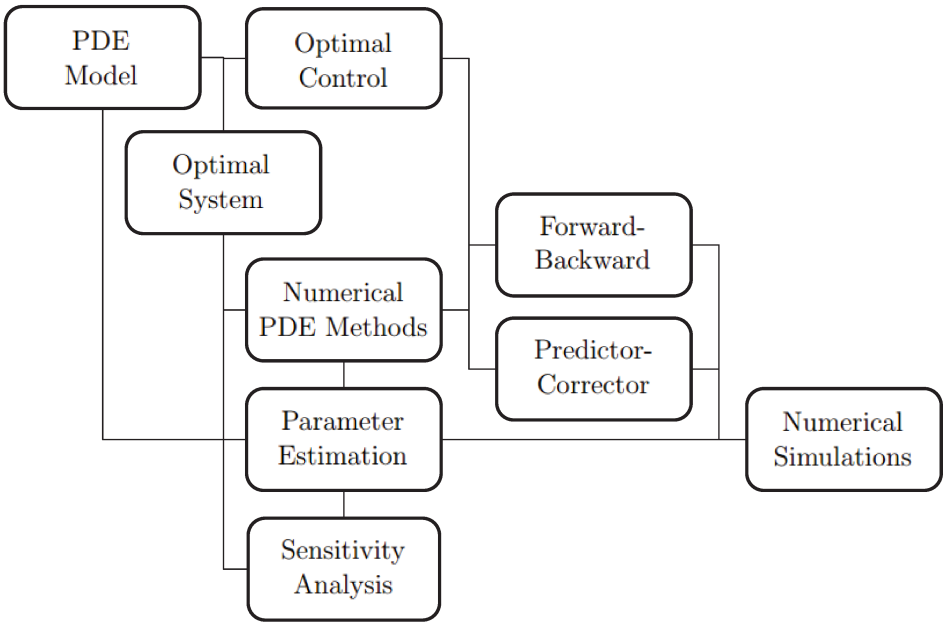

Figure 1 – Flow chart showing a summary of the connections of modeling and methods considered throughout the thesis. The PDE model is defined in Chapter 2 and the optimal control system in Chapter 3. Numerical, forward-backward and predictor-corrector methods are treated in Chapter 4. The parameter estimation procedure and sensitivity analysis are contained in Chapter 5, and numerical simulations in Chapter 6.

Chapter 2
Mathematical modeling

In this chapter we propose a reaction-diffusion compartmental model for Zika virus. The term "reaction" stands for the dynamics within the model, in our case the dynamics of infectious diseases between the compartments in study. It involves transmissions between humans and vector mosquitoes, recovering, birth and death, and other dynamics that should be important, depending on particular interests in the modeling. For more details about infectious disease compartmental models we suggest the excellent books by Edelstein-Keshet [33], Keeling and Rohani [53], and Murray [82].

Diffusion accounts for spatial movement of the populations. Mathematically, it is the mean movement of a random process, and it is modeled by the divergent of a diffusion coefficient multiplied by the gradient of a density [21, 83, 88]. In population dynamics of humans and animals (mosquitoes in the present work), it is impossible to track or represent all movement that occurs at given period. In this sense, diffusion can be interpreted as the mean of all the movement performed by a population at a given time period. When diffusion is combined with infectious disease modeling, it is assumed that local contact transmission occurs when populations occupy the same space. Diffusion coupled with transmission is responsible for the local spread of the disease throughout a certain region, and depends on existing infections for the spread to happen, not considering migration or external sources of infection.

Before passing to the model itself, we review some technical definitions regarding functional analysis, more precisely functional spaces that are necessary in the analysis of PDEs.

2.1 Technical definitions

Due to the necessary theory in the treatment of PDEs, we need to consider specific function spaces, which we define in the following. The integrals are all Lebesgue, and the derivatives in the weak sense. It should be noted that Lebesgue integrals have the same properties as Riemann integrals, as well as derivatives of distributions generalize usual derivatives [11, 25]. We define the spaces for general spatial domains in $\mathbb{R}^n$, but our interest in real life applications restricts to $n = 1$ or $n = 2$, or even $n = 3$ in some

problems. In the present work the application is restricted to $n = 2$, corresponding to spatial areas. More information on the spaces defined below can be found in [36, 57].

Given an open domain $\Omega \subset \mathbb{R}^n$, the space $L^2(\Omega)$ of square integrable functions is defined as:

$$L^2(\Omega) = \left\{ f(\boldsymbol{x}) : \Omega \to \mathbb{R}; \int_\Omega |f(\boldsymbol{x})|^2 \, \mathrm{d}\mu < \infty \right\}.$$

For functions that also depend on time $t \in (0, T)$, given $Q = (0, T) \times \Omega$, the space $L^2((0, T); \Omega) = L^2(Q)$ is the direct extension of $L^2(\Omega)$:

$$L^2((0,T);\Omega) = \left\{ f(\boldsymbol{x}, t) : \Omega \times (0,T) \to \mathbb{R}; \int_\Omega |f(\boldsymbol{x}, t)|^2 \, \mathrm{d}\mu < \infty, \ \forall t \in (0,T) \right\}.$$

The Sobolev space $H^1(\Omega)$ consists of the functions in $L^2(\Omega)$ such that their weak derivatives also belong to $L^2(\Omega)$, that is:

$$H^1(\Omega) = \left\{ f(\boldsymbol{x}) \in L^2(\Omega); \frac{\partial f}{\partial x_1}, \ldots, \frac{\partial f}{\partial x_n} \in L^2(\Omega) \right\}.$$

The dual space of the Sobolev space $H^1(\Omega)$ is $H^1(\Omega)^*$, which consists of linear functionals in $H^1(\Omega)$. That is, any linear form F such that $F : H^1(\Omega) \to \mathbb{R}$. A simple example is the derivative operator acting on functions in $H^1(\Omega)$.

The subspace $H_0^1(\Omega) \subset H^1(\Omega)$ is such that all its functions have compact support (have zero values at the boundary $\partial\Omega$):

$$H_0^1(\Omega) = \left\{ f(\boldsymbol{x}) \in L^2(\Omega); \frac{\partial f}{\partial x_1}, \ldots, \frac{\partial f}{\partial x_n} \in L^2(\Omega), f = 0 \text{ in } \partial\Omega \right\}.$$

We do not need to consider as much restrictive aspects for temporal derivatives in functions that depend on both space and time. We can consider functions such that in space belong to $H^1(\Omega)$, but in time are square integrable. So, we have the space:

$$L^2((0,T); H^1(\Omega)) = \left\{ f(\boldsymbol{x}, t) : \Omega \times (0,T) \to \mathbb{R}; \right.$$
$$\left. \int_\Omega |f(\boldsymbol{x}, t)|^2 \, \mathrm{d}\mu < \infty, \forall t \in (0,T), \frac{\partial f}{\partial x_1}, \ldots, \frac{\partial f}{\partial x_n} \in L^2(\Omega) \right\}.$$

The corresponding dual space is $L^2((0, T); H^1(\Omega)^*)$, consisting on linear forms F such that $F : L^2((0, T); H^1(\Omega)) \to \mathbb{R}$. Later in the optimal control characterization we consider time derivatives in this space.

2.2 Reaction-diffusion model with vaccination

We wish to develop a reaction-diffusion model for the spread of Zika virus in humans and mosquitoes, containing the most important features and being capable of

providing realistic results. Even so, it should be simple enough to analyze and treat, both analytically and numerically. An over complicated model, with many compartments and parameters, brings more uncertainties to the model and possible difficulties in numerical simulations. Also, interpretations of the results would be more complex, particularly in a PDE model, in which spatial and temporal dynamics are both important. Therefore, some simplifying assumptions are necessary. A flow chart for the model is shown in Figure 2, with parameter descriptions in Table 1.

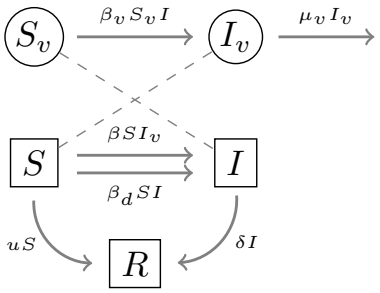

Figure 2 – Flow chart for model (2.1). Squares denote humans and circles mosquitoes. S, I, R denote susceptible, infected, and immune populations, respectively. Reproduction for mosquitoes is of logistic type (not shown in figure). Parameter descriptions can be found in Table 1.

Table 1 – Description and units of quantities from model (2.1).

	Description	Unit
S	Susceptible humans density	humans/km^2
I	Infected humans density	humans/km^2
R	Immune humans density	humans/km^2
S_v	Susceptible mosquitoes density	mosquitoes/km^2
I_v	Infected mosquitoes density	mosquitoes/km^2
u	Vaccination rate	1/days
β	Mosquito to human transmission rate	1/(mosq./km^2 days)
β_v	Human to mosquito transmission rate	1/(hum./km^2 days)
β_d	Human to human transmission rate	1/(hum./km^2 days)
$1/\delta$	Disease duration	days
r_v	Mosquito intrinsic growth rate	days
$1/\mu_v$	Mosquito lifespan	days
κ_v	Mosquito carrying capacity	mosq./km^2
α	Human diffusion coefficient	km^2/days
α_I	Infected human diffusion coefficient	km^2/days
α_v	Mosquito diffusion coefficient	km^2/days
Ω	Spatial domain	km^2
$(0, T)$	Time interval	days

The proposed model consists of five compartments: susceptible (S), infected (I) and immune (R) humans, and susceptible (S_v) and infected (I_v) mosquitoes/vectors [53].

The word "infected" is used to denote that a human or a vector in its corresponding class is able to transmit the virus, even if they are asymptomatic or have the virus in the latent phase. This simplifies the model by eliminating two compartments (asymptomatic and exposed). The immune compartment consists of both humans that acquired the disease and naturally recovered, and the ones that acquired resistance through vaccination.

All populations are able to spatially move, which is described in the model by diffusion. As mentioned before, it represents the mean movement performed at a given time. Throughout the present work we consider constant diffusion coefficients for all populations, assuming that they spread evenly in all spatial directions. Nevertheless, variable diffusion could be considered, if appropriate, depending on the context of application. There is no known transport or preferred direction of movement, so we do not consider advection or convection terms.

The virus is mainly transmitted between humans and mosquitoes: a susceptible human can become infected through bites from mosquitoes carrying the virus, while susceptible mosquitoes can become infected by having blood meals from infected humans. We consider only the *Aedes aegypti* species of mosquito, as it is far more common in the region of our interest (Brazil). A remarkable feature of the Zika virus is direct (sexual) transmission, even though the main course of transmission is through the vector [3]. Little data are available on confirmed direct transmission cases. We consider direct transmission between susceptible and infected humans in the model, but in our numerical simulations we find that it is irrelevant, at least for the set of data we use to parametrize the model. All transmissions are modeled using the mass action principle, which accounts for the mean of the probability of transmission in the spatial contact between susceptible and infected humans or mosquitoes.

Once infected, humans develop mild symptoms which last around 14 days, and after this period are considered to be immune, being unable to transmit the virus and not being able to acquire it anymore. The virus has no effect on the mosquitoes, which remain infected during their lifetime. Deaths caused by the virus are rare, so we do not include them in the model. No natural birth or death rates are included for the humans due to the short time frame for Zika outbreaks. On the other hand, it is important to consider birth and death for mosquitoes since their lifespan is much shorter than that of humans. We chose logistic growth considering that the population of mosquitoes in the region of study is large, but also dependent on resources available for them. Due to simplification aspects, we do not consider different compartments for the life cycle of mosquitoes.

A hypothetical vaccination moves susceptible humans directly into the immune class. The rate of the vaccination of susceptible humans is $u(\boldsymbol{x}, t)$, which is a time and space varying control. It is assumed that the vaccine has 100% of efficiency, but once a real vaccine is approved and applicable, a simple adjustment could be made in order to

include its efficacy. In this way, the new vaccination can be defined as $\bar{u}$, and e_u as the efficacy (in percentage). Then, the vaccination term should be $\bar{u} = e_u u$.

Boundary conditions are chosen as no flux for all populations, with derivatives in the outward normal direction $\boldsymbol{n}$ equal to zero (homogeneous Neumann). This means that there is no flux of humans or mosquitoes at the boundary of the region in study, which is therefore isolated. In other words, the inward and outward flux cancel out at the border, with a resulting zero flux. This kind of behavior is plausible at the border of a state, since we are concentrated in studying the disease spread only within the state. Other boundary conditions could be considered, for example partial flux, with outward normal derivatives proportional to the concentration at the boundary (homogeneous Robin), or proportional to both concentration and an external factor (non homogeneous Robin). Unfortunately, these kinds of boundary conditions would add another parameter to the model, that would be specially hard to estimate since it involves human and mosquito movement across states. A detailed explanation on boundary conditions can be found in [77].

The model is then given by the PDE system (2.1) in $Q = \Omega \times (0, T)$. All populations S, I, R, S_v, I_v and the vaccination rate u are functions of space $\boldsymbol{x} = (x, y)$ and time $t \in (0, T)$, with spatial domain $\Omega \subset \mathbb{R}^2$ and smooth boundary $\partial\Omega$. Populations are seen as densities over space, which is continuous. Initial conditions S_0, I_0, R_0, S_{v0} and I_{v0} are properly defined in each situation of interest. Parameters descriptions and units can be found in Table 1.

$$
\begin{cases}
\dfrac{\partial S}{\partial t} - \nabla \cdot (\alpha \nabla S) = -\beta S I_v - \beta_d S I - uS, \\
\dfrac{\partial I}{\partial t} - \nabla \cdot (\alpha_I \nabla I) = \beta S I_v + \beta_d S I - \delta I, \\
\dfrac{\partial R}{\partial t} - \nabla \cdot (\alpha \nabla R) = uS + \delta I, \\
\dfrac{\partial S_v}{\partial t} - \nabla \cdot (\alpha_v \nabla S_v) = -\beta_v S_v I + r_v \left(S_v + I_v\right) \left(1 - \dfrac{(S_v + I_v)}{\kappa_v}\right), \\
\dfrac{\partial I_v}{\partial t} - \nabla \cdot (\alpha_v \nabla I_v) = \beta_v S_v I - \mu_v I_v, \text{ in } Q, \\
S(\boldsymbol{x}, 0) = S_0,\ I(\boldsymbol{x}, 0) = I_0,\ R(\boldsymbol{x}, 0) = R_0,\ S_v(\boldsymbol{x}, 0) = S_{v0},\ I_v(\boldsymbol{x}, 0) = I_{v0}, \text{ in } \Omega, \\
\dfrac{\partial S}{\partial \boldsymbol{n}} = 0,\ \dfrac{\partial I}{\partial \boldsymbol{n}} = 0,\ \dfrac{\partial R}{\partial \boldsymbol{n}} = 0,\ \dfrac{\partial S_v}{\partial \boldsymbol{n}} = 0,\ \dfrac{\partial I_v}{\partial \boldsymbol{n}} = 0, \text{ in } \partial\Omega \times (0, T).
\end{cases}
\tag{2.1}
$$

Diffusion coefficients are the same for S and R, possibly lower for I due to disease symptoms, and S_v and I_v having the same diffusion coefficient, since the virus does not affect mosquitoes. The transmission terms are proportional to the size of the populations, with the parameter rates β, β_d, β_v regulating the proportionality. The vaccination u and recovery rate δ are also proportional, with the vaccination rate varying in space and time. The other parameters in the model may also depend on space and/or time, but throughout this work they are assumed to be constant. Logistic growth for mosquitoes considers that

both susceptible and infected give birth, and all newborn mosquitoes are susceptible. In this sense, the intrinsic growth rate is given by r_v. Logistic growth also accounts for an embedded mortality due to competition between both susceptible and infected mosquitoes, which limits the population size to the carrying capacity κ_v. Thus, the birth of mosquitoes is greater if the total population $S_v + I_v$ is small (low competition), and gets smaller as this value approaches the carrying capacity (large competition). For infected mosquitoes a proportional natural death term is included with rate μ_v.

Chapter 3
Optimal control

In the modeling, we defined the vaccination rate $u = u(\boldsymbol{x}, t)$ as a space and time variable. It could be constant in both space and time, representing that vaccination should be applied always at the same rate in all space region. Another alternative is time varying, for example with an oscillatory behavior, representing a prevention program at peaks of infections. This kind of situation could be studied with control theory, in which some variable(s) values are varied in order to satisfy a predefined state or condition [62]. This is not our main goal.

It is usually difficult to know exactly at which time and spatial region the disease would spread the most. In this context, a variable rate that adapts to regions and time intervals with most infections could be more efficient, and even the most efficient according to certain criteria. This rate can be obtained by optimal control theory, considering the vaccination as a control variable of an optimization problem. This theory is explored in the present chapter and applied to model (2.1).

We wish to find a vaccination rate that has the best cost-benefit, in terms of costs associated to infections and vaccines, including application costs. In order to specify the optimal control problem, we need to define an associated cost to be minimized or maximized: the objective functional. Once the problem is proposed, the optimal control characterization can be obtained using standard analysis [58]. This involves the sensitivity and adjoint systems, and a directional derivative of the objective functional. In optimal control theory, model (2.1) is also called state system, because its solutions are the state functions (S, I, R, S_v, I_v).

3.1 Definition of the optimal control problem

We wish to obtain the best strategy of vaccination over a spatial region during a time period, considering the vaccination rate u as function of $(\boldsymbol{x}, t)$. Therefore, having the state system (2.1) as a constraint, we wish to minimize the following cost objective functional depending on the vaccination rate u:

$$J(u) = \int_Q (c_1 I(\boldsymbol{x}, t) + c_2 u(\boldsymbol{x}, t) S(\boldsymbol{x}, t) + c_3 u(\boldsymbol{x}, t)^2)\, \mathrm{d}\boldsymbol{x}\mathrm{d}t, \tag{3.1}$$

where c_1, c_2 and c_3 are constant weights, c_1 represents the cost related to infected people, such as medical care and an average cost associated to neurological conditions (possibly including the consequent costs in newborns with microcephaly), c_2 represents the cost related to the implementation of vaccination (per person) in susceptible humans, and c_3 represents the nonlinear cost related to the vaccines themselves, such as production and logistics. The quadratic term $u(\boldsymbol{x}, t)^2$ is chosen to represent a small cost, smaller than a linear term, as the rate $u(\boldsymbol{x}, t)$ is smaller than 1. The integral over $Q = \Omega \times (0, T)$ represents the summed contributions over all space and all time, in a way that all contributions are equally important in the total cost and summarized in a single value. Parameter descriptions and units can be found in Table 2. Looking at a dimensional analysis on the coefficients, it is possible to obtain another look at their interpretation. The unit (\$/hum.)/days from c_1 represents the per capta infection cost per day, meaning that an infected human would in average cost c_1 monetary units \$ per day. Similarly, c_2 would represent the average cost of vaccination per human, \$/hum. On the other hand, c_3, with unit \$/(km^2/days), would represent the average cost of vaccination spent in a unitary area in a day.

Considering bounds $u_{\min}$ and $u_{\max}$ on u, the set of admissible controls is:

$$U = \left\{ u \in L^2(Q), u_{\min} \leqslant u \leqslant u_{\max} \right\}. \tag{3.2}$$

We seek to find the optimal control $u^* \in U$ such that:

$$J(u^*) = \inf_{u \in U} J(u) \tag{3.3}$$

subject to the state equations (2.1). In other words, we seek to find, from all possible controls $u \in U$, the optimal control u^* such that $J(u^*)$ is the minimum among all $J(u)$. It is worth noting that this is an optimization problem in which the variables are functions, so that special care must be taken in the functional analysis involved.

Table 2 – Description and units of parameters for optimal control problem (3.3).

	Description	Unit
c_1	Infected human cost per day	(\$/hum.)/days
c_2	Vaccination cost per human	\$/hum.
c_3	Vaccination cost per area per day	\$/(km^2/days)
$u_{\min}$	Vaccination rate lower bound	1/days
$u_{\max}$	Vaccination rate upper bound	1/days

It is possible to show that weak solutions of system (2.1), with state functions in $L^2((0, T); H^1(\Omega))$ and corresponding time derivatives in $L^2((0, T); H^1(\Omega)^*)$, exist and are unique, as well as the existence and uniqueness of the optimal control, which holds for a sufficiently small time. We do not show these results since they are not in the scope

of our work. Proofs for weak solutions of applied optimal problems can be found in [24, 29, 84], which also contain detailed explanation on the optimal control characterization. In particular, Fister [37] provides a more thorough demonstration of the existence and uniqueness of the optimal solution, using minimizing sequences. These references treat parabolic problems very similar to (2.1), and the provided demonstrations follow the same concepts needed in our case. More theoretical concepts regarding analysis of optimal control problems can be found in [61, 63].

3.2 Derivation of optimal control

We seek to find an optimal control $u^* \in U$ satisfying (3.3), where U is the set of admissible controls defined in (3.2). This optimization problem is subject to the state system (2.1), with state functions in $L^2((0,T); H^1(\Omega))$ and corresponding time derivatives in $L^2((0,T); H^1(\Omega)^*)$. In order to find u^*, we have to solve an optimality system, which consists of the state PDEs, adjoint PDEs, and the optimal control characterization. We also need the sensitivity system, and in order to obtain it we must differentiate the control-to-state map $u \to (S, I, R, S_v, I_v)(u)$. We use that system and the objective functional to find the adjoint system. Then we use the sensitivity and adjoint system to simplify the derivative of the map $u \to J(u)$, finally obtaining the desired optimal control characterization. The derivatives of both of these maps are computed as directional derivatives. In the following, we provide an overview of the derivation of the sensitivity and adjoint equations, and the control characterization.

3.2.1 Sensitivity system

Given a control $u \in U$, consider another control $u + \epsilon\ell$ in U for $\epsilon > 0$, with $\ell \in L^2(Q)$, which represents a perturbation. From the control-to-state map, we define $(S^\epsilon, I^\epsilon, R^\epsilon, S_v^\epsilon, I_v^\epsilon) = (S, I, R, S_v, I_v)(u + \epsilon\ell)$. We then define the sensitivity functions, which are Gateaux derivatives of the control-to-state map:

$$\frac{S^\epsilon - S}{\epsilon} \rightharpoonup \psi_1, \quad \frac{I^\epsilon - I}{\epsilon} \rightharpoonup \psi_2, \quad \frac{R^\epsilon - R}{\epsilon} \rightharpoonup \psi_3, \quad \frac{S_v^\epsilon - S_v}{\epsilon} \rightharpoonup \psi_4, \quad \frac{I_v^\epsilon - I_v}{\epsilon} \rightharpoonup \psi_5, \text{ as } \epsilon \to 0.$$

We also have:

$$S^\epsilon \to S, \ I^\epsilon \to I, \ R^\epsilon \to R, \ S_v^\epsilon \to S_v, \ I_v^\epsilon \to I_v, \text{ as } \epsilon \to 0.$$

The sensitivity functions $\boldsymbol{\psi} = (\psi_1, \psi_2, \psi_3, \psi_4, \psi_5)$ satisfy a system corresponding to a linearized version of the state equations. See works by De Silva et al. [29], Li and Yong [61], and Lions [63] to show justification of such convergence of these quotients and the existence of the sensitivity functions and their PDEs. These equations are used to derive

PDEs for the adjoint $\boldsymbol{\lambda} = (\lambda_1, \lambda_2, \lambda_3, \lambda_4, \lambda_5)$, where each adjoint variable is associated with a state variable.

We now calculate equations for the sensitivity functions, forming the coefficients of the sensitivity functions and then passing the limit. In order to do so we use system (2.1) to write equations for $(S^\epsilon, I^\epsilon, R^\epsilon, S_v^\epsilon, I_v^\epsilon)$ and then form equations for the sensitivity coefficients. Calculating in this way an equation for the S quotient, noting that for S^ϵ, we use $u + \epsilon\ell$ instead of u:

$$\left(\frac{S^\epsilon - S}{\epsilon}\right)_t - \frac{\nabla\cdot(\alpha\nabla S^\epsilon) - \nabla\cdot(\alpha\nabla S)}{\epsilon} = -\beta\left(\frac{S^\epsilon I_v^\epsilon - S^\epsilon I_v + S^\epsilon I_v - SI_v}{\epsilon}\right) - \beta_d\left(\frac{S^\epsilon I^\epsilon - S^\epsilon I + S^\epsilon I - SI}{\epsilon}\right) - u\left(\frac{S^\epsilon - S}{\epsilon}\right) - \ell S^\epsilon.$$

Letting $\epsilon \to 0$, and passing to the limit we get:

$$(\psi_1)_t - \nabla\cdot(\alpha\psi_1) + \beta\left(S\psi_5 + \psi_1 I_v\right) + \beta_d\left(S\psi_2 + \psi_1 I\right) + u\psi_1 = -\ell S.$$

In the same way, letting $\epsilon \to 0$ in

$$\left(\frac{I^\epsilon - I}{\epsilon}\right)_t - \frac{\nabla\cdot(\alpha_I\nabla I^\epsilon) - \nabla\cdot(\alpha\nabla I)}{\epsilon} = \beta\left(\frac{S^\epsilon I_v^\epsilon - S^\epsilon I_v + S^\epsilon I_v - SI_v}{\epsilon}\right) + \beta_d\left(\frac{S^\epsilon I^\epsilon - S^\epsilon I + S^\epsilon I - SI}{\epsilon}\right) - \delta\left(\frac{I^\epsilon - I}{\epsilon}\right)$$

gives an equation for $(\psi_2)_t$:

$$(\psi_2)_t - \nabla\cdot(\alpha_I\psi_2) - \beta\left(S\psi_5 + \psi_1 I_v\right) - \beta_d\left(S\psi_2 + \psi_1 I\right) + \delta\psi_2 = 0.$$

Similarly:

$$\left(\frac{R^\epsilon - R}{\epsilon}\right)_t - \frac{\nabla\cdot(\alpha\nabla R^\epsilon) - \nabla\cdot(\alpha\nabla R)}{\epsilon} = u\left(\frac{S^\epsilon - S}{\epsilon}\right) + \ell S^\epsilon + \delta\left(\frac{I^\epsilon - I}{\epsilon}\right),$$

gives:

$$(\psi_3)_t - \nabla\cdot(\alpha\psi_3) - u\psi_1 - \delta\psi_2 = \ell S.$$

For S_v, we obtain:

$$\left(\frac{S_v^\epsilon - S_v}{\epsilon}\right)_t - \frac{\nabla\cdot(\alpha_v\nabla S_v^\epsilon) - \nabla\cdot(\alpha_v\nabla S_v)}{\epsilon} = -\beta_v\left(\frac{S_v^\epsilon I^\epsilon - S_v^\epsilon I + S_v^\epsilon I - S_v I}{\epsilon}\right) + r_v\left(\frac{S_v^\epsilon - S_v}{\epsilon}\right) + r_v\left(\frac{I_v^\epsilon - I_v}{\epsilon}\right) - \frac{r_v}{\kappa_v}\left(\frac{S_v^\epsilon S_v^\epsilon - S_v^\epsilon S_v + S_v^\epsilon S_v - S_v S_v}{\epsilon}\right) - \frac{2r_v}{\kappa_v}\left(\frac{S_v^\epsilon I_v^\epsilon - S_v^\epsilon I_v + S_v^\epsilon I_v - S_v I_v}{\epsilon}\right) - \frac{r_v}{\kappa_v}\left(\frac{I_v^\epsilon I_v^\epsilon - I_v^\epsilon I_v + I_v^\epsilon I_v - I_v I_v}{\epsilon}\right),$$

which gives:

$$(\psi_4)_t - \nabla\cdot(\alpha_v\psi_4) + \beta_v\left(S_v\psi_2 + \psi_4 I\right) - r_v\left(\psi_4 + \psi_5\right) + \frac{2r_v}{\kappa_v}\left(S_v + I_v\right)\left(\psi_4 + \psi_5\right) = 0.$$

Similarly, for I_v we have:

$$\left(\frac{I_v^\epsilon - I_v}{\epsilon}\right)_t - \frac{\nabla\cdot(\alpha_v\nabla I_v^\epsilon) - \nabla\cdot(\alpha_v\nabla I_v)}{\epsilon} = \beta_v\left(\frac{S_v^\epsilon I^\epsilon - S_v^\epsilon I + S_v^\epsilon I - S_v I}{\epsilon}\right) - \mu_v\left(\frac{S_v^\epsilon - S_v}{\epsilon}\right),$$

and:

$$(\psi_5)_t - \nabla\cdot(\alpha_v\psi_5) - \beta_v\left(S_v\psi_2 + \psi_4 I\right) + \mu_v\psi_5 = 0.$$

In a similar way, we obtain initial conditions:

$$\psi_1(\boldsymbol{x},0) = \psi_2(\boldsymbol{x},0) = \psi_3(\boldsymbol{x},0) = \psi_4(\boldsymbol{x},0) = \psi_5(\boldsymbol{x},0) = 0, \text{ in } \Omega,$$

and boundary conditions:

$$\frac{\partial\psi_1}{\partial\boldsymbol{n}} = \frac{\partial\psi_2}{\partial\boldsymbol{n}} = \frac{\partial\psi_3}{\partial\boldsymbol{n}} = \frac{\partial\psi_4}{\partial\boldsymbol{n}} = \frac{\partial\psi_5}{\partial\boldsymbol{n}} = 0 \text{ in } \partial\Omega\times(0,T).$$

We can now write the sensitivity system in vector form as follows:

$$\boldsymbol{\mathcal{L}}\begin{pmatrix}\psi_1\\ \psi_2\\ \psi_3\\ \psi_4\\ \psi_5\end{pmatrix} = \begin{pmatrix}-\ell S\\ 0\\ \ell S\\ 0\\ 0\end{pmatrix},$$

where:

$$\boldsymbol{\mathcal{L}}\begin{pmatrix}\psi_1\\ \psi_2\\ \psi_3\\ \psi_4\\ \psi_5\end{pmatrix} = \begin{pmatrix}(\psi_1)_t - \nabla\cdot(\alpha\nabla\psi_1)\\ (\psi_2)_t - \nabla\cdot(\alpha_I\nabla\psi_2)\\ (\psi_3)_t - \nabla\cdot(\alpha\nabla\psi_3)\\ (\psi_4)_t - \nabla\cdot(\alpha_v\nabla\psi_4)\\ (\psi_5)_t - \nabla\cdot(\alpha_v\nabla\psi_5)\end{pmatrix} + \boldsymbol{M}\begin{pmatrix}\psi_1\\ \psi_2\\ \psi_3\\ \psi_4\\ \psi_5\end{pmatrix},$$

and the transpose of the matrix $\boldsymbol{M}$ is given by:

$$\boldsymbol{M}^T = \begin{pmatrix}\beta I_v + \beta_d I + u & -\beta I_v - \beta_d I & -u & 0 & 0\\ \beta_d S & \delta - \beta_d S & -\delta & \beta_v S_v & -\beta_v S_v\\ 0 & 0 & 0 & 0 & 0\\ 0 & 0 & 0 & -r_v + \dfrac{2r_v}{\kappa_v}(S_v + I_v) + \beta_v I & -\beta_v I\\ \beta S & -\beta S & 0 & -r_v + \dfrac{2r_v}{\kappa_v}(S_v + I_v) & \mu_v\end{pmatrix}. \tag{3.4}$$

3.2.2 Adjoint system

The adjoint variables $\boldsymbol{\lambda} = (\lambda_1, \lambda_2, \lambda_3, \lambda_4, \lambda_5)$ are each associated with one state variable (S, I, R, S_v, I_v). The adjoint operator $\mathcal{L}^*$ is obtained from the relation:

$$\langle \boldsymbol{\lambda}, \mathcal{L}\boldsymbol{\psi} \rangle = \langle \mathcal{L}^* \boldsymbol{\lambda}, \boldsymbol{\psi} \rangle \tag{3.5}$$

in the appropriate weak $L^2(Q)$ sense and $\langle \cdot, \cdot \rangle$ is the $L^2(Q)$ inner product. The right hand side of the adjoint system is given by the derivatives of the integrand of the objective functional, with respect to the states:

$$\begin{aligned}
\frac{\partial}{\partial S}\left(c_1 I + c_2 u S + c_3 u^2\right) &= c_2 u, \\
\frac{\partial}{\partial I}\left(c_1 I + c_2 u S + c_3 u^2\right) &= c_1, \\
\frac{\partial}{\partial R}\left(c_1 I + c_2 u S + c_3 u^2\right) &= 0, \\
\frac{\partial}{\partial S_v}\left(c_1 I + c_2 u S + c_3 u^2\right) &= 0, \\
\frac{\partial}{\partial I_v}\left(c_1 I + c_2 u S + c_3 u^2\right) &= 0.
\end{aligned}$$

We use expression (3.5) in order to obtain the operators in the adjoint system. This is done using integration by parts on $\langle \boldsymbol{\lambda}, \mathcal{L}\boldsymbol{\psi} \rangle$ and the boundary conditions of the sensitivity equations. The adjoint system obtained this way is:

$$\mathcal{L}^* \begin{pmatrix} \lambda_1 \\ \lambda_2 \\ \lambda_3 \\ \lambda_4 \\ \lambda_5 \end{pmatrix} = \begin{pmatrix} c_2 u \\ c_1 \\ 0 \\ 0 \\ 0 \end{pmatrix}, \tag{3.6}$$

where:

$$\mathcal{L}^* \begin{pmatrix} \lambda_1 \\ \lambda_2 \\ \lambda_3 \\ \lambda_4 \\ \lambda_5 \end{pmatrix} = \begin{pmatrix} -(\lambda_1)_t - \nabla \cdot (\alpha \nabla \lambda_1) \\ -(\lambda_2)_t - \nabla \cdot (\alpha_I \nabla \lambda_2) \\ -(\lambda_3)_t - \nabla \cdot (\alpha \nabla \lambda_3) \\ -(\lambda_4)_t - \nabla \cdot (\alpha_v \nabla \lambda_4) \\ -(\lambda_5)_t - \nabla \cdot (\alpha_v \nabla \lambda_5) \end{pmatrix} + \boldsymbol{M}^T \begin{pmatrix} \lambda_1 \\ \lambda_2 \\ \lambda_3 \\ \lambda_4 \\ \lambda_5 \end{pmatrix}.$$

In the integration by parts, the adjoints must be defined as zero at the final time $t = T$. Thus, the transversality (final time) conditions are given by:

$$\lambda_1(\boldsymbol{x}, T) = 0,\ \lambda_2(\boldsymbol{x}, T) = 0,\ \lambda_3(\boldsymbol{x}, T) = 0,\ \lambda_4(\boldsymbol{x}, T) = 0,\ \lambda_5(\boldsymbol{x}, T) = 0, \quad \text{in } \Omega,$$

and boundary conditions by:

$$\frac{\partial \lambda_1}{\partial \boldsymbol{n}} = 0,\ \frac{\partial \lambda_2}{\partial \boldsymbol{n}} = 0,\ \frac{\partial \lambda_3}{\partial \boldsymbol{n}} = 0,\ \frac{\partial \lambda_4}{\partial \boldsymbol{n}} = 0,\ \frac{\partial \lambda_5}{\partial \boldsymbol{n}} = 0, \quad \text{in } \partial\Omega \times (0, T).$$

3.2.3 Optimal control characterization

We now derive an expression for the optimal control u^* as a function of the state and adjoint variables. The derivative of the map $u \to J(u)$ at u^* in the direction ℓ is:

$$\lim_{\epsilon \to 0^+} \frac{J(u^* + \epsilon\ell) - J(u^*)}{\epsilon},$$

with:

$$\begin{aligned} J(u^* + \epsilon\ell) &= \int_Q \left[c_1 I^\epsilon + c_2(u^* + \epsilon\ell)S^\epsilon + c_3(u^* + \epsilon\ell)^2\right] \mathrm{d}\boldsymbol{x}\mathrm{d}t \\ &= \int_Q \left[c_1 I^\epsilon + c_2 u^* S^\epsilon + \epsilon c_2 \ell S^\epsilon + c_3 (u^*)^2 + 2c_3 u^* \epsilon\ell + c_3 \epsilon^2 \ell^2\right] \mathrm{d}\boldsymbol{x}\mathrm{d}t. \\ J(u^*) &= \int_Q \left[c_1 I + c_2 u^* S + c_3 (u^*)^2\right] \mathrm{d}\boldsymbol{x}\mathrm{d}t. \end{aligned}$$

The * superscript over the state variables denotes optimality, that is: the state solution at the optimal characterization. In order to find the optimal control characterization, we wish to find u^* such that:

$$\lim_{\epsilon \to 0^+} \frac{J(u^* + \epsilon\ell) - J(u^*)}{\epsilon} \geqslant 0.$$

The positivity of the derivative comes from the fact that $J(u^*)$ is minimum among all $J(u)$, $u \in U$. Using the sensitivity and adjoint systems we find a characterization for u^* in the following way:

$$0 \leqslant \lim_{\epsilon \to 0^+} \frac{J(u^* + \epsilon\ell) - J(u^*)}{\epsilon}.$$

Substituting $J(u^* + \epsilon\ell)$ and $J(u^*)$:

$$0 \leqslant \lim_{\epsilon \to 0^+} \int_Q \left[c_1 \frac{I^\epsilon - I}{\epsilon} + c_2 u^* \frac{S^\epsilon - S}{\epsilon} + c_2 \ell S^\epsilon + 2c_3 u^* \ell + c_3 \epsilon \ell^2\right] \mathrm{d}\boldsymbol{x}\mathrm{d}t.$$

Passing to the limit:

$$0 \leqslant \int_Q \left[c_1\psi_2 + c_2 u^* \psi_1 + c_2 \ell S^* + 2c_3 u^* \ell\right] \mathrm{d}\boldsymbol{x}\mathrm{d}t.$$

Rearranging in matrix form:

$$0 \leqslant \int_Q \left[(\psi_1, \psi_2, \psi_3, \psi_4, \psi_5)\,(c_2 u^*, c_1, 0, 0, 0)^T + \ell\,(c_2 S^* + 2c_3 u^*)\right] \mathrm{d}\boldsymbol{x}\mathrm{d}t.$$

Using the fact that $(c_2 u^*, c_1, 0, 0, 0)^T$ is the right hand side of the adjoint operator:

$$0 \leqslant \int_Q \left[(\psi_1, \psi_2, \psi_3, \psi_4, \psi_5)\,\mathcal{L}^*\,(\lambda_1, \lambda_2, \lambda_3, \lambda_4, \lambda_5)^T + \ell\,(c_2 S^* + 2c_3 u^*)\right] \mathrm{d}\boldsymbol{x}\mathrm{d}t.$$

Using the adjoint relation (3.5), in the appropriate weak sense:

$$0 \leqslant \int_Q \left[(\lambda_1, \lambda_2, \lambda_3, \lambda_4, \lambda_5) \, \mathcal{L} \, (\psi_1, \psi_2, \psi_3, \psi_4, \psi_5)^T + \ell \, (c_2 S^* + 2 c_3 u^*) \right] \mathrm{d}\boldsymbol{x}\mathrm{d}t.$$

Substituting the sensitivity operator by its right hand side:

$$0 \leqslant \int_Q \left[(\lambda_1, \lambda_2, \lambda_3, \lambda_4, \lambda_5) \, (-\ell S^*, 0, \ell S^*, 0, 0)^T + \ell \, (c_2 S^* + 2 c_3 u^*) \right] \mathrm{d}\boldsymbol{x}\mathrm{d}t.$$

Rearranging:

$$0 \leqslant \int_Q \left[-\ell \lambda_1 S^* + \ell \lambda_3 S^* + \ell \, (c_2 S^* + 2 c_3 u^*) \right] \mathrm{d}\boldsymbol{x}\mathrm{d}t.$$
$$0 \leqslant \int_Q \ell \left[(-\lambda_1 + \lambda_3 + c_2) \, S^* + 2 c_3 u^* \right] \mathrm{d}\boldsymbol{x}\mathrm{d}t.$$

This has to be true for all $\ell \in L^2(Q)$ on the interior of the control set. In particular, if $\ell \geqslant 0$, then the term in the brackets must also be nonnegative:

$$(-\lambda_1 + \lambda_3 + c_2) \, S^* + 2 c_3 u^* \geqslant 0.$$

And if $\ell \leqslant 0$, then:

$$(-\lambda_1 + \lambda_3 + c_2) \, S^* + 2 c_3 u^* \leqslant 0.$$

So we must necessarily have:

$$(-\lambda_1 + \lambda_3 + c_2) \, S^* + 2 c_3 u^* = 0.$$

Which leads to:

$$u^* = \frac{(\lambda_1 - \lambda_3 - c_2) S^*}{2 c_3}.$$

Due to the boundedness of the control $u_{\min} \leqslant u \leqslant u_{\max}$, we obtain the following optimal control characterization:

$$u^* = \min \left(u_{\max}, \max \left(\frac{(\lambda_1 - \lambda_3 - c_2) S^*}{2 c_3}, u_{\min} \right) \right). \tag{3.7}$$

We can see that the characterization depends both on state and adjoint variables. Also, the adjoint system depends on the states and control, and has a final time condition instead of an initial one. Therefore the state and adjoint systems and the optimal control characterization are coupled, and it is not possible to solve them separately. The forward-backward sweep, which is an iterative numerical approach, is used to overcome this difficulty. The state and adjoint systems must be solved, and for that we use numerical methods for PDEs. The whole procedure for the numerical solutions is the topic of the next chapter.

Chapter 4
Numerical solutions

This chapter presents the use of numerical methods for solutions of partial differential equations, in a clear but not very detailed way. More details about the application and implementation of the same numerical methods used here can be found in [8, 51, 52, 76, 96, 101]. Analytical solutions of PDEs are almost always impossible to be explicitly obtained, even though their existence and uniqueness can be proved. As mentioned in the previous chapter, we do not prove existence and uniqueness of solutions of the states and adjoint systems, although it is possible to do it, and there is an extensive literature for that [25, 36, 37, 96].

The finite element method (FEM), in the classical Galerkin approach, searches for approximated solutions of a PDE in its weak (or variational) formulation, as opposed to the classical (or strong) formulation, in which the problems are usually modeled, as model (2.1). In classical formulations, solutions belong to spaces of continuous and differentiable functions, while in weak formulations the solution spaces are less restrictive. The approximated finite element solution is a linear combination of basis functions in a specific space, usually the space of piecewise polynomial functions. The domain of the problem is approximated by a discrete domain, usually consisting of triangles or quadrilaterals in the two dimensional case. The approximated solution search is done by the calculation of the linear combination coefficients, solving algebraic linear or nonlinear systems of equations. The degrees of freedom used in the interpolation polynomials and the discrete domain refinement define the approximated solution precision in comparison to the analytical solution.

Among the advantages in using FEM, we highlight the following: less regularity required in candidate functions to be approximated solutions; ease of adjustment for non rectangular, real life applicable domains; and simple variation of precision by changing the type of polynomial basis used. For more details about the classical method, we recommend as an introduction the books [8, 52]; for quadrilateral elements [51]; and for a more theoretical point of view [25]. Extensions of the method include adding residual terms to the weak formulation in order to improve stability (specially in advective or convective problems), as SUPG (Streamline Upwind Petrov Galerkin) [18] and GLS (Galerkin Least Squares) methods [39]. In another sense, the discontinuous Galerkin method [15] uses approximated solutions which are piecewise discontinuous, possibly improving stability

for continuous problems. We choose to use the standard Galerkin method because it is reliable, easy to implement, and also sufficient to our purposes.

The finite difference method (FDM) approximates derivatives in ordinary or partial differential equations by difference formulas. Usually, these formulas are obtained by local truncated Taylor approximations, with errors associated to the considered step size. In this way, a continuous problem is transformed into a discrete one, which is a linear or nonlinear algebraic system. Among many possible difference formulas, we chose the backward or implicit Euler method which uses formulas based on a simple linear approximation. Its main advantage is that of being an unconditionally stable method, that is, it is stable for any considered time step. This aspect is important because the class of problems we are interested in solving is stiff. There is no consensus in the definition of a stiff problem, but its classification could involve the steepness of the variation of the solution in function of time; absolute stability region; periodicity; difference between the magnitude of associated eigenvalues [19, 115]. In general, a stiff problem requires a tiny time step to be used in conditionally stable methods, such as the widely used Runge-Kutta methods. In our numerical solutions, the implicit Euler method is enough to correct oscillations that could arise in the time evolution. Also, the implicit Euler method is simple to be used, because it is linear and considers only one time step per iteration. For more details about finite difference methods in general we recommend the introductory books [20, 26], and for a more complete approach [59].

Both in the finite element and finite difference methods, the obtained algebraic systems are computationally large, and with particular sparsity structures, therefore they must be solved by appropriate methods which take advantage of these structures. As examples of direct methods, we cite the LU and Cholesky factorizations which can be implemented for band matrices, the latter one for symmetric positive definite matrices. As examples of iterative methods, we cite the conjugate gradients method, also for symmetric positive definite matrices, in which particular preconditioners can be used in order to accelerate convergence and improve stability. Variants of this method are useful for general matrices, such as the biconjugate conjugate gradients and conjugate gradients squared methods [10, 43, 117].

In the following, we present the numerical methods applied to system (2.1) we wish to solve, at first without considering the optimal control. The procedure for obtaining a numerical solution for the adjoint system is completely analogous as the state, so we omit the details but indicate how it should be done. We then show how the forward-backward sweep is used to solve the optimality system. Finally, we present a numerical error and convergence analyses, comparing the numerical results to a predefined known analytical solution. These analyses show that the numerical method scheme converges to an approximated solution, and give a estimate for the convergence order. A theoretical

proof for this convergence can be made, but falls beyond the scope of our work. Results for similar problems can be found in [25, 51, 59]. The numerical method implementation is done in Fortran 90 in Linux, using sparse compact storage for matrices. This choice provides fast code execution, necessary due to the high number of computations involved.

4.1 Weak formulation

As already mentioned, we apply the finite element method to the weak form of the problem we wish to approximate. We are now going to find the weak form of the PDE system (2.1).

For simplicity in notation, we write, for any functions f, g and considering Lebesgue integrals:

$$(f, g) = \int_\Omega fg \, \mathrm{d}\boldsymbol{x},$$
$$(\nabla f, \nabla g) = \int_\Omega \nabla f \cdot \nabla g \, \mathrm{d}\boldsymbol{x}.$$

Recalling model (2.1), we rewrite it here to facilitate the analysis:

$$\begin{cases} \dfrac{\partial S}{\partial t} - \nabla \cdot (\alpha \nabla S) = -\beta S I_v - \beta_d S I - uS, \\ \dfrac{\partial I}{\partial t} - \nabla \cdot (\alpha_I \nabla I) = \beta S I_v + \beta_d S I - \delta I, \\ \dfrac{\partial R}{\partial t} - \nabla \cdot (\alpha \nabla R) = uS + \delta I, \\ \dfrac{\partial S_v}{\partial t} - \nabla \cdot (\alpha_v \nabla S_v) = -\beta_v S_v I + r_v \left(S_v + I_v\right)\left(1 - (S_v + I_v)/\kappa_v\right), \\ \dfrac{\partial I_v}{\partial t} - \nabla \cdot (\alpha_v \nabla I_v) = \beta_v S_v I - \mu_v I_v, \ \text{in } Q, \\ S(\boldsymbol{x}, 0) = S_0, \ I(\boldsymbol{x}, 0) = I_0, \ R(\boldsymbol{x}, 0) = R_0, \ S_v(\boldsymbol{x}, 0) = S_{v0}, \ I_v(\boldsymbol{x}, 0) = I_{v0}, \ \text{in } \Omega, \\ \dfrac{\partial S}{\partial \boldsymbol{n}} = 0, \ \dfrac{\partial I}{\partial \boldsymbol{n}} = 0, \ \dfrac{\partial R}{\partial \boldsymbol{n}} = 0, \ \dfrac{\partial S_v}{\partial \boldsymbol{n}} = 0, \ \dfrac{\partial I_v}{\partial \boldsymbol{n}} = 0, \ \text{in } \partial\Omega \times (0, T). \end{cases} \tag{2.1}$$

The Neumann boundary conditions in (2.1) are called natural conditions in the finite element context. This name comes from the fact that these type of conditions must not be imposed in the search solution space, but arise naturally in the manipulation of the weak formulation. Robin conditions are also called natural, for the same reason. On the other hand, Dirichlet conditions must be imposed directly in the search solution space, and does not appear in the weak formulation. Due of this reason they are called essential conditions.

The process of obtaining the weak form associated to (2.1) consists in multiplying the state equations, for S, I, R, S_v, I_v, by test functions $v \in H^1(\Omega)$ and integrating

them over Ω. Doing this procedure we obtain:

$$\begin{cases} \left(\frac{\partial S}{\partial t}, v\right) - \left(\nabla \cdot \left(\alpha \nabla S\right), v\right) = -\left(\beta S I_v, v\right) - \left(\beta_d S I, v\right) - \left(uS, v\right), \\ \left(\frac{\partial I}{\partial t}, v\right) - \left(\nabla \cdot \left(\alpha_I \nabla I\right), v\right) = \left(\beta S I_v, v\right) + \left(\beta_d S I, v\right) - \left(\delta I, v\right), \\ \left(\frac{\partial R}{\partial t}, v\right) - \left(\nabla \cdot \left(\alpha \nabla R\right), v\right) = \left(uS, v\right) + \left(\delta I, v\right), \\ \left(\frac{\partial S_v}{\partial t}, v\right) - \left(\nabla \cdot \left(\alpha_v \nabla S_v\right), v\right) = -\left(\beta_v S_v I, v\right) + \left(r_v \left(S_v + I_v\right)\left(1 - \left(S_v + I_v\right)/\kappa_v\right), v\right), \\ \left(\frac{\partial I_v}{\partial t}, v\right) - \left(\nabla \cdot \left(\alpha_v \nabla I_v\right), v\right) = \left(\beta_v S_v I, v\right) - \left(\mu_v I_v, v\right). \end{cases}$$

We observe that all parameters are inside the integrals, because they may depend on space variables. If we consider constant parameters, we can simply take them out of the integrals. Using integration by parts (Green's first identity), the diffusive term in the first equation becomes:

$$-\left(\nabla \cdot \left(\alpha \nabla S\right), v\right) = \left(\alpha \nabla S, \nabla v\right) - \oint_{\partial\Omega} \alpha \frac{\partial S}{\partial \boldsymbol{n}} v \, \mathrm{d}S,$$

where $\boldsymbol{n}$ is the unit normal vector exterior to $\partial\Omega$. Due to the natural boundary conditions the normal derivative is null, and so is the line integral. Thus:

$$-\left(\nabla \cdot \left(\alpha \nabla S\right), v\right) = \left(\alpha \nabla S, \nabla v\right).$$

Due to the natural boundary conditions, there is no need to modify anything else in the implementation of the method, besides the equivalence above. Analogous expressions hold for the other equations. Substituting these results, we obtain the weak form of problem (2.1): Find S, I, R, S_v, and I_v belonging to $\mathcal{V} = L^2((0,T); H^1(\Omega))$ and solutions of:

$$\begin{cases} \left(\frac{\partial S}{\partial t}, v\right) + \left(\alpha \nabla S, \nabla v\right) = -\left(\beta S I_v, v\right) - \left(\beta_d S I, v\right) - \left(uS, v\right), \\ \left(\frac{\partial I}{\partial t}, v\right) + \left(\alpha_I \nabla I, \nabla v\right) = \left(\beta S I_v, v\right) + \left(\beta_d S I, v\right) - \left(\delta I, v\right), \\ \left(\frac{\partial R}{\partial t}, v\right) + \left(\alpha \nabla R, \nabla v\right) = \left(uS, v\right) + \left(\delta I, v\right), \\ \left(\frac{\partial S_v}{\partial t}, v\right) + \left(\alpha_v \nabla S_v, \nabla v\right) = -\left(\beta_v S_v I, v\right) + \left(r_v \left(S_v + I_v\right)\left(1 - \left(S_v + I_v\right)/\kappa_v\right), v\right), \\ \left(\frac{\partial I_v}{\partial t}, v\right) + \left(\alpha_v \nabla I_v, \nabla v\right) = \left(\beta_v S_v I, v\right) - \left(\mu_v I_v, v\right). \end{cases} \tag{4.1}$$

This way $\mathcal{V} = L^2((0,T); H^1(\Omega))$ is called the set of admissible functions and $H^1(\Omega)$ the set of test functions. We now look for an approximated solution of this problem by the Galerkin method.

4.2 Galerkin method

The Galerkin method consists in the search for approximated solutions, called Galerkin solutions, in a finite dimensional subspace $\mathcal{V}_N \subset \mathcal{V}$. By reducing the problem to a finite dimensional space we can numerically calculate solutions S_N, I_N, R_N, S_{vN} I_{vN} as linear combinations of vectors that form a basis for $\mathcal{V}_N$. Assuming that Galerkin solutions admit separation of space and time variables, we consider the search space $\mathcal{V}_N = \mathcal{V}_h(\Omega_h) \times \mathcal{V}_h(0,T)$, where $\mathcal{V}_h(\Omega_h)$ is a finite dimensional subspace of $H^1(\Omega_h)$, $\mathcal{V}_h(0,T)$ is a finite dimensional subspace of $L^2(0,T)$, and Ω_h is a discrete partition that approximates Ω.

Considering a generic basis $\mathcal{B} = \{\varphi_1(\boldsymbol{x}), \ldots, \varphi_N(\boldsymbol{x})\}$ for $\mathcal{V}_h(\Omega_h)$ and using separation of variables, the Galerkin solutions are given by:

$$\begin{aligned}
S(\boldsymbol{x},t) \approx S_N(\boldsymbol{x},t) &= \sum_{j=1}^{N} s_j(t)\varphi_j(\boldsymbol{x}),\\
I(\boldsymbol{x},t) \approx I_N(\boldsymbol{x},t) &= \sum_{j=1}^{N} i_j(t)\varphi_j(\boldsymbol{x}),\\
R(\boldsymbol{x},t) \approx R_N(\boldsymbol{x},t) &= \sum_{j=1}^{N} r_j(t)\varphi_j(\boldsymbol{x}),\\
S_v(\boldsymbol{x},t) \approx S_{vN}(\boldsymbol{x},t) &= \sum_{j=1}^{N} s_{vj}(t)\varphi_j(\boldsymbol{x}),\\
I_v(\boldsymbol{x},t) \approx I_{vN}(\boldsymbol{x},t) &= \sum_{j=1}^{N} i_{vj}(t)\varphi_j(\boldsymbol{x}).
\end{aligned} \tag{4.2}$$

These approximations are linear combinations of elements from $\mathcal{B}$ with time-

dependent coefficients, to be later determined. Substituting (4.2) in (4.1) and rearranging:

$$
\begin{cases}
\displaystyle\sum_{j=1}^{N} \frac{\mathrm{d}s_j}{\mathrm{d}t}\,(\varphi_j, v) + \sum_{j=1}^{N} s_j \Big\{ (\alpha\nabla\varphi_j, \nabla v) + \sum_{k=1}^{N} i_{vk}\,(\beta\varphi_j\varphi_k, v) + \sum_{k=1}^{N} i_k\,(\beta_d\varphi_j\varphi_k, v) \\
\qquad\qquad + (u(\boldsymbol{x},t)\varphi_j, v) \Big\} = 0, \\
\displaystyle\sum_{j=1}^{N} \frac{\mathrm{d}i_j}{\mathrm{d}t}\,(\varphi_j, v) + \sum_{j=1}^{N} i_j \Big\{ (\alpha_I\nabla\varphi_j, \nabla v) - \sum_{k=1}^{N} s_k\varphi_k\,(\beta_d\varphi_j, v) + (\delta\varphi_j, v) \Big\} \\
\qquad\qquad = \displaystyle\sum_{k=1}^{N} s_k \sum_{\ell=1}^{N} i_{v\ell}\,(\beta\varphi_k\varphi_\ell, v)\,, \\
\displaystyle\sum_{j=1}^{N} \frac{\mathrm{d}r_j}{\mathrm{d}t}\,(\varphi_j, v) + \sum_{j=1}^{N} r_j \Big\{ (\alpha\nabla\varphi_j, \nabla v) \Big\} = \sum_{k=1}^{N} s_k\,(u(\boldsymbol{x},t)\varphi_k, v) + \sum_{k=1}^{N} i_k\,(\delta\varphi_k, v)\,, \\
\displaystyle\sum_{j=1}^{N} \frac{\mathrm{d}s_{vj}}{\mathrm{d}t}\,(\varphi_j, v) + \sum_{j=1}^{N} s_{vj} \Big\{ (\alpha_v\nabla\varphi_j, \nabla v) + \sum_{k=1}^{N} i_k\,(\beta_v\varphi_j\varphi_k, v) \Big\} \\
\quad = \left(r_v \left(\displaystyle\sum_{j=1}^{N} s_{vj}\varphi_j + \sum_{k=1}^{N} i_{vk}\varphi_k \right) \left(1 - \left(\sum_{j=1}^{N} s_{vj}\varphi_j + \sum_{k=1}^{N} i_{vk}\varphi_k \right) / \kappa_v \right), v \right), \\
\displaystyle\sum_{j=1}^{N} \frac{\mathrm{d}i_{vk}}{\mathrm{d}t}\,(\varphi_j, v) + \sum_{j=1}^{N} i_{vj} \Big\{ (\alpha_v\nabla\varphi_j, \nabla v) + (\mu_v\varphi_j, v) \Big\} = \sum_{k=1}^{N} s_{vk} \sum_{\ell=1}^{N} i_\ell\,(\beta_v\varphi_k\varphi_\ell, v)\,.
\end{cases}
$$

The control variable remains with usual notation $u(\boldsymbol{x}, t)$, because it is not approximated by a Galerkin solution. In order to obtain a characterization of the Galerkin solution, we need to substitute the test functions v by a linear combination of vectors from basis $\mathcal{B}$, such as $v = \displaystyle\sum_{i=1}^{N} b_i\varphi_i$, for constants b_i, $i = 1, \ldots, N$. After substituting, in the resulting system we find that it is enough to consider each φ_i, $i = 1, \ldots, N$ one at a time

in place of v. This way we obtain the following equations, for $i = 1, \ldots, N$:

$$\begin{cases} \displaystyle\sum_{j=1}^{N} \frac{\mathrm{d}s_j}{\mathrm{d}t}\,(\varphi_j, \varphi_i) + \sum_{j=1}^{N} s_j \Bigg\{ (\alpha \nabla\varphi_j, \nabla\varphi_i) + \sum_{k=1}^{N} i_{vk}\,(\beta\varphi_j\varphi_k, \varphi_i) + \sum_{k=1}^{N} i_k\,(\beta_d\varphi_j\varphi_k, \varphi_i) \\ \qquad\qquad + (u(\boldsymbol{x},t)\varphi_j, \varphi_i) \Bigg\} = 0, \\ \displaystyle\sum_{j=1}^{N} \frac{\mathrm{d}i_j}{\mathrm{d}t}\,(\varphi_j, \varphi_i) + \sum_{j=1}^{N} i_j \Bigg\{ (\alpha_I \nabla\varphi_j, \nabla\varphi_i) - \sum_{k=1}^{N} s_k\varphi_k\,(\beta_d\varphi_j, \varphi_i) + (\delta\varphi_j, \varphi_i) \Bigg\} \\ \qquad\qquad = \displaystyle\sum_{k=1}^{N} s_k \sum_{\ell=1}^{N} i_{v\ell}\,(\beta\varphi_k\varphi_\ell, \varphi_i)\,, \\ \displaystyle\sum_{j=1}^{N} \frac{\mathrm{d}r_j}{\mathrm{d}t}\,(\varphi_j, \varphi_i) + \sum_{j=1}^{N} r_j \Bigg\{ (\alpha\nabla\varphi_j, \nabla\varphi_i) \Bigg\} = \sum_{k=1}^{N} s_k\,(u(\boldsymbol{x},t)\varphi_k, \varphi_i) + \sum_{k=1}^{N} i_k\,(\delta\varphi_k, \varphi_i)\,, \\ \displaystyle\sum_{j=1}^{N} \frac{\mathrm{d}s_{vj}}{\mathrm{d}t}\,(\varphi_j, \varphi_i) + \sum_{j=1}^{N} s_{vj} \Bigg\{ (\alpha_v \nabla\varphi_j, \nabla\varphi_i) + \sum_{k=1}^{N} i_k\,(\beta_v\varphi_j\varphi_k, \varphi_i) \Bigg\} \\ \quad = \left(r_v \left(\displaystyle\sum_{j=1}^{N} s_{vj}\varphi_j + \sum_{k=1}^{N} i_{vk}\varphi_k \right) \left(1 - \left(\sum_{j=1}^{N} s_{vj}\varphi_j + \sum_{k=1}^{N} i_{vk}\varphi_k \right) / \kappa_v \right), \varphi_i \right), \\ \displaystyle\sum_{j=1}^{N} \frac{\mathrm{d}i_{vk}}{\mathrm{d}t}\,(\varphi_j, \varphi_i) + \sum_{j=1}^{N} i_{vj} \Bigg\{ (\alpha_v \nabla\varphi_j, \nabla\varphi_i) + (\mu_v\varphi_j, \varphi_i) \Bigg\} = \sum_{k=1}^{N} s_{vk} \sum_{\ell=1}^{N} i_\ell\,(\beta_v\varphi_k\varphi_\ell, \varphi_i)\,. \end{cases} \tag{4.3}$$

As we know all functions φ_j, φ_i, $i, j = 1, \ldots, N$, from basis $\mathcal{B}$, we know how to calculate all integrals appearing in (4.3). Thus, equations (4.3) consist in a system of ordinary differential equations (ODEs) on time variable t, or precisely, an initial value problem (IVP). Initial conditions are given by Galerkin solutions applied in the initial conditions of system (2.1):

$$\begin{aligned} S_0(\boldsymbol{x}) \approx S_N(\boldsymbol{x}, 0) &= \sum_{j=1}^{N} s_j(0)\varphi_j(\boldsymbol{x}), \\ I_0(\boldsymbol{x}) \approx I_N(\boldsymbol{x}, 0) &= \sum_{j=1}^{N} i_j(0)\varphi_j(\boldsymbol{x}), \\ R_0(\boldsymbol{x}) \approx R_N(\boldsymbol{x}, 0) &= \sum_{j=1}^{N} r_j(0)\varphi_j(\boldsymbol{x}), \\ S_{v0}(\boldsymbol{x}) \approx S_{vN}(\boldsymbol{x}, 0) &= \sum_{j=1}^{N} s_{vj}(0)\varphi_j(\boldsymbol{x}), \\ I_{v0}(\boldsymbol{x}) \approx I_{vN}(\boldsymbol{x}, 0) &= \sum_{j=1}^{N} i_{vj}(0)\varphi_j(\boldsymbol{x}). \end{aligned} \tag{4.4}$$

4.3 Backward Euler method

In order to obtain a numerical solution of the IVP (4.3) we use the backward (or implicit) Euler method. Dividing the time interval $(0, T)$ in n_t subintervals with regular size Δt, in the partition $\Pi_t : 0 = t_0 < t_1 < \ldots < t_{n_t} = T$, the method uses the following difference formula:

$$\frac{du_j^{n+1}}{dt} = \frac{u_j^{n+1} - u_j^n}{\Delta t} + \mathcal{O}(\Delta t), \tag{4.5}$$

for $n = 1, \ldots, n_t$ and a given j. The index n is related to time and j to space, so that u_j^{n+1} represents the j-th coefficient of a Galerkin solution at time t_{n+1}. The term $\mathcal{O}(\Delta t)$ means that the formula has an error of order Δt. Substituting these formulas for each derivative in (4.3), we obtain for $i = 1, \ldots, N$ and $n = 0, \ldots, n_t - 1$:

$$\begin{cases}
\displaystyle\sum_{j=1}^{N} s_j^{n+1} \Bigg\{ (\varphi_j, \varphi_i) + \Delta t \left(\alpha \nabla \varphi_j, \nabla \varphi_i\right) + \sum_{k=1}^{N} i_{v_k}^{n+1} \Delta t \left(\beta \varphi_j \varphi_k, \varphi_i\right) \\
\qquad + \displaystyle\sum_{k=1}^{N} i_k^{n+1} \Delta t \left(\beta_d \varphi_j \varphi_k, \varphi_i\right) + \Delta t \left(u(\boldsymbol{x}, t_{n+1}) \varphi_j, \varphi_i\right) \Bigg\} = \displaystyle\sum_{j=1}^{N} s_j^n \left(\varphi_j, \varphi_i\right), \\
\displaystyle\sum_{j=1}^{N} i_j^{n+1} \Bigg\{ (\varphi_j, \varphi_i) + \Delta t \left(\alpha_I \nabla \varphi_j, \nabla \varphi_i\right) - \sum_{k=1}^{N} s_k^{n+1} \varphi_k \Delta t \left(\beta_d \varphi_j, \varphi_i\right) + \Delta t \left(\delta \varphi_j, \varphi_i\right) \Bigg\} \\
\qquad = \displaystyle\sum_{j=1}^{N} i_j^n \left(\varphi_j, \varphi_i\right) + \sum_{k=1}^{N} s_k^{n+1} \sum_{\ell=1}^{N} i_{v_\ell}^{n+1} \Delta t \left(\beta \varphi_k \varphi_\ell, \varphi_i\right), \\
\displaystyle\sum_{j=1}^{N} r_j^{n+1} \Bigg\{ (\varphi_j, \varphi_i) + \Delta t \left(\alpha \nabla \varphi_j, \nabla \varphi_i\right) \Bigg\} = \sum_{j=1}^{N} r_j^n \left(\varphi_j, \varphi_i\right) + \sum_{k=1}^{N} s_k^{n+1} \Delta t \left(u(\boldsymbol{x}, t_{n+1}) \varphi_k, \varphi_i\right) \\
\qquad + \displaystyle\sum_{k=1}^{N} i_k^{n+1} \Delta t \left(\delta \varphi_k, \varphi_i\right), \\
\displaystyle\sum_{j=1}^{N} s_{v_j}^{n+1} \Bigg\{ (\varphi_j, \varphi_i) + \Delta t \left(\alpha_v \nabla \varphi_j, \nabla \varphi_i\right) + \sum_{k=1}^{N} i_k^{n+1} \Delta t \left(\beta_v \varphi_j \varphi_k, \varphi_i\right) \Bigg\} \\
\qquad = \displaystyle\sum_{j=1}^{N} s_{v_j}^n \left(\varphi_j, \varphi_i\right) + \Delta t \Bigg(r_v \left(\sum_{j=1}^{N} s_{v_j}^{n+1} \varphi_j + \sum_{k=1}^{N} i_{v_k}^{n+1} \varphi_k \right) \\
\qquad\qquad \left(1 - \left(\displaystyle\sum_{j=1}^{N} s_{v_j}^{n+1} \varphi_j + \sum_{k=1}^{N} i_{v_k}^{n+1} \varphi_k \right) / \kappa_v \right), \varphi_i \Bigg), \\
\displaystyle\sum_{j=1}^{N} i_{v_j}^{n+1} \Bigg\{ (\varphi_j, \varphi_i) + \Delta t \left(\alpha_v \nabla \varphi_j, \nabla \varphi_i\right) + \Delta t \left(\mu_v \varphi_j, \varphi_i\right) \Bigg\} = \sum_{j=1}^{N} i_{v_j}^n \left(\varphi_j, \varphi_i\right) \\
\qquad + \displaystyle\sum_{k=1}^{N} s_{v_k}^{n+1} \sum_{\ell=1}^{N} i_\ell^{n+1} \Delta t \left(\beta_v \varphi_k \varphi_\ell, \varphi_i\right).
\end{cases} \tag{4.6}$$

The notation $u(\boldsymbol{x}, t_{n+1})$ denotes that the control variable must be calculated at time t_{n+1}.

For simplicity we can write equations (4.6) in matrix form:

$$\begin{cases} (\mathbf{A}_s + \mathbf{B}_s)\, \boldsymbol{s}^{n+1} = (\mathbf{C}_s + \mathbf{D}_s)\, \boldsymbol{s}^n + \boldsymbol{f}_s, \\ (\mathbf{A}_i + \mathbf{B}_i)\, \boldsymbol{i}^{n+1} = (\mathbf{C}_i + \mathbf{D}_i)\, \boldsymbol{i}^n + \boldsymbol{f}_i, \\ (\mathbf{A}_r + \mathbf{B}_r)\, \boldsymbol{r}^{n+1} = (\mathbf{C}_r + \mathbf{D}_r)\, \boldsymbol{r}^n + \boldsymbol{f}_r, \\ (\mathbf{A}_{s_v} + \mathbf{B}_{s_v})\, \boldsymbol{s}_v^{n+1} = (\mathbf{C}_{s_v} + \mathbf{D}_{s_v})\, \boldsymbol{s}_v^n + \boldsymbol{f}_{s_v}, \\ (\mathbf{A}_{i_v} + \mathbf{B}_{i_v})\, \boldsymbol{i}_v^{n+1} = (\mathbf{C}_{i_v} + \mathbf{D}_{i_v})\, \boldsymbol{i}_v^n + \boldsymbol{f}_{i_v}. \end{cases} \tag{4.7}$$

Where $\mathbf{A}_s$, $\mathbf{A}_i$, $\mathbf{A}_r$, $\mathbf{A}_{s_v}$, $\mathbf{A}_{i_v}$, $\mathbf{C}_s$, $\mathbf{C}_i$, $\mathbf{C}_r$, $\mathbf{C}_{s_v}$, and $\mathbf{C}_{i_v}$ contain the linear terms in each equation in (4.6); $\mathbf{B}_s$, $\mathbf{B}_i$, $\mathbf{B}_r$, $\mathbf{B}_{s_v}$, $\mathbf{B}_{i_v}$, $\mathbf{D}_s$, $\mathbf{D}_i$, $\mathbf{D}_r$, $\mathbf{D}_{s_v}$, $\mathbf{D}_{i_v}$, $\mathbf{f}_s$, $\mathbf{f}_i$, $\mathbf{f}_r$, $\mathbf{f}_{s_v}$, and $\mathbf{f}_{i_v}$ the non linear terms (depending on the variables); and $\boldsymbol{s}^n = [s_j^n]$, $\boldsymbol{i}^n = [i_j^n]$, $\boldsymbol{r}^n = [r_j^n]$, $\boldsymbol{s}_v^n = [s_{v_j}^n]$, and $\boldsymbol{i}_v^n = [i_{v_j}^n]$ are the solution vectors for $j = 1, , \ldots, N$ and $n = 1, \ldots, n_t - 1$. The non linear terms depend on the solutions both at time n and $n+1$: $(\boldsymbol{s}^n, \boldsymbol{i}^n, \boldsymbol{r}^n, \boldsymbol{s}_v^n, \boldsymbol{i}_v^n)$ and $\left(\boldsymbol{s}^{n+1}, \boldsymbol{i}^{n+1}, \boldsymbol{r}^{n+1}, \boldsymbol{s}_v^{n+1}, \boldsymbol{i}_v^{n+1}\right)$. At each time step we must solve five matrix equations in order to obtain the solutions, willing to ultimately find solutions at the final step size $n = n_t$, $(\boldsymbol{s}^{n_t}, \boldsymbol{i}^{n_t}, \boldsymbol{r}^{n_t}, \boldsymbol{s}_v^{n_t}, \boldsymbol{i}_v^{n_t})$. Starting from initial conditions for $n = 0$, we use known values at time n to find solutions at time $n+1$, and so on successively. However, as the system is nonlinear, at a given time n it is not possible to obtain all values in the non linear matrix coefficients, because some of them depend on $n+1$. We thus need a method that can deal with non linearities.

4.4 Predictor-corrector linearization method

The matrix equations in (4.7) are coupled due to the nonlinearities in system (2.1). To overcome this issue, we use a predictor-corrector method consisting of successive linearizations, due to Douglas and Dupont [31, 32] in problems similar to ours.

For a time step n, the method uses predictors for solutions at time $n+1$ and iterates until a corrector is accepted, then it moves to the next time step. It starts using as predictors solutions at time step n:

$$\left(\boldsymbol{s}^{n+1}, \boldsymbol{i}^{n+1}, \boldsymbol{r}^{n+1}, \boldsymbol{s}_v^{n+1}, \boldsymbol{i}_v^{n+1}\right) \approx (\boldsymbol{s}^\star, \boldsymbol{i}^\star, \boldsymbol{r}^\star, \boldsymbol{s}_v^\star, \boldsymbol{i}_v^\star) = (\boldsymbol{s}^n, \boldsymbol{i}^n, \boldsymbol{r}^n, \boldsymbol{s}_v^n, \boldsymbol{i}_v^n)\,.$$

Substituting $(\boldsymbol{s}^\star, \boldsymbol{i}^\star, \boldsymbol{r}^\star, \boldsymbol{s}_v^\star, \boldsymbol{i}_v^\star)$ in the matrix equations in (4.7), they become linear. Solving this linearized system, the solutions give the correctors $(\boldsymbol{s}^{\star\star}, \boldsymbol{i}^{\star\star}, \boldsymbol{r}^{\star\star}, \boldsymbol{s}_v^{\star\star}, \boldsymbol{i}_v^{\star\star})$. These solutions are now the new predictors for solutions at time step $n+1$:

$$\left(\boldsymbol{s}^{n+1}, \boldsymbol{i}^{n+1}, \boldsymbol{r}^{n+1}, \boldsymbol{s}_v^{n+1}, \boldsymbol{i}_v^{n+1}\right) \approx (\boldsymbol{s}^{\star\star}, \boldsymbol{i}^{\star\star}, \boldsymbol{r}^{\star\star}, \boldsymbol{s}_v^{\star\star}, \boldsymbol{i}_v^{\star\star})\,.$$

Then the method iterates again and new solutions are calculated. The process is repeated until the relative errors between two successive iterations:

$$\frac{\left\|(\boldsymbol{s}^{\star\star}, \boldsymbol{i}^{\star\star}, \boldsymbol{r}^{\star\star}, \boldsymbol{s}_v^{\star\star}, \boldsymbol{i}_v^{\star\star}) - (\boldsymbol{s}^\star, \boldsymbol{i}^\star, \boldsymbol{r}^\star, \boldsymbol{s}_v^\star, \boldsymbol{i}_v^\star)\right\|}{\left\|(\boldsymbol{s}^{\star\star}, \boldsymbol{i}^{\star\star}, \boldsymbol{r}^{\star\star}, \boldsymbol{s}_v^{\star\star}, \boldsymbol{i}_v^{\star\star})\right\|}$$

become smaller than a certain predefined tolerance, for a given norm $\|\cdot\|$. In our simulations we use a tolerance of 10^{-6} with the max (infinite) norm, and the method converges in up to 4 iterations. Once the tolerance is reached, the latest corrector is accepted at the solution at $n+1$, and the linearization method starts again with predictors for time step $n+2$. The method proceeds until the final step size, n_t.

4.5 Finite element basis

In the finite element context, the basis $\mathcal{V}_h(\Omega_h)$ consists of piecewise polynomial functions. The discretized domain Ω_h usually consists of triangles or quadrilaterals called *elements*, that disjointly cover the entire domain Ω. The piecewise polynomials are constructed in one element from the partition Ω_h with nodal values and are null outside this element. In this way the integrals in (4.6) are simply calculated, because they are all polynomial multiplications, and thus have a small support. Also, because of the local support, these functions lead to sparse matrices in system (4.7), simplifying their resolution. Furthermore, using informations about the discrete mesh and with appropriate variable transformations, the integrals are systematically calculated, transforming each element in Ω_h to a single reference element $\hat{E}$ and using Gaussian quadratures [20, 26], which exactly integrates polynomials depending on the number of quadrature points used. The use of transformations also allows the use of unstructured meshes in an easy way, which are widely used in real life applications.

Possible spaces to be used are $\mathcal{P}_r$, consisting of the space with polynomials with degree less than or equal to r. Another possibility is the space $\mathcal{Q}_r$, which is defined as the tensorial product of $\mathcal{P}_r$ with itself, that is: $\mathcal{Q}_r = \mathcal{P}_r \otimes \mathcal{P}_r$ [51]. In $\mathbb{R}^2$, this space consists in polynomials in x and y with sum of exponents less than or equal to r. As examples, we can cite linear elements in $\mathcal{P}_1$ (triangles with 3 nodes), quadratic elements in $\mathcal{P}_2$ (triangles with 6 nodes), bilinear elements in $\mathcal{Q}_1$ (quadrilaterals with 4 nodes), biquadratics in $\mathcal{Q}_2$ (quadrilaterals with 9 nodes), and bicubics in $\mathcal{Q}_3$ (quadrilaterals with 16 nodes). These reference elements are schematically shown in Figure 3.

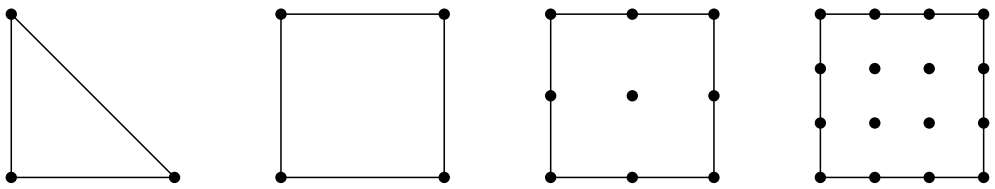

(a) Linear (b) Bilinear (c) Biquadratic (d) Bicubic

Figure 3 – Examples of reference elements used in the finite element method.

We implemented the method for $\mathcal{P}_1$, but it is readily adaptable for $\mathcal{P}_2$, $\mathcal{Q}_1$, $\mathcal{Q}_2$,

and so on. We use isoparametric transformations, which can transform general quadrilaterals or triangles, even curved ones. These are more general than affine transformations, which can only transform triangles and parallelograms. Results on approximation capabilities and errors can be found in [6]. In section 4.9 we present a numerical error and convergence analysis for the finite element and finite difference methods.

Let p_i, $i = 1, \ldots, nen$ denote the polynomial basis functions, nen the number of element nodes exemplified in the previous paragraph, $\boldsymbol{x}$ the real coordinates, and $\boldsymbol{\xi}$ the coordinates in the reference element $\hat{E}$. Also, let $\boldsymbol{x}_i$, $i = 1, \ldots, nen$ denote the nodes in any element E in the domain discretization Ω_h. Then the isoparametric transformation from $\hat{E}$ to $\mathbb{R}^2$ is given by:

$$\boldsymbol{x}(\boldsymbol{\xi}) = \sum_{i=1}^{nen} p_i(\boldsymbol{\xi})\boldsymbol{x}_i. \tag{4.8}$$

Transformation (4.8) relates the real coordinates $\boldsymbol{x}$ in the element E with the coordinates $\boldsymbol{\xi}$ in the reference element $\hat{E}$. There is one transformation (4.8) for each element E, which takes $\boldsymbol{\xi}_j$ in $\hat{E}$ to $\boldsymbol{x}_j$ in E, for $j = 1, \ldots, nen$, where $\boldsymbol{\xi}_j$ are the element nodes as shown in Figure 3, in an arbitrary enumeration, usually counterclockwise. The functions $p_i(\boldsymbol{\xi})$ are such that $p_i(\boldsymbol{\xi}_j) = \delta_{ij}$ (Kronecker delta), for $i, j = 1, \ldots, nen$. These properties facilitates the calculation of the integrals in (4.6). For example, let us see how an integral involving gradients can be calculated, changing variables from $\boldsymbol{x}$ in E to $\boldsymbol{\xi}$ in $\hat{E}$. The gradient of a basis function in $\boldsymbol{x}$ coordinates is:

$$\nabla\varphi(\boldsymbol{x}) = \left(\frac{\partial\varphi}{\partial x_1}, \frac{\partial\varphi}{\partial x_2}\right).$$

Using the chain rule, we can calculate the gradient of $\hat{\varphi}$, the basis function in the reference element:

$$\begin{aligned}
\frac{\partial\hat{\varphi}}{\partial\xi_1} &= \frac{\partial\varphi}{\partial x_1}\frac{\partial x_1}{\partial\xi_1} + \frac{\partial\varphi}{\partial x_2}\frac{\partial x_2}{\partial\xi_1}, \\
\frac{\partial\hat{\varphi}}{\partial\xi_2} &= \frac{\partial\varphi}{\partial x_1}\frac{\partial x_1}{\partial\xi_2} + \frac{\partial\varphi}{\partial x_2}\frac{\partial x_2}{\partial\xi_2}.
\end{aligned}$$

This can be rewritten as:

$$\nabla\hat{\varphi}(\boldsymbol{\xi}) = \begin{pmatrix} \dfrac{\partial x_1}{\partial\xi_1} & \dfrac{\partial x_2}{\partial\xi_1} \\ \dfrac{\partial x_1}{\partial\xi_2} & \dfrac{\partial x_2}{\partial\xi_2} \end{pmatrix} \begin{pmatrix} \dfrac{\partial\varphi}{\partial x_1} \\ \dfrac{\partial\varphi}{\partial x_2} \end{pmatrix} = J^T\nabla\varphi(\boldsymbol{x}),$$

where J is the Jacobian of the isoparametric transformation (4.8), which is easily calculated. Inverting the transpose of the Jacobian matrix gives a relation between the gradients:

$$\nabla\varphi(\boldsymbol{x}) = (J^T)^{-1}\nabla\hat{\varphi}(\boldsymbol{\xi}).$$

This way, an integral involving gradients can be calculated as:

$$\int_E \nabla\varphi_j \cdot \nabla\varphi_i \,\mathrm{d}\boldsymbol{x} = \int_{\hat{E}} \left[(J^T)^{-1}\nabla\hat{\varphi}_j\right] \cdot \left[(J^T)^{-1}\nabla\hat{\varphi}_j\right] \det(J) \,\mathrm{d}\boldsymbol{x}. \tag{4.9}$$

The other integrals from system (4.6) can be calculated in the same way, passing from coordinates $\boldsymbol{x}$ in E to coordinates $\boldsymbol{\xi}$ in $\hat{E}$, for all elements E in Ω_h.

4.6 Solutions of linear systems arising in discretization

For each time step we also have intermediate iterations due to the predictor-corrector method, so that we need to solve a great ammount of linear systems in order to obtain solutions at the final time step, $(\boldsymbol{s}^{n_t}, \boldsymbol{i}^{n_t}, \boldsymbol{r}^{n_t}, \boldsymbol{s}_{\boldsymbol{v}}^{n_t}, \boldsymbol{i}_{\boldsymbol{v}}^{n_t})$. Thus it is important to solve the systems carefully.

As already mentioned, the systems have the property of being sparse. Also, a well known result in finite element theory states that the matrices arising from the method applied to reaction-diffusion problems are symmetric and positive definite [51, 52]. The matrix structure also depends on the kind of finite element mesh being used. If a structured mesh is used, for example, a rectangle divided in regular small triangles or quadrilaterals, the resulting matrices would have a band structure. In this case, it is recommended to use direct methods implemented in a way that takes advantage of the band, such as Cholesky factorization [117]. Real life problems usually have domains that require an unstructured mesh, in which each element is different from the other. The resulting matrices in this case do not have a regular band structure, although the sparsity is the same. Thus, an iterative method should be used, for example the preconditioned conjugate gradients method [10]. In our simulations we use the conjugate gradients method, with diagonal preconditioning suited to a compact sparse storage structure. This structure consists of non zero elements only, and storages the $i, j-$th element together with the i and j indexes. Scalar products, matrix multiplications and other calculations are also implemented according to this structure, eliminating useless computations and speeding up the code execution. Details on these storage structure can be found in [70, 94].

4.7 Adjoint system solutions

In order to find the optimal control characterization, we need to numerically solve the adjoint system. This is done using the same methods as for the state system, and the procedure is analogous, since it is also a nonlinear reaction-diffusion system, with a few adjustments. We will comment the procedure in the following. Writing the adjoint

system (3.6) in equation form:

$$\begin{cases} -\dfrac{\partial \lambda_1}{\partial t} - \nabla \cdot (\alpha \nabla \lambda_1) + (\beta I_v + \beta_s I + u)\,\lambda_1 - (\beta I_v + \beta_s I)\lambda_2 - u\lambda_3 = c_2 u, \\ -\dfrac{\partial \lambda_2}{\partial t} - \nabla \cdot (\alpha_I \nabla \lambda_2) + \beta_s S \lambda_1 + (\delta - \beta_s S)\lambda_2 - \delta \lambda_3 + \beta_v S_v \lambda_4 - \beta_v S_v \lambda_5 = c_1, \\ -\dfrac{\partial \lambda_3}{\partial t} - \nabla \cdot (\alpha \nabla \lambda_3) = 0, \\ -\dfrac{\partial \lambda_4}{\partial t} - \nabla \cdot (\alpha_v \nabla \lambda_4) + \left(\beta_v I - r_v + \dfrac{2r_v}{\kappa_v}(S_v + I_v)\right)\lambda_4 - \beta_v I \lambda_5 = 0, \\ -\dfrac{\partial \lambda_5}{\partial t} - \nabla \cdot (\alpha_v \nabla \lambda_5) + \beta S \lambda_1 - \beta S \lambda_2 + \left(-r_v + \dfrac{2r_v}{\kappa_v}(S_v + I_v)\right)\lambda_4 \\ \qquad\qquad + \mu_v \lambda_5 = 0, \text{ in } Q. \\ \lambda_1(\boldsymbol{x}, T) = 0,\ \lambda_2(\boldsymbol{x}, T) = 0,\ \lambda_3(\boldsymbol{x}, T) = 0,\ \lambda_4(\boldsymbol{x}, T) = 0,\ \lambda_5(\boldsymbol{x}, T) = 0, \text{ in } \Omega. \\ \dfrac{\partial \lambda_1}{\partial \boldsymbol{n}} = 0,\ \dfrac{\partial \lambda_2}{\partial \boldsymbol{n}} = 0,\ \dfrac{\partial \lambda_3}{\partial \boldsymbol{n}} = 0,\ \dfrac{\partial \lambda_4}{\partial \boldsymbol{n}} = 0,\ \dfrac{\partial \lambda_5}{\partial \boldsymbol{n}} = 0, \text{ in } \partial\Omega. \end{cases} \tag{4.10}$$

We can see that the adjoint equations are coupled with the state and control variables. Because of this, it is not possible to obtain independent solutions. In order to deal with this, we use a specific strategy to solve each system separately and then combine the results. For now, we derive numerical solutions for the adjoint system (4.10) considering known values for the states (S, I, R, S_v, I_v) and control u, and solving the system for $(\lambda_1, \lambda_2, \lambda_3, \lambda_4, \lambda_5)$.

In order to apply the finite element method, system (4.10) is transformed to its weak form, as in (4.1). Then we look for Galerkin solutions similar to (4.2), obtaining a final value problem (FVP), due to the transversality (final time) conditions, as opposed to the IVP (4.3). Using a simple change of variables in t, $\tau = T - t$, it is possible to transform this FVP in an IVP. This way, the backward Euler method is readily applicable, resulting in algebraic equations to be solved, as (4.6), or its matrix form (4.7). The predictor-corrector linearization method is then applied, and linear systems must be solved by the same methods as before.

4.8 Optimality system solutions: forward-backward sweep

In Chapter 3 we showed that the optimality system consists of the state and adjoint equations, and the optimal control characterization, all of them coupled. While the state system has initial conditions, the adjoint has final time (transversality) conditions. Thus, it is not possible to solve them simultaneously. We overcome this using the forward-backward sweep, which is an iterative method [46]. As the optimal control problem has a unique solution, it is possible to use an iterative method. Thus, if it converges to one solution, we know that it is the correct one. A detailed explanation of the method for ODEs can be found in [58], but its application is totally analogous for PDEs.

The method starts with an initial guess for u^*, which can be defined as $u^* = 0$ in all $Q = \Omega \times (0, T)$ for convenience. Then, the state system (2.1) is numerically solved forward in time, and the solution is stored for all time and space. Using this obtained state solution, the adjoint system is solved backward in time, and its solution is also stored for all Q. Afterwards, the optimal control u^* is updated as a convex combination (usually the average) between the old control and the characterization (3.7), that we rewrite here for convenience:

$$u^* = \min\left(u_{\max}, \max\left(\frac{(\lambda_1 - \lambda_3 - c_2)S^*}{2c_3}, u_{\min}\right)\right). \tag{3.7}$$

Also, the relative change between successive old and new states and controls is checked, through some norm $\|\cdot\|$. If the relative changes are greater than a predefined tolerance, the procedure is iterated again, until convergence is obtained. The adjoint solutions are also iteratively calculated, but there is no need to consider their norm, because if the states and control converge, the adjoint will converge as well. We use in our simulations the vector 1 norm (sum of linear absolute errors), and a tolerance of 10^{-2}. In this way the method converges in about 10 iterations. The procedure can be summarized in the following algorithm:

1. Define $u^* = 0$ (initial guess).
2. Using u^*, solve state equations (2.1) forward in time.
3. Using state solutions and u^*, solve adjoint equations (4.10) backward in time.
4. Update u^* as the average of u^* and (3.7).
5. Check convergence through relative errors between old and new solutions. If the errors are greater than the tolerance, return to step 2. Otherwise stop, and the current solutions are optimal.

After the optimal solution is obtained, we calculate the value of the total cost $J(u^*)$, using (3.1):

$$J(u^*) = \int_Q (c_1 I^*(\boldsymbol{x}, t) + c_2 u^*(\boldsymbol{x}, t) S^*(\boldsymbol{x}, t) + c_3 u^*(\boldsymbol{x}, t)^2)\, \mathrm{d}\boldsymbol{x}\mathrm{d}t. \tag{4.11}$$

Remembering that $Q = \Omega \times (0, T)$, this integral depends on both space $\boldsymbol{x} \in \Omega$ and time $t \in (0, T)$. It is numerically calculated using quadratures in space, with the same formulas used in the finite element integrals, and using repeated trapezoidal formulas in time, since the time grid is regular. Other quantities of interest can be calculated as integrals, using these same approximations. More of these values will be discussed in Chapter 6.

4.9 Numerical error and convergence analysis

In numerical solutions of partial or ordinary differential equations, a single given solution that approximates the exact solution of the problem may be apparently acceptable, showing good and expected behavior, although incorrect. Thus, it is important to verify the quality of the obtained solutions, usually by the error between the numerical and exact solutions, u_h and $\bar{u}$ respectively, where h is a step size associated to the mesh in which the solutions are being calculated. We can measure the error using a given norm $\|\cdot\|$, so that the absolute error is $\|u_h - \bar{u}\|$. The absolute value for this error often does not represent the quality of the solution, because it depends on the scale of the problem. The relative error $\|u_h - \bar{u}\|/\|\bar{u}\|$ is thus more appropriate. For the results of this section we will use the $\mathcal{O}(h^r)$ notation, meaning that the approximation is of order r, that is, the error has the form Ch^r for a constant C that does not depend on h. We will also consider the following norms:

$$\text{Norm in } L^2(\Omega)\text{: } \|u\|_{L^2} = \sqrt{\iint_\Omega |u|^2 \, \boldsymbol{x}}.$$

$$\text{Gradient norm in } L^2(\Omega)\text{: } \|\nabla u\|_{L^2} = \sqrt{\iint_\Omega |\nabla u|^2 \, \mathrm{d}\boldsymbol{x}}.$$

$$\text{Vector 2 norm: } \|\boldsymbol{u}\|_2 = \sqrt{\sum_{i=1}^{N} h|u_i|^2}.$$

An important result in approximation theory of finite element states that errors in $\mathcal{P}_1$ calculated in the $L^2(\Omega)$ norm are $\mathcal{O}(h^2)$, and in the $L^2(\Omega)$ gradient norm are $\mathcal{O}(h)$, where h is the maximum diameter among all elements in the mesh [6]. The error of the backward Euler method is $\mathcal{O}(\Delta t)$, and can be obtained by truncation error analysis [59].

With these results it is possible to numerically calculate the convergence rate p obtained by the methods. Considering u_1 and u_2 solutions in meshes with step sizes $h = h_1$ and $h = h_2 = h_1/2$, respectively, and $\bar{u}$ the exact solution of the problem, we have, asymptotically:

$$\|u_1 - \bar{u}\| = Ch^p, \quad \|u_2 - \bar{u}\| = C\left(\frac{h}{2}\right)^p.$$

Dividing both errors:

$$\frac{\|u_1 - \bar{u}\|}{\|u_2 - \bar{u}\|} = \frac{Ch^p}{Ch^p} 2^p.$$

Applying logarithm at both sides and rearranging we isolate p:

$$p = \log\left(\frac{\|u_1 - \bar{u}\|}{\|u_2 - \bar{u}\|}\right) \frac{1}{\log 2}. \tag{4.12}$$

If the analytical solution $\bar{u}$ is not available, an analogous procedure can be done, comparing solutions in three different meshes with consecutive refinements, with h_1, $h_2 = h_1/2$ e $h_3 = h_2/2$. Another option is to assume that an approximated solution in a very fine mesh is a sufficiently good approximation to the analytical solution, and use it as $\bar{u}$. In any of the approaches mentioned, the tendency is that as h gets smaller, the numerical rate p gets closer to the theoretical, aside from floating point numerical errors [59], and the numerical solution gets closer to the analytical. Once the convergence of the method is verified, it is enough to consider numerical simulations with a not so refined mesh, because it is known that the results are trustworthy.

In real life problems, as the ones we are interested in solving, the analytical solution is not available. However, we can test the numerical results by imposing a predefined analytical solution and adding a source term to the differential equation, in a way that the predefined solution satisfies the modified equation. In order to do that, it suffices to take a source term corresponding to the differential equation evaluated at the predefined solution. For problem (2.1), imposing known solutions $\bar{S}$, $\bar{I}$, $\bar{R}$, $\bar{S}_v$, and $\bar{I}_v$, we add the following source terms to each of the system's equations:

$$\begin{aligned}
g_S =& \frac{\partial \bar{S}}{\partial t} - \nabla \cdot \left(\alpha \nabla \bar{S}\right) + \beta \bar{S} \bar{I}_v + \beta_d \bar{S} \bar{I} + u \bar{S}, \\
g_I =& \frac{\partial I}{\partial t} - \nabla \cdot \left(\alpha_I \nabla \bar{I}\right) - \beta \bar{S} \bar{I}_v - \beta_d \bar{S} \bar{I} + \delta \bar{I}, \\
g_R =& \frac{\partial \bar{R}}{\partial t} - \nabla \cdot \left(\alpha \nabla \bar{R}\right) - u \bar{S} - \delta \bar{I}, \\
g_{S_v} =& \frac{\partial \bar{S}_v}{\partial t} - \nabla \cdot \left(\alpha_v \nabla \bar{S}_v\right) + \beta_v \bar{S}_v \bar{I} - r_v \left(\bar{S}_v + \bar{I}_v\right) \left(1 - \left(\bar{S}_v + \bar{I}_v\right)/\kappa_v\right), \\
g_{I_v} =& \frac{\partial \bar{I}_v}{\partial t} - \nabla \cdot \left(\alpha_v \nabla \bar{I}_v\right) - \beta_v \bar{S}_v \bar{I} + \mu_v \bar{I}_v.
\end{aligned} \tag{4.13}$$

It is straightforward to see that $\bar{S}$, $\bar{I}$, $\bar{R}$, $\bar{S}_v$, and $\bar{I}_v$ are solutions for the modified system. As we use known $\bar{S}$, $\bar{I}$, $\bar{R}$, $\bar{S}_v$, and $\bar{I}_v$, the derivatives and all terms in the expression above can be directly calculated, except for u. However, we also add source terms similar to (4.13) to the adjoint system (4.10), so that we also have predefined known adjoint solutions. Thus, using the optimal control characterization (3.7), we can calculate $u = u^*$ directly in terms of the known state and adjoint solutions. Approximated solutions for the modified systems can be obtained using the forward-backward sweep, with a procedure completely analogous to the one showed in the previous sections.

In our tests, we used the predefined solutions:

$$\begin{aligned}
\bar{S}(\boldsymbol{x},t) &= \left(\frac{x^3}{3}-x\right)\left(\frac{y^2}{2}-y\right)\cos(\pi t),\\
\bar{I}(\boldsymbol{x},t) &= \left(\frac{x^3}{3}-\frac{x^2}{2}\right)\left(\frac{y^3}{3}-\frac{y^2}{2}\right)\cos(\pi t),\\
\bar{R}(\boldsymbol{x},t) &= \left(\frac{x^3}{3}-x\right)\left(\frac{y^3}{3}-\frac{y^2}{2}\right)\cos(\pi t),\\
\bar{S}_v(\boldsymbol{x},t) &= \left(\frac{x^5}{5}-\frac{x^2}{2}\right)\left(\frac{y^3}{3}-y\right)\cos(\pi t),\\
\bar{I}_v(\boldsymbol{x},t) &= \left(\frac{x^2}{2}-x\right)\left(\frac{y^5}{5}-\frac{y^3}{3}\right)\cos(\pi t).
\end{aligned}$$

And same functions for the adjoint variables, that is: $\left(\bar{\lambda}_1,\bar{\lambda}_2,\bar{\lambda}_3,\bar{\lambda}_4,\bar{\lambda}_5\right)=\left(\bar{S},\bar{I},\bar{R},\bar{S}_v,\bar{I}_v\right)$. These functions satisfy homogeneous Neumann boundary conditions in the test domain $\Omega=(0,1)\times(0,1)$. Initial conditions are set by taking $t=0$. We decided to use these functions because they are simple and well behaved, both in space and time. Visualization of these functions can be seen in Figure 4, for $t=0$, but the spatial shape is the same for any given time t, due to the particular form of the functions. In the following we present the error analysis for the state equations. There is no need to do the analysis for the adjoint equations, since the systems are coupled.

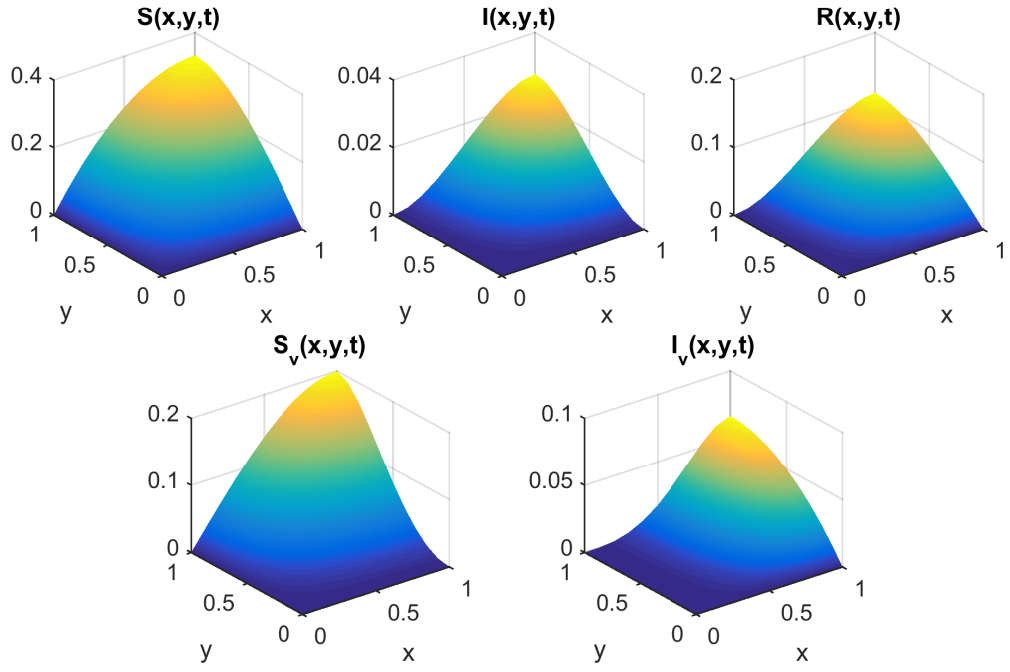

Figure 4 – Spatial plots of the functions considered as exact solutions for the error analysis.

For the error analysis of the finite element method, we considered a final time of $T=0.01$, and $n_t=2^{10}$ time intervals, obtaining a time step of $\Delta t=9.77\times10^{-6}$, a sufficiently small value so that the time discretization would not interfere in the spatial

numerical error. As we are using regular meshes, the number of divisions in x and y directions is the same, denoted by n, and each element maximum diameter denoted by h. We vary the number of divisions n in order to lower the error and find the numerical rate p of the method. The results are presented in Tables 3 and 4, which contains n, absolute errors in L^2 or L^2 gradient norms and convergence rate, respectively. Figure 5 displays plots of the error by h in log $\times$ log scale, with linear regressions for each case. It is possible to see that the errors have the expected rates in all cases: $p \approx 2$ for L^2 norm and $p \approx 1$ for L^2 gradient norm.

Table 3 – Errors and convergence rates of the finite element method in the L^2 norm.

	S		I		R		S_v		I_v	
n	error	rate	error	rate	error	rate	error	rate	error	rate
4	6.0e−3		5.1e−4		2.0e−3		3.8e−3		1.5e−3	
8	1.5e−3	1.99	1.3e−4	1.95	5.2e−4	1.97	9.7e−4	1.95	4.0e−4	1.92
16	3.7e−4	2.01	3.3e−5	1.99	1.3e−4	2.00	2.4e−4	1.99	1.0e−4	1.98
32	9.2e−5	2.02	8.3e−6	2.01	3.2e−5	2.01	6.1e−5	2.01	2.5e−5	2.00
64	2.5e−5	1.89	2.0e−6	2.05	8.0e−6	2.01	1.5e−5	2.06	6.2e−6	2.04

Table 4 – Errors and convergence rates of the finite element method in the L^2 gradient norm.

	S		I		R		S_v		I_v	
n	error	rate	error	rate	error	rate	error	rate	error	rate
4	8.6e−2		7.3e−3		2.9e−2		5.3e−2		2.2e−2	
8	4.3e−2	1.00	3.8e−3	0.96	1.5e−2	0.98	2.7e−2	0.97	1.1e−2	0.94
16	2.1e−2	1.00	1.9e−3	0.99	7.4e−3	0.99	1.4e−2	0.99	5.7e−3	0.98
32	1.1e−2	1.00	9.5e−4	1.00	3.7e−3	1.00	6.9e−3	1.00	2.9e−3	1.00
64	5.8e−3	0.90	4.7e−4	1.00	1.9e−3	0.97	3.4e−3	1.00	1.4e−3	1.00

For the error analysis of the backward Euler method, we considered a final time $T = 1$ and $n = 2^6$ divisions in both x and y directions. We vary the number of time steps n_t in order to refine the time step $h = \Delta t = T/n_t$. We calculated the error using the vector 2 norm, applied to the integral of S, I, R, S_v and I_v over the whole domain. The results are presented in Table 5, which contains $h = \Delta t$, absolute errors in vector 2 norm and convergence rate. In Figure 6 we present error plots by $h = \Delta t$ in log $\times$ log scale, with linear regressions for each case. It is possible to see that the errors have the expected rates $p \approx 1$ in all cases.

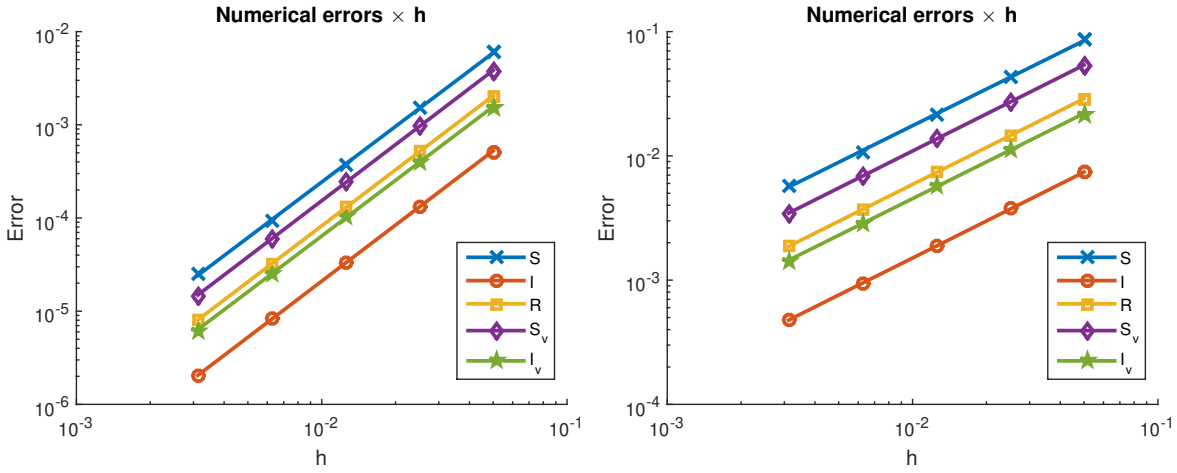

Figure 5 – At left: numerical errors in L^2 norm by element step sizes. At right: numerical errors in L^2 gradient norm by element step sizes. Linear regressions are shown for each case.

Table 5 – Errors and convergence rates of the backward Euler method in the vector 2 norm.

	S		I		R		S_v		I_v	
n	error	rate	error	rate	error	rate	error	rate	error	rate
4	4.5e−2		2.3e−3		1.1e−2		1.8e−2		5.5e−3	
8	2.1e−2	1.12	1.1e−3	1.11	5.2e−3	1.12	8.1e−3	1.13	2.5e−3	1.12
16	1.0e−2	1.06	5.1e−4	1.06	2.5e−3	1.06	3.9e−3	1.07	1.2e−3	1.06
32	4.9e−3	1.03	2.5e−4	1.03	1.2e−3	1.03	1.9e−3	1.03	6.0e−4	1.03
64	2.4e−3	1.02	1.2e−4	1.02	6.0e−4	1.02	9.4e−4	1.02	2.9e−4	1.02
128	1.2e−3	1.02	6.2e−5	1.01	3.0e−4	1.01	4.6e−4	1.02	1.5e−4	1.02
256	5.9e−4	1.02	3.1e−5	1.02	1.5e−4	1.02	2.3e−4	1.02	7.2e−5	1.02
512	2.9e−4	1.04	1.5e−5	1.03	7.2e−5	1.03	1.1e−4	1.04	3.5e−5	1.04
1024	1.4e−4	1.07	7.2e−6	1.05	3.4e−5	1.06	5.2e−5	1.08	1.6e−5	1.09

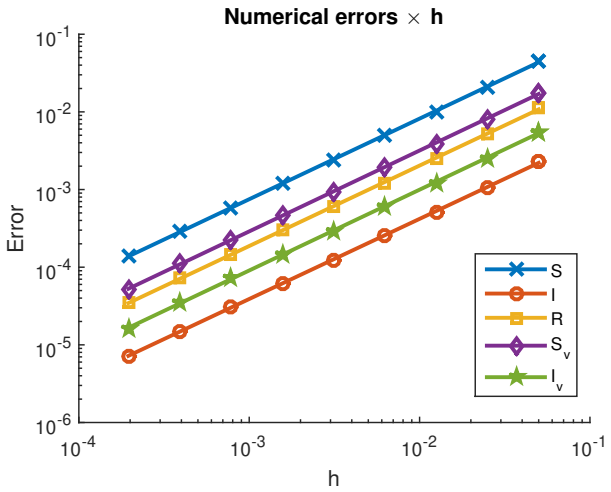

Figure 6 – Numerical errors in vector 2 norm by time step sizes. Linear regressions are shown for each case.

Chapter 5
Parameter estimation

With all tools needed to obtain reliable numerical solutions of model (2.1) and the optimal problem (3.3), we can focus on applying them to a real life problem. In order to do so, we need to find numerical values for the parameters involved in the model. There are some information available in literature, for example for the disease duration and mosquito lifespan [41, 50]. However, some of the parameters, specially transmission rates, could have different values depending on location and climate, since mosquito behavior, biting rates, and other factors are dependent on the weather [80]. For this reason, we wish to connect our model to some real life Zika data in order to get closer to reality.

Unfortunately, it is not easy to find reliable datasets containing the number of infected cases in Brazil. Lots of suspected cases could be unreported or misdiagnosed, specially with vector-borne diseases as dengue, chikungunya and Zika that have similar symptoms and are present in the same seasons. Moreover, Zika virus was completely absent in Brazil before its introduction around 2013. A surveillance protocol was published by the Brazilian Health Ministry in December 2015, in order to identify and confirm Zika suspected infections and microcephaly cases in newborns [75]. Before that, Zika cases were difficult to diagnose and suspected and confirmed cases were not of compulsory notification.

There are some public data available for the notified Zika, dengue, and chikungunya cases in the Brazilian Health Ministry website, but only after 2016, when the surveillance protocol was active. We are interested in simulating scenarios for the beginning of the outbreak, when Zika was introduced in Brazil, back in 2015. The only dataset we were able to find for this time frame was for Rio Grande do Norte State, in northeastern Brazil, one of the first states to have confirmed cases in Brazil [104].

In this chapter, we create a finite element mesh using Matlab (R2015a) to approximate the geographical boundary of Rio Grande do Norte state, and find some estimates for some parameters of model (2.1). Then, we use a parameter estimation method based on nonlinear least squares to connect our model to the dataset. We define a residual between the number of new cases from data and from the model, and minimize its square in terms of a set of parameters. Some tests are also carried out in order to verify the capacity of the proposed method in obtaining reliable results.

5.1 Application to 2015 Zika outbreak in Brazil

Weekly reported cases for the initial 2015 Zika outbreak in Rio Grande do Norte state in Brazil are available from the State Health Office website [104], from 5th to 26th epidemiological weeks of that year, and separated by cities. Most cities have few reported cases, so we decided to consider only the 13 cities with relevant number of cases. We show the number of reported cases by weeks in Table 6, and city locations in the state in Figure 8. There is no available information about confirmed cases and reporting rates, so we assume an under-reporting rate equal to the symptomatic rate of 20% [118]. This way the number of new cases (also called incidence throughout this work) is the reported cases from data divided by 20%. The sum of all reported cases is 4486, which rescaled gives a total of 22430 assumed infections. A schematic bar plot for the rescaled number of cases is shown in Figure 7.

Table 6 – Number of reported Zika cases in Rio Grande do Norte state in 2015.

	Epidemiological week																			
City	7	8	9	10	11	12	13	14	15	16	17	18	19	20	21	22	23	24	25	26
Apodi	0	0	0	0	0	0	0	0	0	0	4	6	5	11	0	6	6	4	7	11
Areia Branca	0	0	0	0	0	0	0	0	0	0	0	1	38	4	30	52	33	11	11	1
Caicó	0	0	0	0	0	0	2	0	1	1	87	73	67	67	37	9	3	14	1	5
Canguaretama	0	0	0	0	0	0	0	3	0	14	16	19	19	25	21	14	16	34	29	17
Ceará Mirim	33	94	16	17	70	42	1	31	59	72	38	11	28	23	18	16	13	3	9	8
João Câmara	0	0	0	3	8	0	0	0	0	0	4	25	5	5	3	3	0	0	0	0
Mossoró	0	0	0	2	2	3	7	6	25	154	163	131	130	57	59	61	42	27	26	19
Natal	0	1	0	9	2	2	3	0	36	45	96	196	230	196	155	190	106	100	126	82
Parnamirim	0	0	0	0	0	0	0	0	0	11	21	30	24	25	16	28	22	22	13	14
Rio do Fogo	0	0	0	0	0	0	1	0	0	3	6	11	8	8	3	9	2	1	0	0
Santa Cruz	0	0	0	0	0	0	0	0	0	0	1	2	2	14	0	5	3	10	3	0
Santo Antônio	0	0	0	0	0	0	1	0	0	1	24	13	11	11	22	23	16	11	4	5
S. G. Amarante	0	0	0	0	1	0	0	0	3	2	1	4	7	14	2	3	1	2	3	1
Total	33	95	16	31	83	47	15	40	124	303	461	522	574	460	366	419	263	239	232	163

Using Google Earth software [45], we created a numerical representation for the boundary of Rio Grande do Norte state, using geographical coordinates. More precisely, we defined 33 nodes to approximate the boundary. As coordinates from Google Earth are tridimensional, we projected the points into a plane. After that, the coordinates were converted from geodetic coordinates (latitude, longitude and altitude) to ECEF (earth-centered, earth-fixed) in kilometers using `lla2ecef` function from the aerospace toolbox in Matlab [69]. This way we have (x, y) coordinates in kilometers for the boundary of the state. There is no loss of accuracy in the projection because the altitude in the state is irrelevant compared to the length – the state has approximately 400 km in the latitudinal direction, 240 km in the longitudinal direction and 300 m elevation.

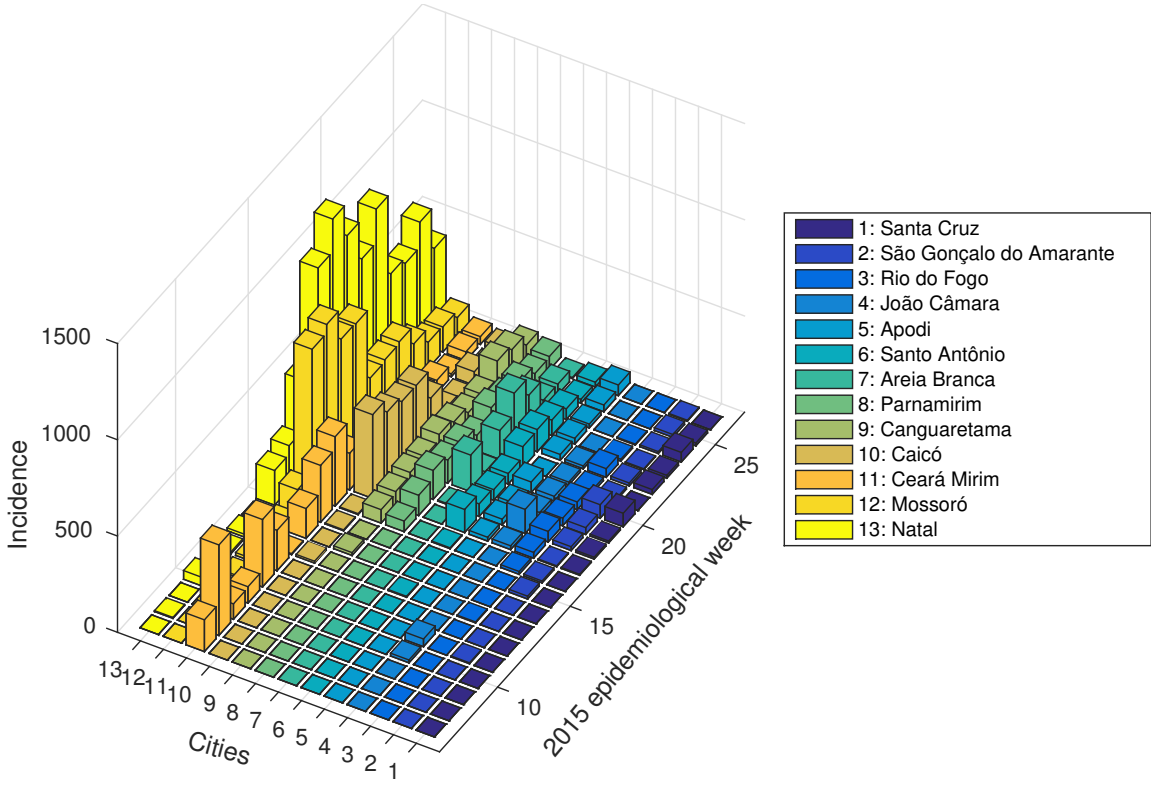

Figure 7 – Rescaled incidence in selected cities by epidemiological weeks of 2015.

With the boundary coordinates we created a linear finite element mesh, using Matlab's PDE toolbox [72]. We create a PDE model with function `createpde`, in which it is possible to define a domain, boundaries, and finite element meshes. Then with function `decsg` we create a decomposed geometry, in which we define the boundary and interior of the domain. This geometry is included in the PDE model with function `geometryFromEdges`. Finally we create the linear finite element mesh (consisting of 3 node triangles) using `generateMesh`. We export this mesh as a file and load it in our Fortran 90 finite element implementation. The mesh and location of cities from data are shown in Figure 8.

From the data, the first reported cases were in the city of Ceará-Mirim, at the 7th epidemiological week. This means that there were 33 reported Zika cases between the 6th and 7th weeks, but there is no information on the exact date. So we assume that the first infections happened one week before the data starts, between the 6th and 7th epidemiological weeks. To include this in the model, we define I_{0I} as the number of infected people at Ceará-Mirim divided by the approximated area of the city, between weeks 6 and 7. This way, I_{0I} represents density of the first infected humans arriving in the state. We have 20 weeks of data as in Table 6, so we start at $t = 0$ days counting from the 6th epidemiological week, and simulate a final time of $T = 140$ days (corresponding to the 26th epidemiological week).

Analyzing the dataset we find that the virus started to spread in the eastern

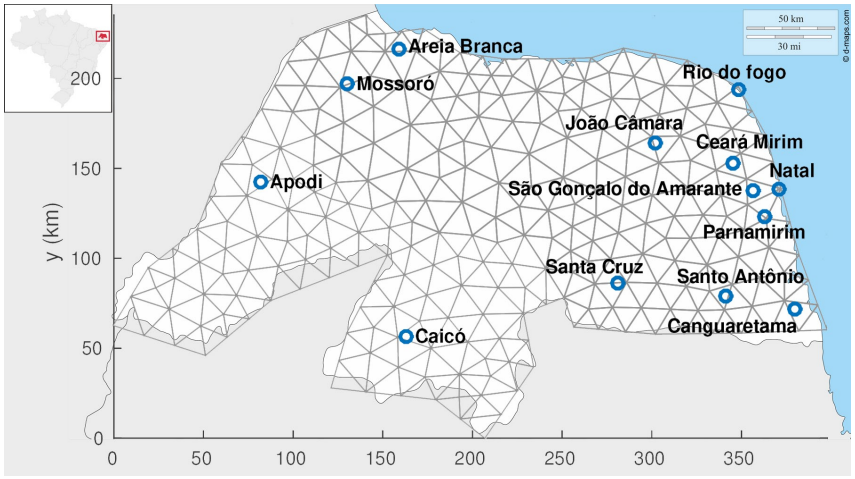

Figure 8 – Linear finite element mesh approximating Rio Grande do Norte state. Circles represent cities with relevant incidence data.

region of the state, where the capital city Natal and its densely populated metropolitan region are located, and most number of cases were also located in that region. However, infected cases started to appear in the western region in the 10th week in the city of Mossoró, and in the southern region in the 13th week in the city of Caicó (Figures 7 and 8). At this time, the virus had not spread over a large region in the state from the initial focus in the east. Thus, instead of local transmission, we consider those new infections to be originated from immigration of infected people from other locations. In order to consider this in our model, we include this data as an additional source function $f(\boldsymbol{x}, t)$ in the I equation of the state (2.1), acting in a specific spatial region and time period. It acts by adding new infected humans in the model, as an external source. The addition of this function does not change the adjoint system neither the optimal control characterization, because it does not depend on any of the state variables (S, I, R, S_v, I_v). For simplicity, $f(\boldsymbol{x}, t)$ is defined as constant in periods of time length τ and adds a number of infected humans coming from outside, in an region $\bar{\omega}_i \subset \Omega$, $i = 1, 2$, having the following form:

$$f(\boldsymbol{x}, t) = \begin{cases} \dfrac{(\text{infected humans})}{\tau |\bar{\omega}_i|}, \text{ if } \bar{t}_j \leqslant t \leqslant \bar{t}_j + \tau, \ \boldsymbol{x} \in \bar{\omega}_i, \ i, j = 1, 2, \\ 0, \text{ otherwise.} \end{cases} \tag{5.1}$$

Considering $(\bar{t}_j, \bar{t}_j + \tau)$ as the time interval between two successive weeks as in data, we must have $\tau = 7$ days. The region $\bar{\omega}_i$ is a small part of the domain, with $|\bar{\omega}_i|$ representing its area measure. We consider $\bar{\omega}_i$ as an approximation of the area of each city in which the new infected source is being added. We also define I_{0M} and I_{0C} as the number of infected humans in the right hand side of (5.1) for the cities of Mossoró and Caicó, respectively. These functions are added between epidemiological weeks 9 and 10 ($7 \leqslant t \leqslant 14$, if counting from $t = 0$ days) for Mossoró, and weeks 12 and 13 ($28 \leqslant t \leqslant 35$,

if counting from $t = 0$ days) for Caicó. This way the source function (5.1) turns into:

$$f(\boldsymbol{x}, t) = \begin{cases} \dfrac{I_{0M}}{7|\bar{\omega}_1|}, \text{ if } 7 \leqslant t \leqslant 14 \text{ and } \boldsymbol{x} \in \bar{\omega}_1, \\ \dfrac{I_{0C}}{7|\bar{\omega}_2|}, \text{ if } 28 \leqslant t \leqslant 35 \text{ and } \boldsymbol{x} \in \bar{\omega}_2, \\ 0, \text{ otherwise.} \end{cases} \tag{5.2}$$

As an approximation to each $|\bar{\omega}_i|, i = 1, 2$, we use the area of the triangular element closest to the city location in the mesh, as in Figure 8.

In order to simulate the initial spread of Zika virus in Rio Grande do Norte state, we define the initial conditions as following. For susceptible humans and vectors the density is constant in the whole domain, representing the total human population and the mosquitoes at carrying capacity. For infected humans, the initial condition is zero in the whole domain, except for a small region corresponding to the city of Ceará-Mirim (the mesh triangle closest to the city), that has I_{0I} infected humans per area. The density for immune humans and infected vectors are zero in the entire domain. A representation of the initial condition is depicted in Figure 25 in Chapter 6.

5.2 Parameter estimates

Our model is limited to the time interval connected with data, a period of 140 days, or 20 weeks, between February and June, a period with no great changes in environmental features affecting mosquitoes, such as temperature and precipitation, and thus we are not considering seasonality, opting instead for constant parameters. Relating these factors with entomological parameters could also be a difficult task, specially in PDE models. The values for all parameters used in simulations are shown in Table 1.

We adapted values for some of the parameters in our model from [41], obtaining a recovery period of $1/\delta = 15$ days, and mosquitoes incubation period and lifespan of $1/r_v = 1/\mu_v = 14$ days. The total human population in Rio Grande do Norte state is approximately 3.4 million [104], which leads to a density of 64.28 humans/km^2, value used as the initial condition for susceptible humans. Also, assuming a rate of 5 mosquitoes per human, we have a maximum density of $\kappa_v = 321.4$ mosquitoes/km^2.

According to Honório et al. [50], an *Aedes aegypti* mosquito can fly up to 300 meters per day. We have to connect this speed to the diffusion coefficient, which is the mean spread of an area over time. In order to do so, let us consider a reaction-diffusion equation for mosquitoes only, with logistic growth and without external influence, that is, the equation for S_v in (2.1) with I and I_v equal to zero. Then it is possible to find that the traveling wave speed of the solution is given by $2\sqrt{\alpha_v r_v}$, as done in [56]. Solving $2\sqrt{\alpha_v r_v} = 300$ for α_v we find an approximated diffusion coefficient of $\alpha_v = 0.315$ km^2/days.

Table 7 – Parameter values used in simulations.

	Value	Unit	Source
β	1.28×10^{-5}	1/(mosq./km^2 days)	estimated
β_v	1.55×10^{-2}	1/(hum./km^2 days)	estimated
β_d	0	1/(hum./km^2 days)	estimated
$1/\delta$	15	days	[41]
$1/r_v$	14	days	[41]
$1/\mu_v$	14	days	[41]
κ_v	321.4	mosq./km^2	assumed
α	5	km^2/days	[50, 56]
α_I	5	km^2/days	[50, 56]
α_v	0.315	km^2/days	[50, 56]
c_1	66.67	(\$/hum.)/days	assumed
c_2	100	\$/hum.	assumed
c_3	1000	\$/(km^2/days)	assumed
$u_{\min}$	0	1/days	assumed
$u_{\max}$	0.005	1/days	assumed
T	140	days	[104]
N	64.28	hum./km^2	[104]
I_{0I}	133	hum./km^2	estimated
I_{0M}	107	hum./km^2	estimated
I_{0C}	107	hum./km^2	estimated

The movement scale for humans is completely different and depends on a variety of factors [17]. Zika symptoms are mild when symptomatic and there is no relevant difference in movement from different humans classes, so we assume a mean diffusion coefficient of $\alpha = \alpha_I = 5$ km^2/days for humans.

As there are still no vaccines publicly available we have to make assumptions for the parameters related to them. It is important to note that for the optimal control characterization we need to use well balanced weights c_1, c_2, and c_3, so we are considering these values relative to an unit "\$" (United States Dollars). Nevertheless, it is important to consider these costs relatively realistic. A cost of \$1000 per infection day was considered for infected humans, giving $c_1 =$ \$66.67 per hum./days, considering 15 days for the disease duration. The costs related to vaccine were assumed to be $c_2 =$ \$100 per human vaccinated, and $c_3 =$ \$1000 per (km^2/days), the latter being the cost related to vaccination per area and per day. These values provide the ratios $c_2/c_1 = 1.5$ and $c_3/c_1 = 15$, which are reasonable in realistic terms. Again, we emphasize that the most important factor is the relative size of c_1, c_2 and c_3, as the cost functional (3.1) can be normalized if divided by c_1. The vaccine application should be non negative, and we assumed a maximum rate of 0.005 per day, corresponding to approximately 0.5% of susceptible humans or less being vaccinated each day. Since $u << 1$ and the c_3 term is associated with u^2, it contributes much less to J than the terms with c_1 and c_2. As these choices are somewhat uncertain

we later consider a sensitivity analysis on the parameters.

All transmission rates, β, β_d, and β_v may depend on local conditions, such as weather and behavior of humans and mosquitoes, so we decided to estimate them from data. We also have to estimate the number of infected humans in the initial condition, I_{0I}, and the number of infected humans from immigration, I_{0M} and I_{0C}. The estimation procedure is detailed in next section, and the values obtained are in Table 1. We note that the estimation for β_d as zero corroborates the hypothesis that direct transmission is irrelevant in the spread of Zika virus, at least for the set of data we are using [3].

5.3 Parameter estimation using least squares

We wish to estimate some parameters of model (2.1) from the available data in Table 6. In order to do so, we need to consider a measure to fit the model to data, as performed in other parameter estimation works [5, 22, 109]. The dataset consists of the number of cases, or incidence, so we need to define a measure for a equivalent quantity in the model. The incidence from model (2.1) in a spatial region $\omega_i \subset \Omega$ and at a time interval $(t_j, t_j + \tau)$ is defined as:

$$\mathcal{Y}_{ij} = \int_{t_j}^{t_j+\tau} \int_{\omega_i} (\beta S I_v + \beta_d S I) \, \mathrm{d}\boldsymbol{x}\mathrm{d}t, \tag{5.3}$$

where ω_i denotes the spatial region of the i-th city and $(t_j, t_j + \tau)$ the time length of the j-th week of interest, with $\tau = 7$ days. The integrals represent the sum over a specific space and time. The integrand consists of the rates of new infections, and its form is given by the positive components at the right hand side of the equation for I in model (2.1), except for the external source of immigration.

We define $\overline{\mathcal{Y}}_{ij}$ as the incidence from data, that is, data from Table 6 seen as a matrix and divided by the report rate of 20%, with $i = 1, \ldots, 13$ (representing the cities), $j = 1, \ldots, 20$ (representing the weeks). Then it is possible to compare the model incidence $\mathcal{Y}_{ij}$ to the data incidence $\overline{\mathcal{Y}}_{ij}$. In order to do so, we define the normalized residual between the incidence from data and from model (2.1):

$$\mathcal{R} = \sqrt{\frac{\sum\limits_{i\in\mathcal{I}, j\in\mathcal{J}} \left(\overline{\mathcal{Y}}_{ij} - \mathcal{Y}_{ij}\right)^2}{\sum\limits_{i\in\mathcal{I}, j\in\mathcal{J}} \left(\overline{\mathcal{Y}}_{ij}\right)^2}}. \tag{5.4}$$

In the residual, we consider only indexes $i \in \mathcal{I}$ and $j \in \mathcal{J}$ such that $\overline{\mathcal{Y}}_{ij}$ is different from zero, for $i = 1, 2, \ldots, 13$ (one for each city) and $j = 1, 2, \ldots, 20$ (one for each week). The geometric interpretation for this expression is the euclidean distance between the two quantities. The normalization only helps to keep the absolute value of the residual

small. Therefore, by minimizing $\mathcal{R}$, or equivalently $\mathcal{R}^2$ to eliminate the square root, we try to obtain parameters for model (2.1) that produce results close to data. Formally, we wish to find a vector of parameters $\boldsymbol{\theta} \in \Theta$ such that $\boldsymbol{\theta} = \arg\min \mathcal{R}^2$, subject to system (2.1). This is a nonlinear least squares problem [5, 79], that should be solved appropriately. The choice of which parameters $\boldsymbol{\theta}$ should be considered as variables depend on the information available on the problem, as well as the set of possible values Θ. Usually, and this is the way we proceed, Θ consists of lower and upper bounds for each parameter, such that $L_k \leqslant \theta_k \leqslant U_k$, for each k-th parameter. In our case, the parameters we wish to estimate are $\boldsymbol{\theta} = (\beta, \beta_v, \beta_d, I_{0I}, I_{0M}, I_{0C})$, as mentioned before. For each set of parameters, the state system (2.1) is solved using the methods discussed in Chapter 4 and the residual $\mathcal{R}$ is calculated using quadratures and trapezoids.

Several optimization methods are available for solving nonlinear least squares problems, for example we can cite, in Fortran, TANGO (Trustable Algorithms for Nonlinear General Optimization) [13], and TOLMIN (a tolerant algorithm for linearly constrained optimization calculations) [93], and Matlab optimization toolbox with several methods [71]. Our choice is BOBYQA (Bounded Optimization by Quadratic Approximation), a bound constrained derivative-free algorithm [92], because it is very simple to use and to connect with the finite element implementation in Fortran 90. It is also very reliable and appropriate to our problem, as we can see in the results. In a brief explanation, BOBYQA uses a trust region method that forms quadratic models by interpolation of the objective function – in our case the residual $\mathcal{R}$. Each iteration produces a new point $\boldsymbol{\theta}$, usually by solving a trust region subproblem subject to the bound constraints. Alternatively, it chooses a point to replace an interpolation point in order to provide good linear independence in the interpolation conditions.

Lower bounds for β, β_v, β_d, I_{0I}, I_{0M}, I_{0C} were taken as small values close to zero, and upper bounds according to realistic approximations of each parameters – bounds are shown in Table 8. We vary the initial guess of the optimization method to guarantee that we find a global minimum instead of a local one. The initial guesses were uniformly random generated based on the lower and upper bounds and simulated 100 times.

Best fit results are shown in Table 8, with a normalized residual of $\mathcal{R} = 0.821$. We show in Figure 9 the simulated incidence in each city, and in Figure 10 the simulated incidence summed over the 13 cities. Overall, we can see that the result from simulation qualitatively agrees with data, although it is very difficult to obtain a good fit for all the cities at once. The rate β_d is estimated at the lower bound, so we assume its value as zero, meaning that direct transmission is irrelevant for the dataset used.

In the next section we run some tests in order to verify that the methodology is reliable. However, before that we give a brief summary of the parameter estimation procedure, which can be readily applied to other problems of interest:

Table 8 – Parameter bounds and estimation results.

	$\mathcal{R}$	β	β_v	β_d	I_{0I}	I_{0M}	I_{0C}
Lower bounds	0	10^{-6}	10^{-6}	10^{-6}	1	1	1
Upper bounds	0	10^{-1}	10^{-1}	10^{-1}	133	107	107
Results	0.821	6.438×10^{-5}	1.561×10^{-2}	0	133	107	107

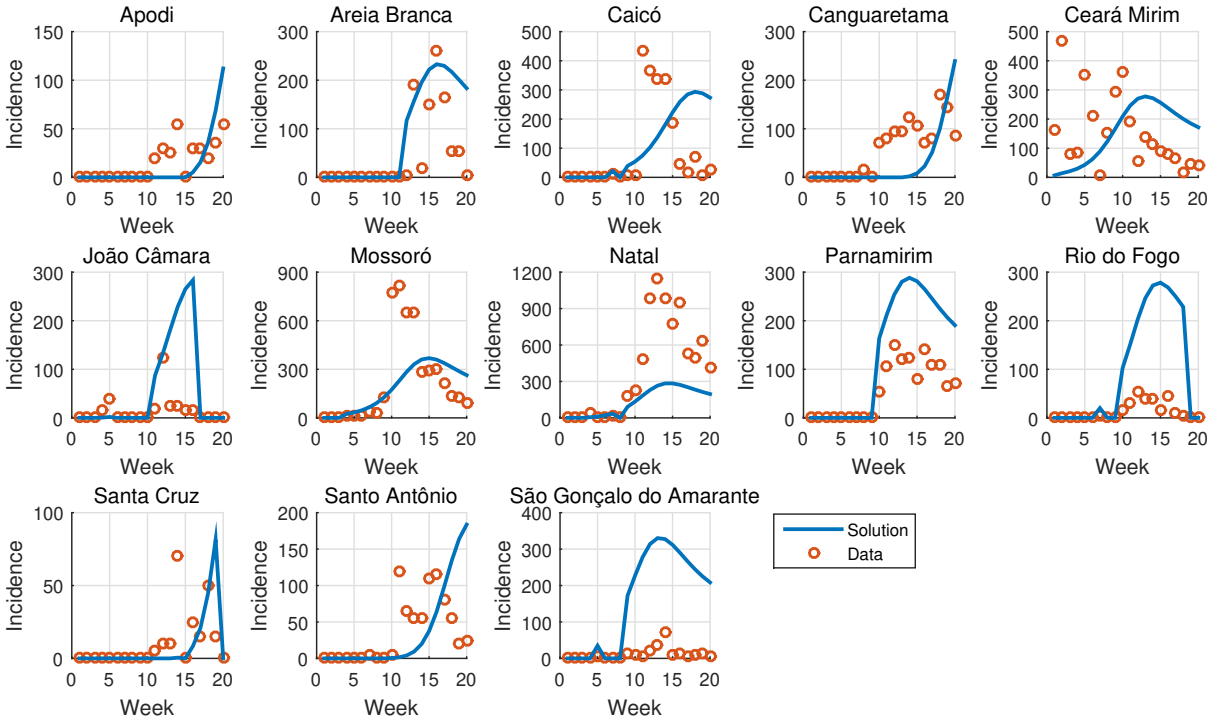

Figure 9 – Comparison between the sum in each city of data and simulated incidence.

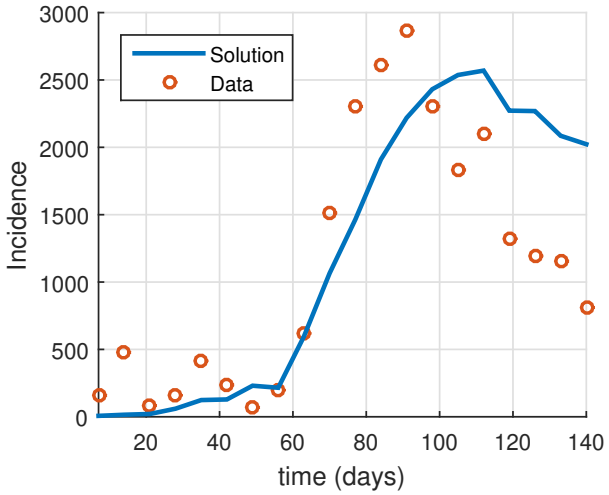

Figure 10 – Comparison between the sum from data and from simulated incidence.

- We use a dataset with reported Zika cases from Rio Grande do Norte state in Brazil, for 20 weeks, or 140 days.
- We created a finite element mesh to approximate the state, and cities are approxi-

mated by mesh triangles.

- We introduced a function $f(\boldsymbol{x}, t)$ to account for immigrated infections.
- Most parameter values are obtained from literature [41, 50, 56, 104].
- The incidence (number of new infections) from model (2.1) is given by (5.3).
- The residual (5.4) between model and data incidence is minimized in order to estimate parameters.
- The estimated parameters are the transmission rates β, β_v, and β_d, and number of initial infections I_{0I}, I_{0M}, and I_{0C}.

5.4 Tests with generated data

In order to verify that our parameter estimation methodology is reliable, in this section we run some tests with artificially generated data, trying to imitate the set of available data from Table 7. The generated set is defined by running a simulation using the parameters values obtained in the previous section (all parameters from Table 7) and then calculating the corresponding incidence by expression (5.3) in the relevant cities for which we have data (cities from Table 7), for 20 weeks. However, in order to get closer to a real data set, we use data only from weeks in which values from the real data set is different from zero. In other words, the set of partial data consists of the incidence $\mathcal{Y}_{ij}$, for $i \in \mathcal{I}$ and $j \in \mathcal{J}$, as defined in (5.4). Both complete and partial generated data is shown in Figure 11, and summed complete and partial generated data is shown in Figure 12, in which partial data is visibly different from full data.

Real life collected data often is affected by noise, coming for example from measurement errors, uncertain report rates, misleading diagnosis, and uncertainty in modeling. Thus, we add random noise in the generated data set in order to include some of these factors. A good way to add random noise is to use white noise, a vector in which each component is a random variable with zero mean and finite variance. We define variance as a predefined maximum variation from the generated data. For example, if the maximum variation is 10%, each variance is proportional to the baseline data and maximum variation, and the data with added noise ranges between 90% and 110% from the baseline value. In this way, let $\hat{\boldsymbol{\mathcal{Y}}}$ be the artificial generated data matrix, and $\boldsymbol{\varepsilon}$ the white noise matrix, then the noisy data set is given by $\hat{\boldsymbol{\mathcal{Y}}} + \boldsymbol{\varepsilon}$.

We considered five different noisy scenarios, corresponding to 0%, 30%, 50%, 70%, and 100% of maximum variation from generated data. In each of these scenarios, different white noise was added to $\hat{\boldsymbol{\mathcal{Y}}}$, producing five different datasets. Using our least squares approach as in the previous section, we estimated β, β_v, I_{0I}, I_{0M}, and I_{0C} for

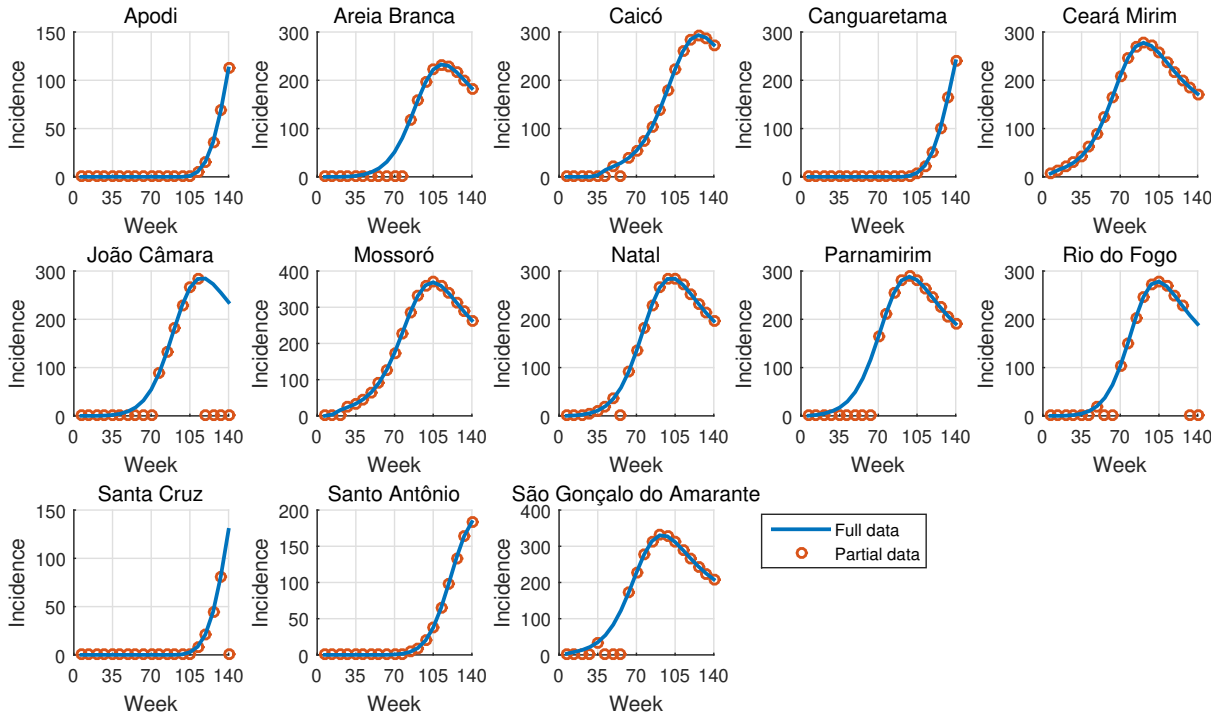

Figure 11 – Full and partial artificially generated incidence data. The latter is used in the parameter estimation tests.

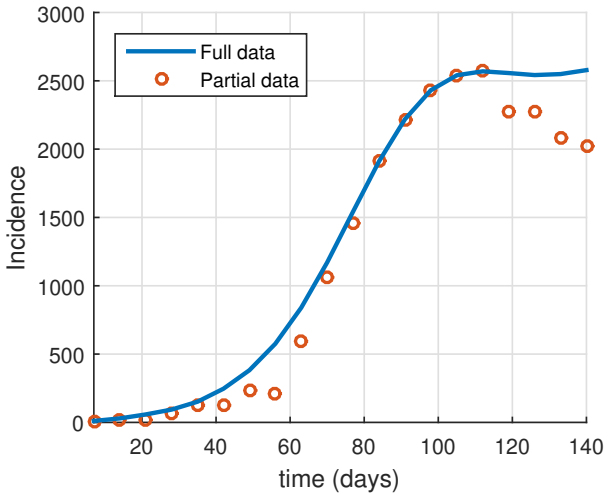

Figure 12 – Full and partial summed artificially generated incidence data. The latter is used in the parameter estimation tests.

each one of these datasets. The direct transmission rate β_d was not estimated because we have found that its value is irrelevant and very close to zero. In the case of 0% variation, corresponding to no added noise, the method was able to exactly retrieve the predefined parameters. Results are shown in Table 9, which contains the predefined values for the parameters (denoted by true values), estimated parameters for each dataset, residuals $\mathcal{R}$ calculated as in (5.4), and relative errors between the estimated parameters and true values. In Figure 13 we graphically show the residuals $\mathcal{R}$ and relative errors of the parameters, in order to have a geometric overview of the results. It is possible to see that β and β_v have

small relative errors in all considered noise scenarios, but not for the other parameters. Also, the 100% noise scenario gives the highest residual $\mathcal{R}$, but returns small relative errors for all parameters. This means that relative errors for the parameters do not uniquely define accuracy in the results. By accuracy we mean a small residual between simulated and data incidence – a small value for $\mathcal{R}$. Nevertheless, all of the scenarios produced a small residual $\mathcal{R}$, representing a good fit to each of the dataset considered in the estimation procedure.

Table 9 – Results of parameter estimation tests with artificially generated noisy data.

	$\mathcal{R}$	β	β_v	I_{0I}	I_{0M}	I_{0C}
True values	**0**	$\mathbf{6.438 \times 10^{-5}}$	$\mathbf{1.561 \times 10^{-2}}$	**133**	**107**	**107**
30% noise	7.17×10^{-2}	6.709×10^{-5}	1.501×10^{-2}	133	94.67	105.94
Rel. error		4.2%	3.9%	0.0%	11.5%	1.0%
50% noise	1.56×10^{-1}	6.542×10^{-5}	1.544×10^{-2}	122.64	90.45	93.30
Rel. error		1.6%	1.1%	7.8%	15.5%	12.8%
70% noise	2.00×10^{-1}	6.807×10^{-5}	1.527×10^{-2}	90.14	75.04	88.75
Rel. error		5.7%	2.2%	32.2%	29.9%	17.1%
100% noise	3.05×10^{-1}	6.396×10^{-5}	1.561×10^{-2}	133	97.28	105.30
Rel. error		0.6%	0%	0%	9.1%	1.6%

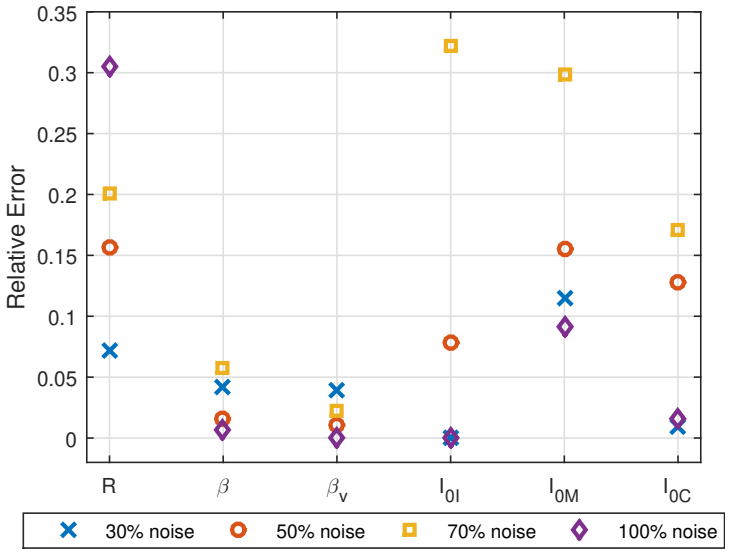

Figure 13 – Residual $\mathcal{R}$ and relative errors of estimated parameters using artificially generated data with 30%, 50%, 70%, and 100% added noise.

In Figures 14 – 21 we show the results from the parameter estimation with noisy generated datasets. Figures 14, 16, 18, and 20 show the simulated incidence with estimated parameters, original generated incidence data (without noise), and incidence data with added noise. Figures 15, 17, 19, 21 show these same contents summed over the 13 cities with relevant data.

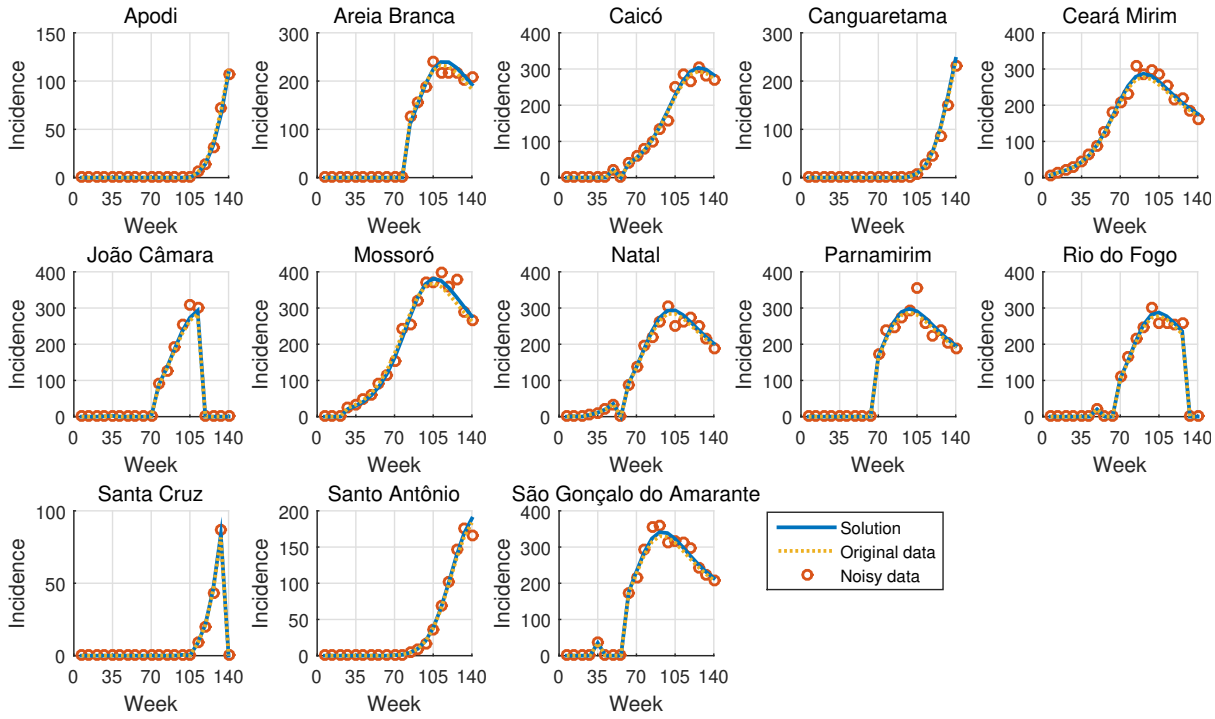

Figure 14 – Incidence in each city (blue solid lines) with estimated parameters $\beta = 6.709 \times 10^{-5}$, $\beta_v = 1.501 \times 10^{-2}$, $I_{0I} = 133$, $I_{0M} = 94.67$, $I_{0C} = 105.94$, obtained using artificially generated data with 10% added noise. The corresponding residual is $\mathcal{R} = 7.17 \times 10^{-2}$. Data with 10% added noise (red circles) and without noise (yellow dotted lines) are also shown.

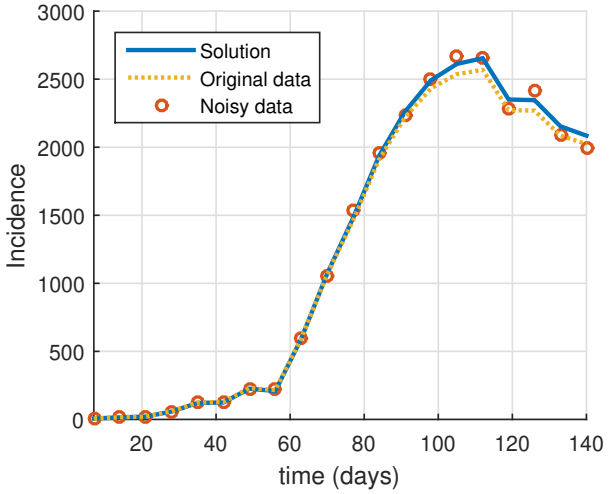

Figure 15 – Summed incidence in all cities (blue solid line) with estimated parameters $\beta = 6.709 \times 10^{-5}$, $\beta_v = 1.501 \times 10^{-2}$, $I_{0I} = 133$, $I_{0M} = 94.67$, $I_{0C} = 105.94$, obtained using artificially generated data with 10% added noise. The corresponding residual is $\mathcal{R} = 7.17 \times 10^{-2}$. Summed data with 30% added noise (red circles) and without noise (yellow dotted line) are also shown.

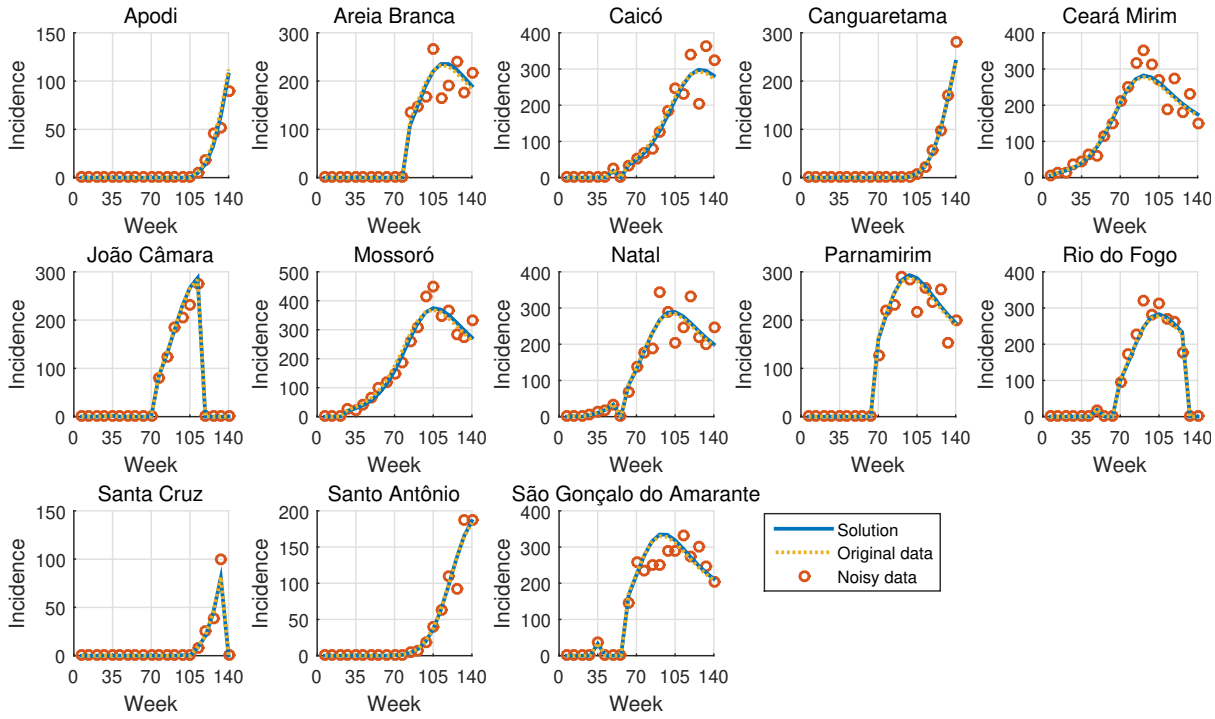

Figure 16 – Incidence in each city (blue solid lines) with estimated parameters $\beta = 6.542 \times 10^{-5}$, $\beta_v = 1.544 \times 10^{-2}$, $I_{0I} = 122.62$, $I_{0M} = 90.45$, $I_{0C} = 93.30$, obtained using artificially generated data with 50% added noise. The corresponding residual is $\mathcal{R} = 1.56 \times 10^{-1}$. Data with 10% added noise (red circles) and without noise (yellow dotted lines) are also shown.

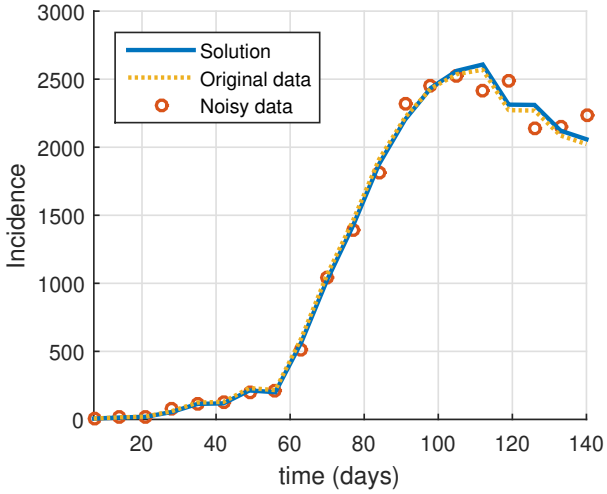

Figure 17 – Summed incidence in all cities (blue solid line) with estimated parameters $\beta = 6.542 \times 10^{-5}$, $\beta_v = 1.544 \times 10^{-2}$, $I_{0I} = 122.62$, $I_{0M} = 90.45$, $I_{0C} = 93.30$, obtained using artificially generated data with 10% added noise. The corresponding residual is $\mathcal{R} = 1.56 \times 10^{-1}$. Summed data with 50% added noise (red circles) and without noise (yellow dotted line) are also shown.

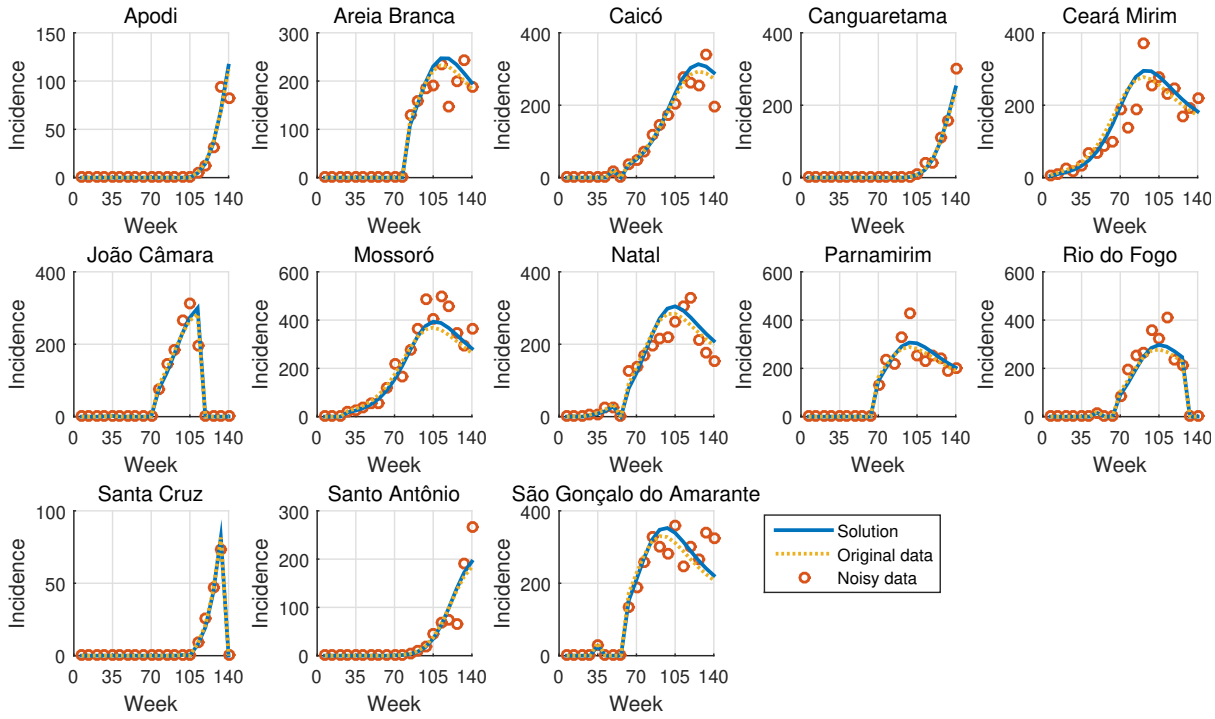

Figure 18 – Incidence in each city (blue solid lines) with estimated parameters $\beta = 6.807\times10^{-5}, \beta_v = 1.527\times10^{-2}, I_{0I} = 90.14, I_{0M} = 75.04, I_{0C} = 88.75$, obtained using artificially generated data with 70% added noise. The corresponding residual is $\mathcal{R} = 2.00 \times 10^{-1}$. Data with 70% added noise (red circles) and without noise (yellow dotted lines) are also shown.

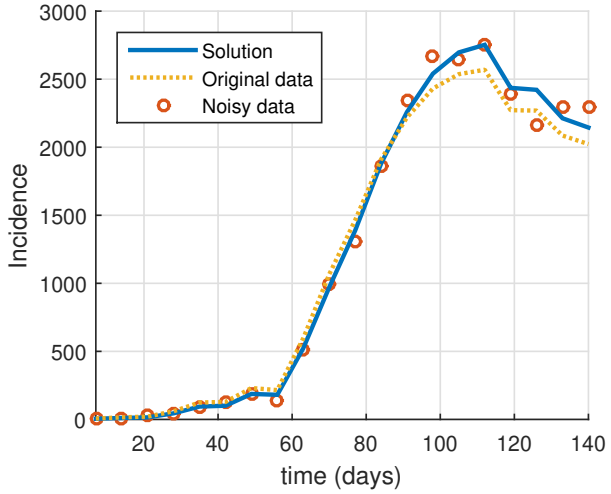

Figure 19 – Summed incidence in all cities (blue solid line) with estimated parameters $\beta = 6.807\times10^{-5}, \beta_v = 1.527\times10^{-2}, I_{0I} = 90.14, I_{0M} = 75.04, I_{0C} = 88.75$, obtained using artificially generated data with 70% added noise. The corresponding residual is $\mathcal{R} = 2.00 \times 10^{-1}$. Summed data with 70% added noise (red circles) and without noise (yellow dotted line) are also shown.

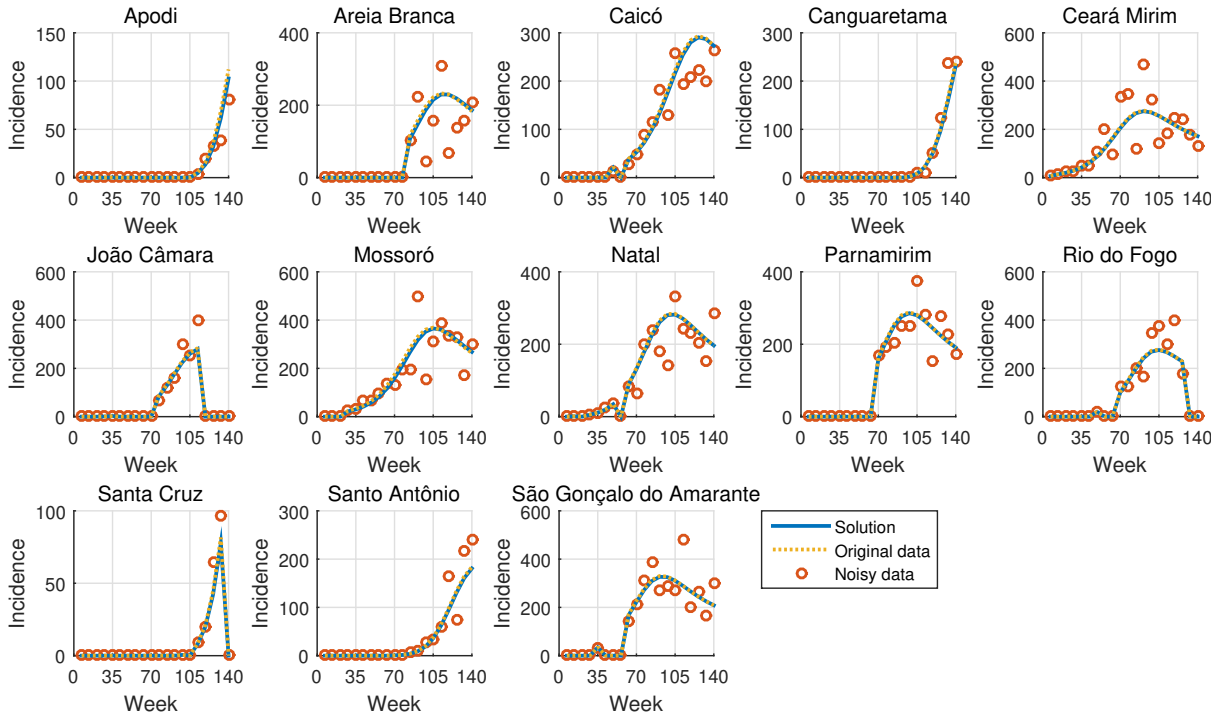

Figure 20 – Incidence in each city (blue solid lines) with estimated parameters $\beta = 6.396 \times 10^{-5}$, $\beta_v = 1.561 \times 10^{-2}$, $I_{0I} = 133$, $I_{0M} = 97.28$, $I_{0C} = 105.30$, obtained using artificially generated data with 100% added noise. The corresponding residual is $\mathcal{R} = 3.05 \times 10^{-1}$. Data with 100% added noise (red circles) and without noise (yellow dotted lines) are also shown.

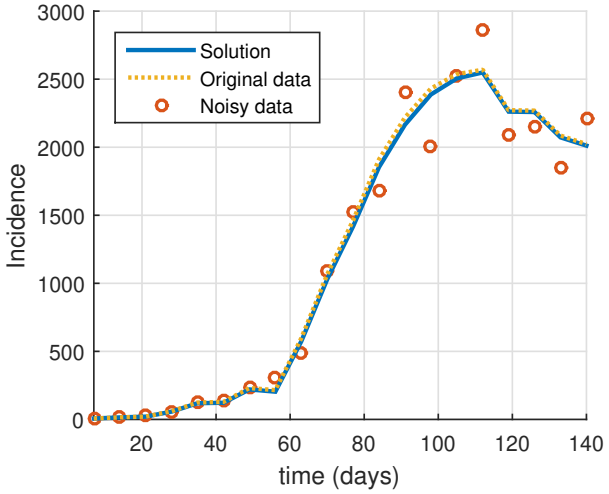

Figure 21 – Summed incidence in all cities (blue solid line) with estimated parameters $\beta = 6.396 \times 10^{-5}$, $\beta_v = 1.561 \times 10^{-2}$, $I_{0I} = 133$, $I_{0M} = 97.28$, $I_{0C} = 105.30$, obtained using artificially generated data with 100% added noise. The corresponding residual is $\mathcal{R} = 3.05 \times 10^{-1}$. Summed data with 100% added noise (red circles) and without noise (yellow dotted line) are also shown.

In Figures 14 and 15 we can see that a maximum variation of 30% does not change much the generated incidence, and the simulated incidence in this case is very close to the original data. This also happens in Figures 16 and 17, with a 50% noise, although the variation is a little bit higher. In Figures 18 and 19, 70% noisy data is relatively far for original simulated data, which causes a visible difference between the incidence with estimated parameters and original incidence. In Figures 20 and 21, 100% of maximum variation significantly changes the behavior of the noisy data from the original incidence curves, but the estimated solution still approximates the original data without added noise.

The results in this section show that the proposed parameter estimation methodology is able to retrieve good results in terms of parameters and output, producing small least squares residuals even when white noise is present in data. It is not clear how errors in estimated and true parameters are related to the residual $\mathcal{R}$ in the presence of noise, since small errors in parameters could provide a higher residual. However, more variation in noise produced results with higher $\mathcal{R}$, even though all of the incidence solutions obtained were close to the artificially generated data without noise.

5.5 Global Sensitivity Analysis

A complete analysis of parameters should also account for sensitivities in model (2.1), which are able to verify which parameters have the most impact in a particular model output. In order to search for these key parameters, we perform a global sensitivity analysis, accounting for the influence of all the parameters at once. We assess the impact of variations in the model parameters on the outputs using partial rank correlation coefficients (PRCCs) [67]. These coefficients are similar to the common Pearson correlation coefficient, but also deal with nonlinearities, as long as the output is monotonic in the parameters.

PRCC analysis is a sample based method, which means it requires several trials (or samples) of the model. These trials are usually random generated in a Monte Carlo sense [47]. The idea is to generate several random sets of parameters for model (2.1), and then numerically solve it for each set, obtaining a corresponding set of outputs, which are used for the calculation of the correlation coefficients. In this sense it is expected that as the number of trials increase, a better overview of the model outputs should be provided, eventually covering a large amount of parameter combinations. Asymptotically, the considered sets of parameters should cover all the possible combinations of the search space.

Latin hypercube sampling (LHS) is a particular Monte Carlo method that relies on sampling without replacement, with the advantage that it requires fewer samples than simple random sampling with the same accuracy [73]. This is specially important

in the present work, as numerical solutions for PDEs can be very time-consuming. Each parameter range is divided into N_{sim} equally spaced intervals, with N_{sim} being the number of trials. Each interval for each parameter is then sampled only once, that is, without replacement, so that the entire range is explored, for each of the parameters. The results of the sampling are put in a matrix that consists of one column per parameter, with the sampling results in each of the N_{sim} rows. Once the matrix is assembled, N_{sim} model solutions are simulated, using each combination of parameters of the matrix rows.

The PRCCs are calculated with the N_{sim} latin hypercube samples. Briefly, the procedure is as following: for a j-th parameter input x_j and output y, the x_j, y data is rank transformed, by putting it in ascending order from 1 to the sample size, N_{sim}. Then, linear effects of the other parameters on the output are disregarded from linear regressions. The correlation coefficient is then calculated, and it describes the linear correlation of the rank-transformed data, which corresponds to nonlinear correlation of the original data. Each PRCC has an associated p-value, that accounts for the significance (or in a less technical word, reliability) of the result. More details on the coefficient calculations can be found in [67, 103]. A detailed and thorough PRCC analysis for an ODE model with optimal control can be found in [48], and a corresponding shorter version in [49].

We performed two analyses, one using the cost $J(u^*)$ as output, and the other using incidence (total number of new infections). $J(u^*)$ is a single number output that accounts for all time and space at once, so its sensitivities are also single numbers, one for each parameter. On the other hand, the total incidence from the model can be viewed as a function over time, so the PRCCs can also be seen that way.

The Latin hypercube sampling was simulated with $N_{\text{sim}} = 200$ trials, and parameters from model (2.1) were considered following normal distributions, with baseline values given by the estimated parameters in the previous sections. Ranges were chosen corresponding to 15% of maximum variation from their baselines for β and c_3, 10% for δ, r_v and μ_v, and 5% for the other parameters. These values can be found in Table (10). The direct transmission rate β_d was not considered because we considered its value as zero. The normal distributions are defined within these ranges, with means at the baselines and standard deviations according to the lower and upper bounds. More precisely, values were chosen such that lower and upper bounds were within three standard deviations from the mean, according to the *three sigma rule* [100]. We considered a significance level of 0.05, meaning that PRCCs with p-values greater than 0.05 are assumed to be not significant. A PRCC value lower than 0.2 is also considered insignificant, due to the low impact it has on the output. Monotonicity was verified in for the parameters between lower and upper bounds, with $J(u^*)$ being decreasing in δ, μ_v, and c_1, and increasing in the other parameters. Scatter plots of rank-transformed data are shown in Figures (23) and (24). Both axis scales in the plots result from the rank transformation and linear regression,

and do not represent the real values for the output and parameters in the simulations.

Table 10 – Parameter baseline values and ranges used in the PRCC analysis.

	Baseline value	Lower bound	Upper bound	Variation
β	1.28×10^{-5}	1.09×10^{-5}	1.47×10^{-5}	15%
β_v	1.55×10^{-2}	1.47×10^{-2}	1.63×10^{-2}	5%
δ	0.067	0.0603	0.0737	10%
r_v	0.071	0.0639	0.0781	10%
μ_v	0.071	0.0639	0.0781	10%
κ_v	321.4	305.33	337.47	5%
α	5	4.75	5.25	5%
α_I	5	4.75	5.25	5%
α_v	0.315	0.299	0.331	5%
c_1	66.67	63.34	70	5%
c_2	100	95	105	5%
c_3	1000	850	1150	15%

PRCC results and p-values considering the cost $J(u^*)$ as output are shown in Tables 11 and 12. We found that both transmission rates β, β_v, mosquitoes carrying capacity κ_v, and costs associated with infected humans c_1 are positive correlated with $J(u^*)$, while the recovery rate δ and mortality rate of mosquitoes μ_v are negative correlated to $J(u^*)$. The other parameters have insignificant PRCCs. In Figure 23 it is possible to see the apparent linear correlation in the transformed data (which corresponds to a nonlinear correlation of the original data) for β, δ, β_v, κ_v, μ_v, and c_1. There is no visible trend in the other parameter plots, as they seem to be evenly spread. In both cases the plots confirm the results from the PRCC values.

Table 11 – Significant PRCCs with $J(u^*)$ as output.

Parameter	β	δ	β_v	κ_v	μ_v	c_1
PRCC	0.9698	−0.8490	0.7808	0.6324	−0.7463	0.5618
p-value	0	0	0	0	0	0

Table 12 – Insignificant PRCCs with $J(u^*)$ as output.

Parameter	r_v	α	α_I	α_v	c_2	c_3
PRCC	−0.09	0.00	−0.06	−0.04	0.07	0.15
p-value	0.206	0.974	0.375	0.530	0.330	0.031

Considering incidence as a time varying output, we can calculate PRCC values at each time, assessing parameter sensitivity over time. Significant PRCCs calculated this way are shown in Figure 22, and rank-transformed scatter plots at the final time of

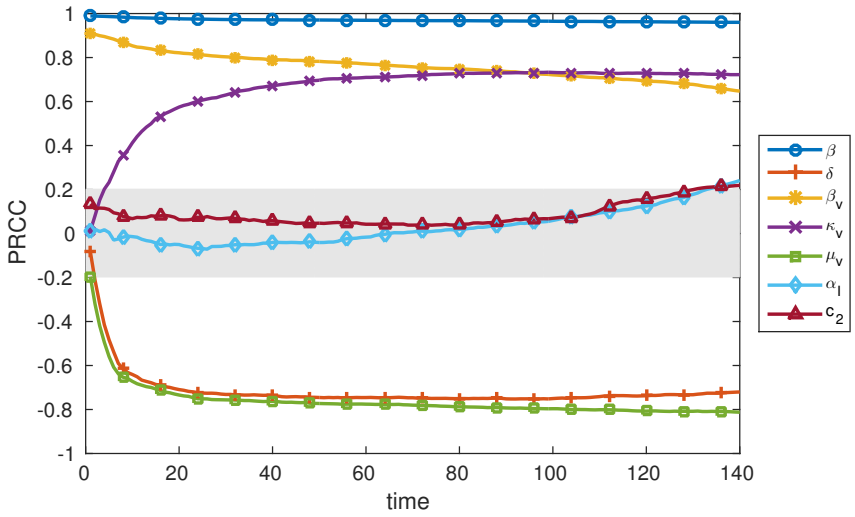

Figure 22 – Significant PRCCs over time, using incidence as output. Shaded area indicates region where PRCC is not significant.

simulation ($t = 140$ days) in Figure 24. We can see that there is a great variation in the PRCCs for κ_v, μ_v, and δ in the beginning of the simulations, when the correlations are low (in absolute values), and then they increase over time. There is a moderate variation in the PRCCs for β_v, α_I, and c_2 over the whole time interval. PRCCs for α_I, and c_2 are insignificant in most of the time, but increase at the end of the simulation. The recovery rate δ and mortality rate of mosquitoes μ_v are again negatively correlated to the output, while the other parameters are positively correlated. In Figure 24 it is possible to see the linear correlation trend of the parameters and incidence at $t = 140$ days for β, δ, β_v κ_v, μ_v. Although slight, it is also possible to see the correlation for α_I and c_2. These results are again in accordance to the PRCC values as seen in Figure 22.

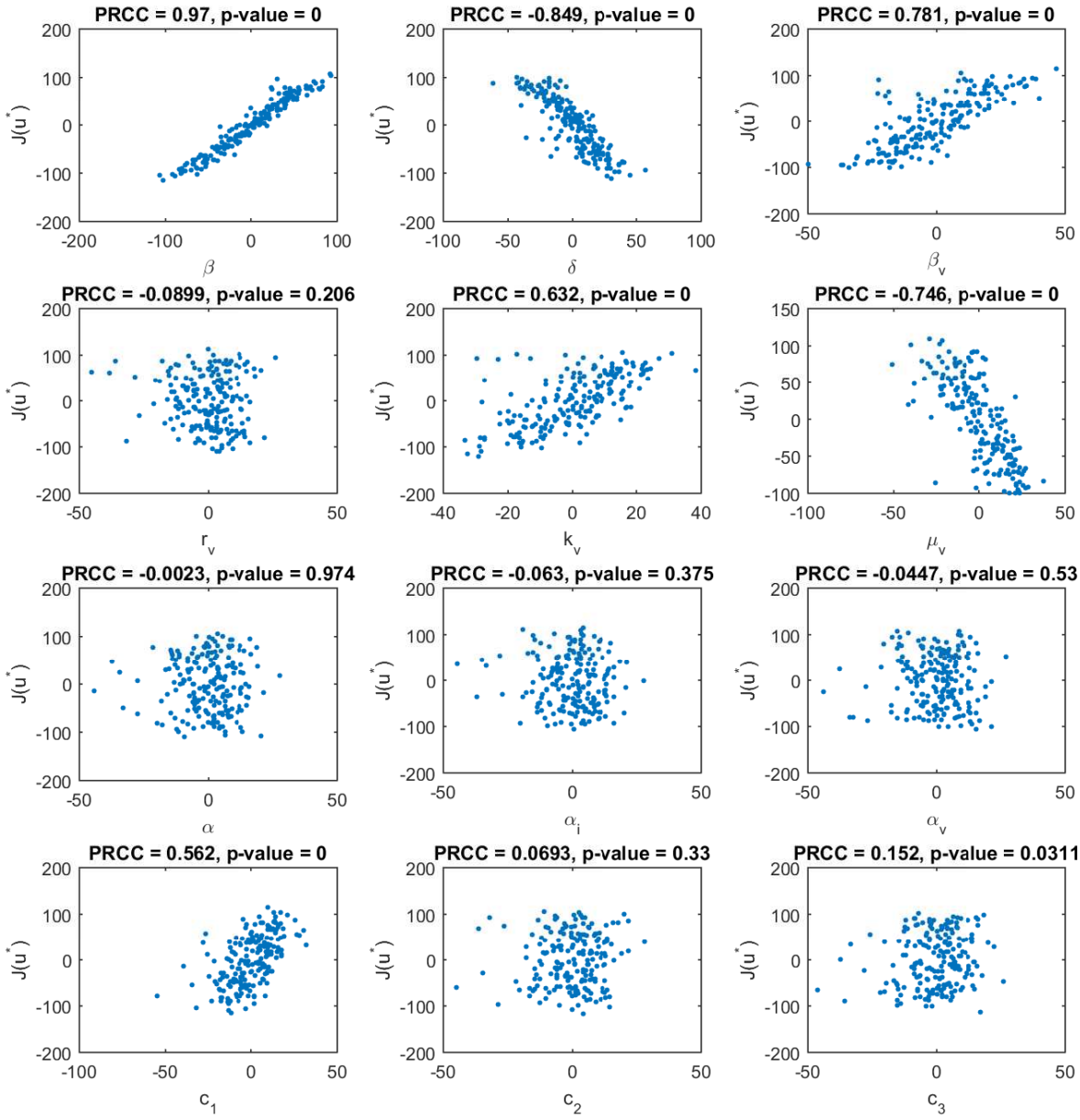

Figure 23 – Scatter plots of rank-transformed data with $J(u^*)$ as output. A PRCC is considered significant if it is greater than 0.2 or if its p-value is less than 0.05. Scales in both axes result from rank transformation and linear regression. It is possible to see positive linear trends of correlation for β, β_v, κ_v, and c_1, and negative ones for δ and μ_v.

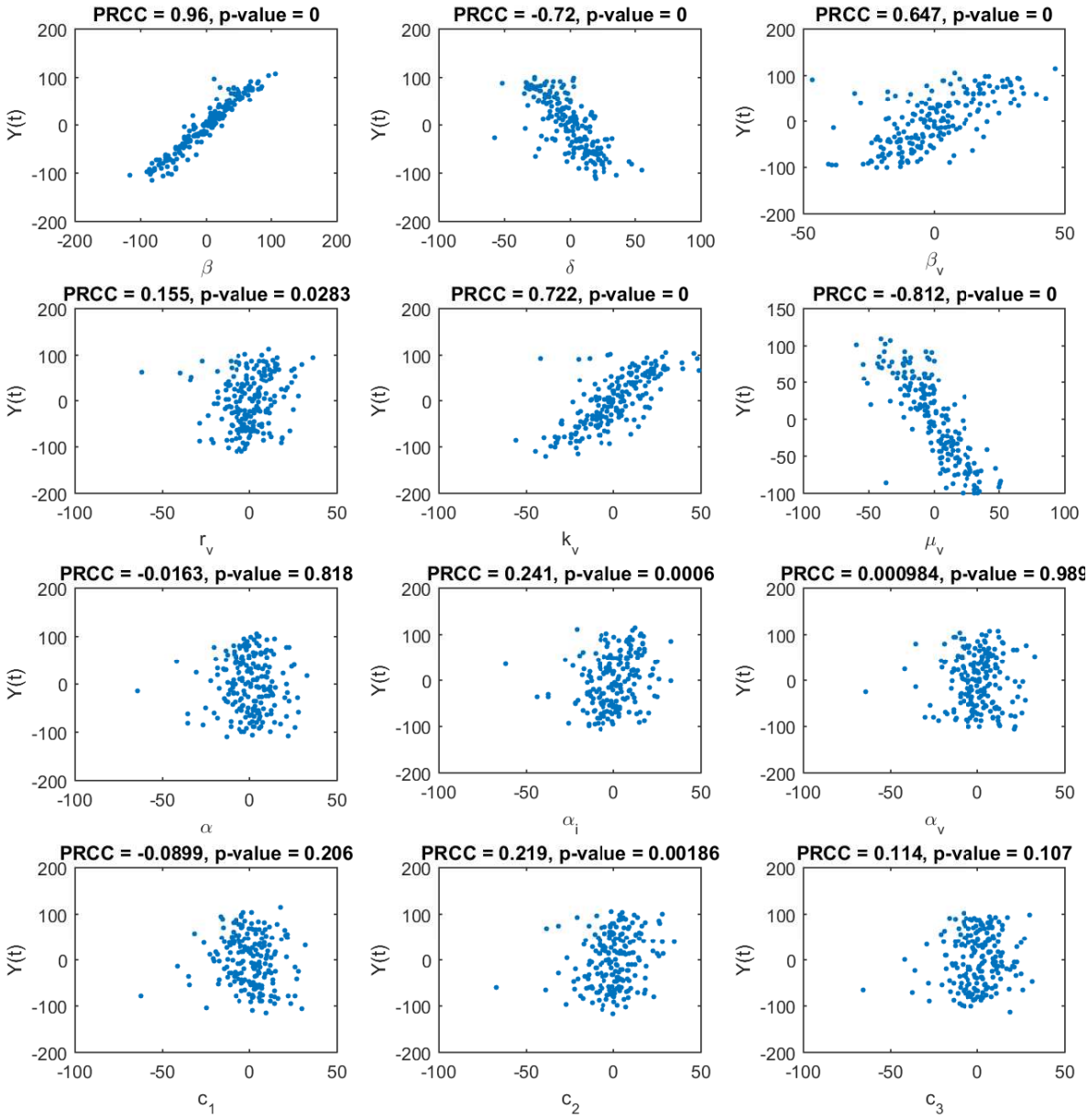

Figure 24 – Scatter plots of rank-transformed data with incidence as output. Results are showed for $t = 140$ days. A PRCC is considered significant if it is greater than 0.2 or if its p-value is less than 0.05. Scales in both axes result from rank transformation and linear regression. It is possible to see positive linear trends of correlation for β, β_v, κ_v, α_I and c_2, and negative ones for δ and μ_v.

Chapter 6
Numerical results

Using parameter values obtained in Chapter 5, we now focus on simulating different scenarios for the spread of Zika virus, also considering optimal vaccination strategies, with methods described in Chapter 4. The parameters used in the simulations are from Table 1, which were estimated in Chapter 5.

We first consider a scenario without control, trying to recreate the spread of the virus in Rio Grande do Norte state in 2015, based on the dataset from Table 6. After that, we wish to evaluate scenarios with the introduction of vaccination control. It is expected that the earlier the control is applied, the better the results will be, with lower costs $J(u^*)$ and infections. However, due to practical factors it is almost impossible to begin the vaccination program as soon as the virus is detected in the population. Even if the vaccine is readily available, there are operational procedures such as allocation of resources and transportation of vaccine to health care facilities. Therefore, we simulate optimal control scenarios with introduction of vaccination starting at different times: 35, 52, 70, and 105 days. These scenarios are simulated without control until the specified starting time, and then the vaccination is introduced by solving the optimal system. We vary the time of introduction of vaccination to verify if there is a significant impact on the overall output. Furthermore, constant control scenarios are simulated with u always at the upper bound, that is, $u = u_{\max}$, also starting at times 35, 52, 70, and 105 days, in order to show the advantages of a spatial and time varying optimal control. For these scenarios, we do not show the state solution plots, only the overall cost $J(u_{\max})$ values.

Some quantities of interest are calculated, in order to have a comparison overview between all scenarios, namely: the total incidence from the model (total number of new infected cases in the simulated time and over all space), the total number of vaccinated humans, the total optimal cost $J(u^*)$, the cost with constant control at the upper bound, $J(u_{\max})$, and the ratio $J(u^*)/J(u_{\max})$. These quantities of interest are

calculated as integrals:

$$\begin{aligned}\text{Total incidence} &= \int_Q \beta S I_v \,\mathrm{d}\boldsymbol{x}\mathrm{d}t,\\ \text{Total vaccinated} &= \int_Q uS \,\mathrm{d}\boldsymbol{x}\mathrm{d}t,\\ \text{Total cost: } J(u) &= \int_Q \left(c_1 I + c_2 uS + c_3 u^2\right) \,\mathrm{d}\boldsymbol{x}\mathrm{d}t.\end{aligned}$$

The total cost can be calculated for the optimal control $u = u^*$ or constant at the upper bound $u = u_{\max}$. The integrals are calculated over $Q = \Omega \times (0, T)$, gathering contributions from both space and time. Their approximation are made by quadratures and trapezoids, as explained in Chapter 4. Results are compared to the scenario without control in order to quantify, in percentages, the advantages of the control application. Quantities of interest results are shown in Table 13.

In the next sections, we show spatial plots for the scenarios without control and with optimal control, for selected times. The plots consist of scaled 2D heatmaps, with scaled colors representing different densities of each population. The selected times are $t = 35$, 52, 70, 105 and 140 days, chosen as intermediate intervals in order to represent a good overview of the temporal dynamics.

We also show plots of the total number of each model compartment through time, calculated by integrals over space. In mathematical terms, the integrals are given by:

$$\begin{aligned}S(t) &= \int_\Omega S(x, y, t) \,\mathrm{d}x,\\ I(t) &= \int_\Omega I(x, y, t) \,\mathrm{d}x,\\ R(t) &= \int_\Omega R(x, y, t) \,\mathrm{d}x,\\ S_v(t) &= \int_\Omega S_v(x, y, t) \,\mathrm{d}x,\\ I_v(t) &= \int_\Omega I_v(x, y, t) \,\mathrm{d}x,\\ u(t) &= \int_\Omega u(x, y, t) \,\mathrm{d}x,\end{aligned}$$

in which the integral over space represents the total number of each compartment over time $t \in (0, T)$. In this way, the above functions over time are similar to ordinary differential equation solutions, which helps in the interpretation of the results. Plots for these functions are shown in Figure 31, for the scenarios without control, and with optimal control starting at 35, 52, and 70 days, all together in the same figure to facilitate comparisons.

As mentioned before in Chapter 5, the initial conditions are the same for all scenarios, and are shown in Figure 25. For susceptible humans and vectors the density

Table 13 – Optimal control results compared to the scenario without control.

	without control	control starting at $t = 35$ days	control starting at $t = 52$ days	control starting at $t = 70$ days	control starting at $t = 105$ days
Total incidence % of no control	4.719×10^5	2.746×10^5 58.18%	3.271×10^5 69.32%	3.811×10^5 80.75%	4.628×10^5 98.06%
Total vaccinated		4.951×10^5	4.072×10^5	2.939×10^5	4.472×10^4
$J(u^*)$ % of no control	3.341×10^8	2.454×10^8 73.44%	2.759×10^8 82.58%	3.040×10^8 90.98%	3.335×10^8 99.81%
$J(u_{\max})$ % of no control		3.093×10^8 92.56%	3.326×10^8 99.53%	3.536×10^8 105.83%	3.687×10^8 110.36%
$J(u_{max})/J(u^*)$		126.03%	120.53%	116.33%	110.56%

is constant in the whole domain, representing the total human population (3.4 million spread over the total area or 64.25 hum./km^2) and the mosquitoes at carrying capacity (17 million spread over the total area or 321.5 mosq./km^2). For infected humans, the initial condition is zero in the whole domain, except for a small region corresponding to the city of Ceará-Mirim (the mesh triangle closest to the city), that has I_{0I} infected humans per area. The density for immune humans and infected vectors are zero in the entire domain.

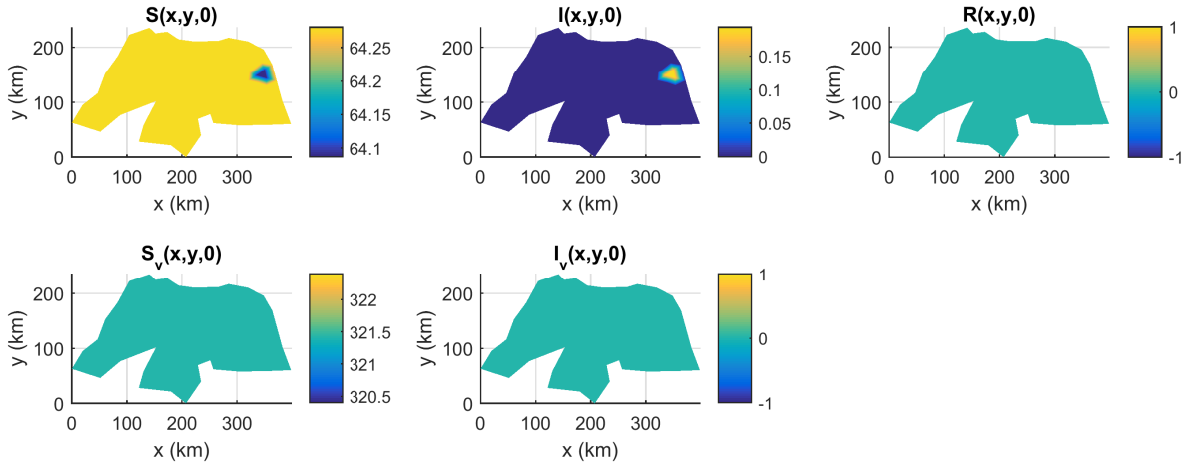

Figure 25 – Plots of initial conditions in space ($t = 0$ days), for all scenarios. Each plot has a different scale.

6.1 Simulation without control

Results without control over space at selected times are shown in Figures 26 – 30. We can see the spread over time of each infected source due to diffusion, as both susceptible humans and mosquitoes are being infected, and humans recover, becoming immune. As the simulation time passes, S and S_v have lower densities in the regions where infections are located, while I, I_v and R have higher ones. Each infected source, the initial (I_{0I}) and the two added sources at times $t = 7$ (I_{0M}) and $t = 28$ (I_{0C}) days,

act independently with non overlapping supports – they reach each other only at the end of the simulation, as seen in Figure (30). We can see that the spread due to the initial condition, in the eastern region, is bigger than the others, which reflects the data and the fact that it is where the initial condition is located. At the final time, 140 days – Figure (30), we can see that the virus has spread through a major region of the state, in the form of circular waves due to the homogeneity of diffusion.

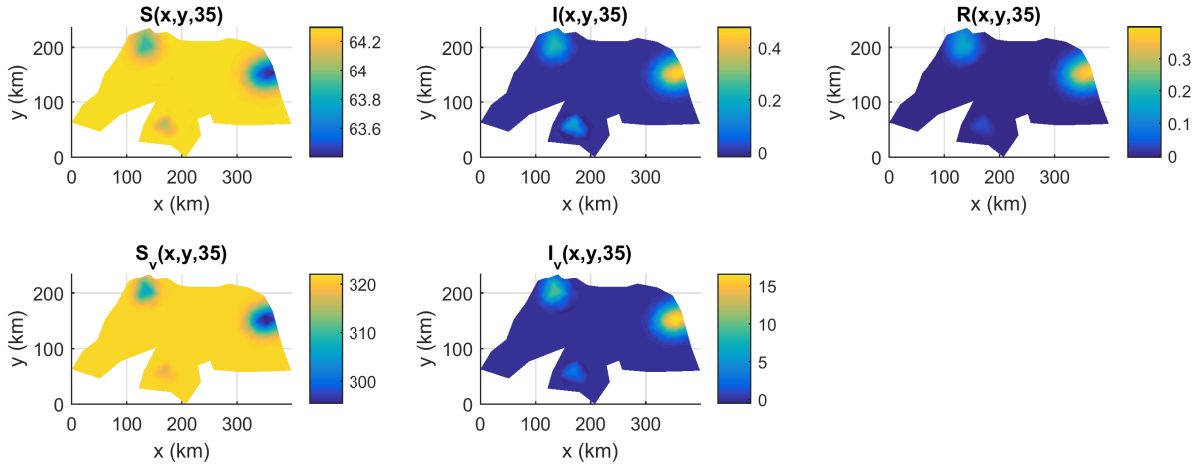

Figure 26 – Plots of solutions in space at $t = 35$ days, scenario without control. Each plot has a different scale.

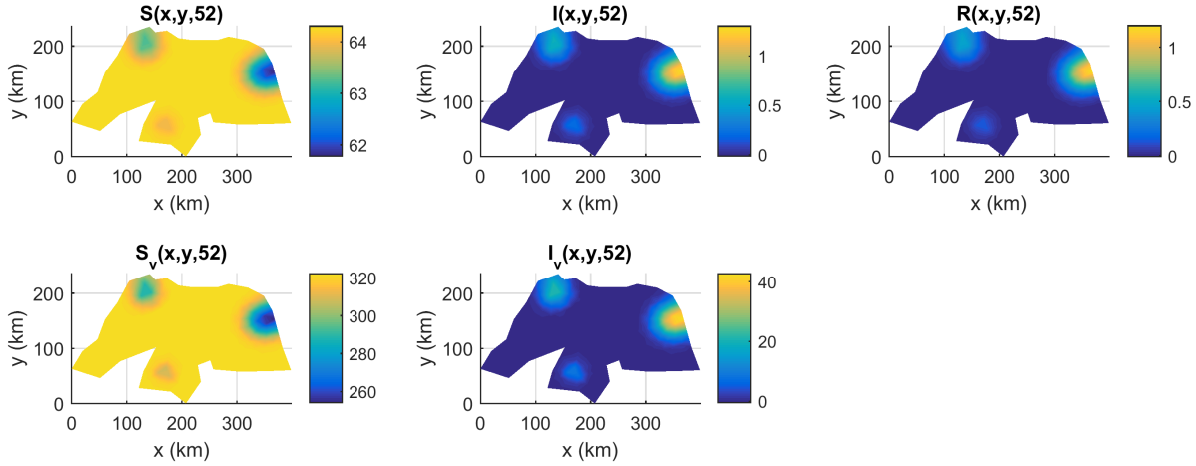

Figure 27 – Plots of solutions in space at $t = 52$ days, scenario without control. Each plot has a different scale.

In the time plots of Figure 31, we can see the increase in the infected human population (I), the corresponding increase in the removed (R) and infected vector (I_v) populations, and the corresponding decrease in the susceptible human (S) and vector (S_v) populations. Also, the infected human population is always increasing, which reflects the initial phase of the disease outbreak. By comparing the numbers in the scales we see that at the end of 140 days, the approximately 140 thousand infected humans is not so large compared to the total population in the state, 3.4 million.

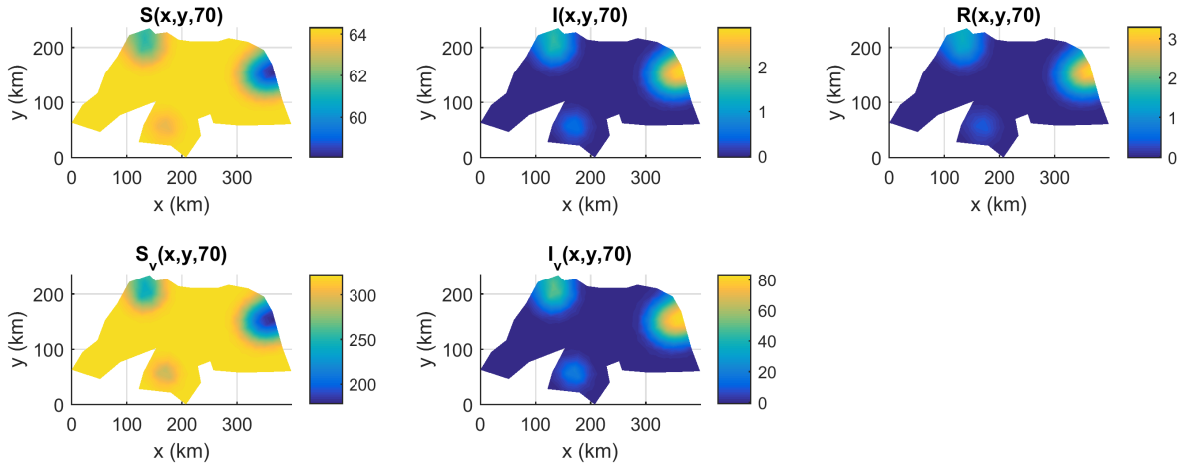

Figure 28 – Plots of solutions in space at $t = 70$ days, scenario without control. Each plot has a different scale.

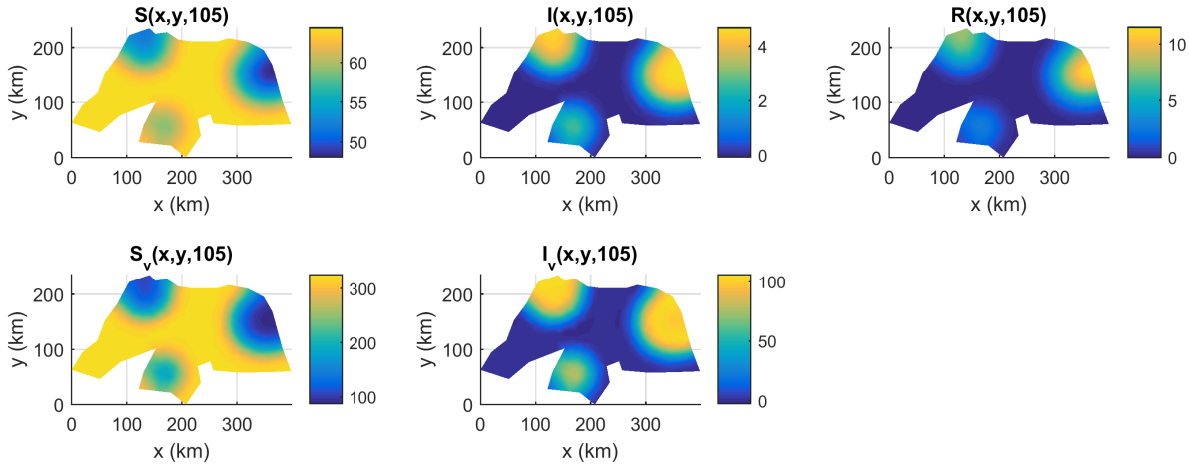

Figure 29 – Plots of solutions in space at $t = 105$ days, scenario without control. Each plot has a different scale.

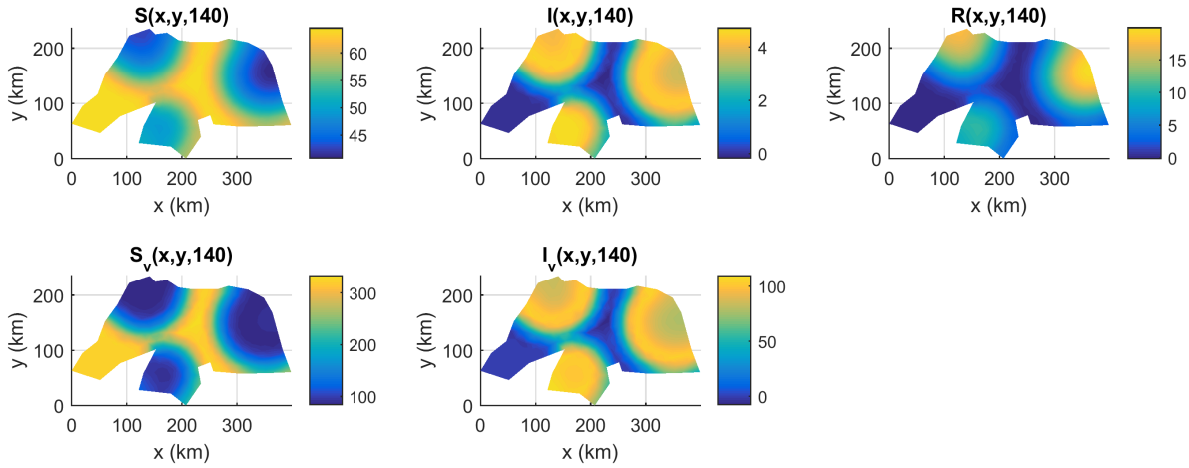

Figure 30 – Plots of solutions in space at $t = 140$ days, scenario without control. Each plot has a different scale.

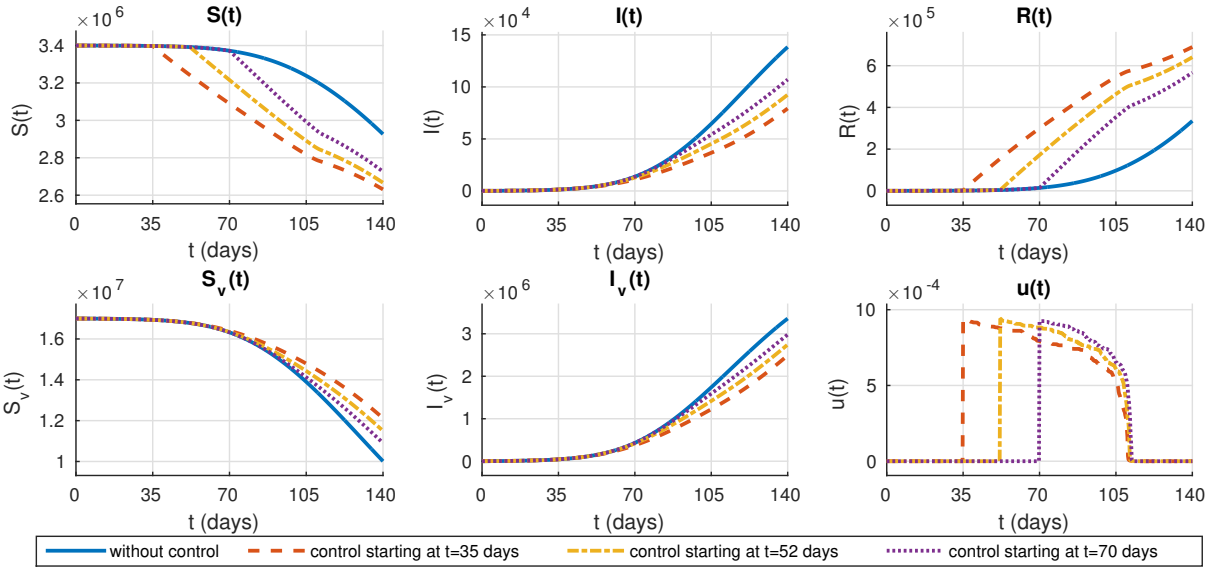

Figure 31 – Integrals of state solutions and optimal control over space. Scenarios without control, and with optimal control starting at $t = 35$, 52 and 70 days.

Quantities of interest for this scenario are shown in the second column of Table 13. The total number of new infections is 471, 900 humans, corresponding to approximately 14% of the total population in the state. As we are assuming that the report rate is 20%, the total reported infections, or equivalently the total symptomatic, would be 2.8%. The associated cost $J(u = 0)$ is 3.34×10^8, which corresponds to the cost of infected people only, as there is no vaccination being applied. As mentioned before, these values are taken as baseline for comparison of efficacy of the vaccination scenarios.

6.2 Simulation with optimal control starting at 35 days

We can see in Figures 32 – 36 that the optimal control application does not change much of the spatial spread in the solutions over time, except for the susceptible and immune humans, which now have much lower and higher density values over space, respectively. The infected sources continue to spread the same way as in the case without control, but the densities are lower, as it can be seen comparing the difference in scale of solutions at $t = 140$ days in Figures 30 and 36. The control starts acting with values at the upper bound $u_{\max} = 0.005$, and is non-zero in a region that covers where the infected humans are. The reason for this is because the optimal control solution accounts for all time, so that it tries to prevent the spread of infection as soon as possible, introducing higher vaccination at the beginning. As time passes, until $t = 70$ days, Figure 34, we can see that the control shrinks covering a smaller part of the spatial domain, but always where there are the most infected humans, with the optimal control staying at the upper bound. We see that at $t = 112$ days, Figure 35, the control is positive at a smaller part of the domain. From $t = 119$ to $t = 140$ days the control is zero, because the optimal

characterization requires it to be that way at the final time, as seen in Figure 36.

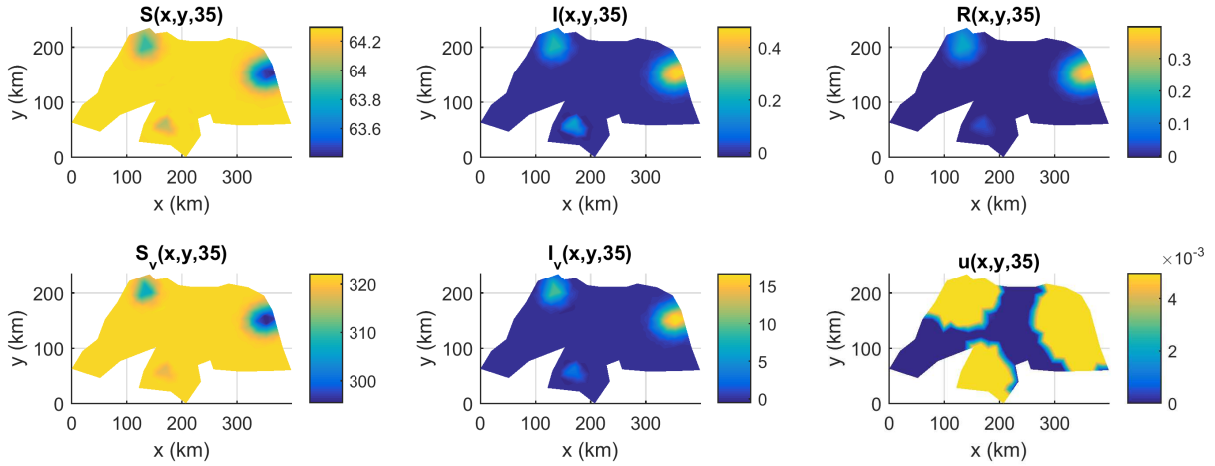

Figure 32 – Plots of solutions in space at $t = 35$ days, scenario with optimal control starting at $t = 35$ days. Each plot has a different scale.

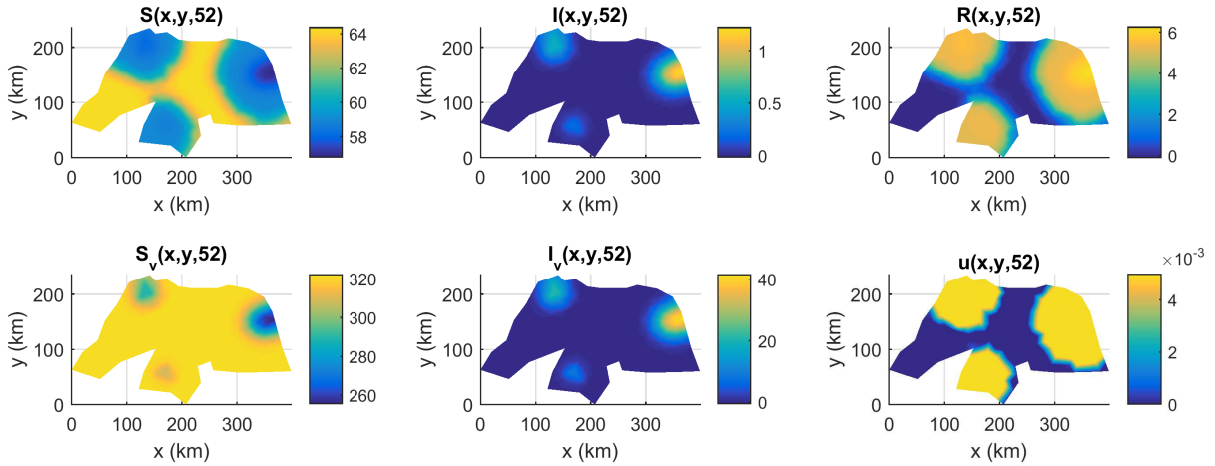

Figure 33 – Plots of solutions in space at $t = 52$ days, scenario with optimal control starting at $t = 35$ days. Each plot has a different scale.

In the time plots, Figure 31, we can see that the control is highest at the time it starts, and then lowers until zero, confirming the spatial results. We can see the control effects in the other population plots, starting at $t = 35$ days, mainly in the susceptible humans and removed, in which the control acts. When the control starts, the susceptible human population sharply decreases, with the corresponding increase in the immune population. This behavior changes approximately at $t = 105$ days, when the control application starts to lower to zero.

From Table 13, the number of new infected humans is $274,600$, corresponding to 58.18% of the incidence with no control, and the cost $J(u^*)$ is reduced to 73.44% from that case. Both values had considerable reduction, showing a successful application of vaccination. We note that these values were obtained with almost 500 thousand vaccinated humans, which is a relatively low number, about 15% of the total human population

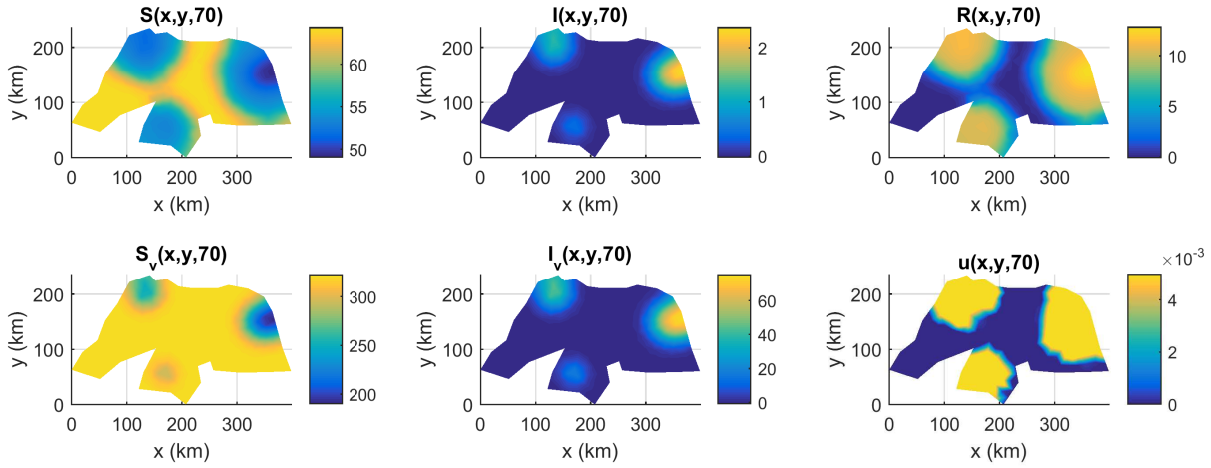

Figure 34 – Plots of solutions in space at $t = 70$ days, scenario with optimal control starting at $t = 35$ days. Each plot has a different scale.

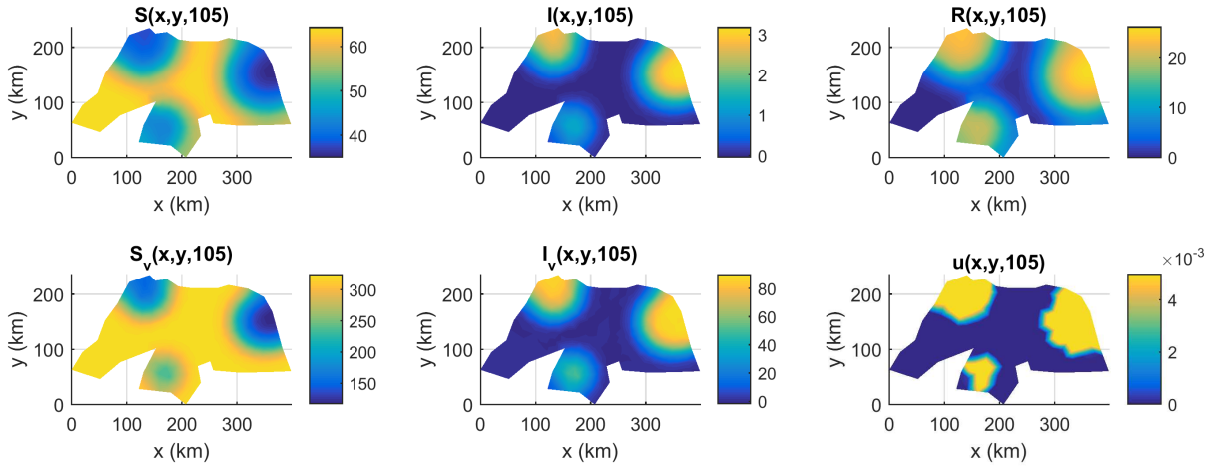

Figure 35 – Plots of solutions in space at $t = 105$ days, scenario with optimal control starting at $t = 35$ days. Each plot has a different scale.

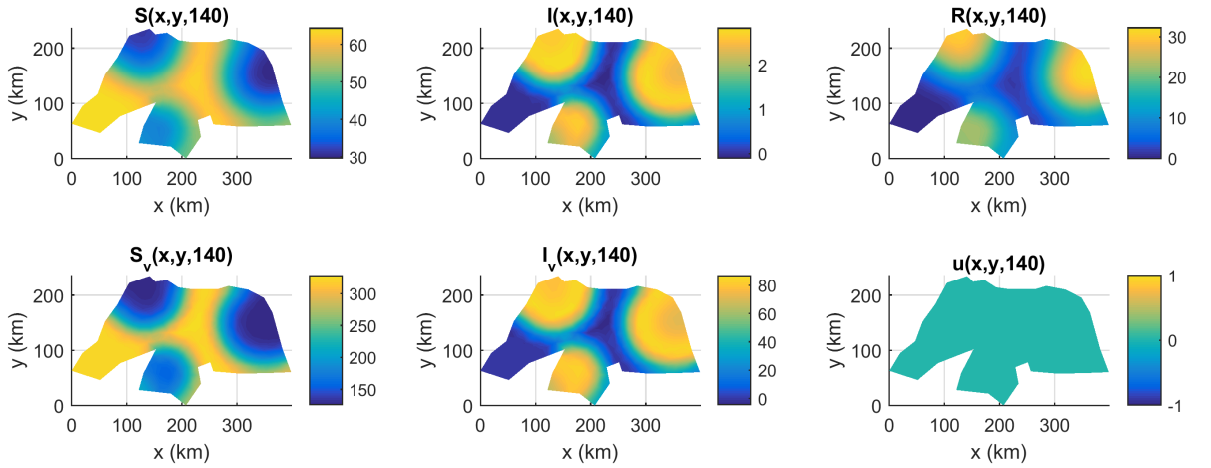

Figure 36 – Plots of solutions in space at $t = 140$ days, scenario with optimal control starting at $t = 35$ days. Each plot has a different scale.

(3.4 million). This means that there is no need to vaccinate a high proportion of the population to reduce infections, as 15% of vaccinated humans is enough to reduce incidence by 40%. The scenario with constant control starting at $t = 35$ days returned a cost $J(u_{\max})$ corresponding to 92.56% of the cost without control and 126.03% of the optimal control cost, so there is a significant difference between constant and optimal controls.

6.3 Simulation with optimal control starting at 52 days

Starting the optimal control at $t = 52$ days results in a similar spatial behavior for state and control solutions, as shown in Figures 37 – 40. The most prominent difference in this scenario is again in the scale, as there are less immune humans due to less vaccination, and consequently more infections. The control rate again starts at the upper bound and covers the same part of the domain as before, and keeps shrinking as time passes until it becomes zero.

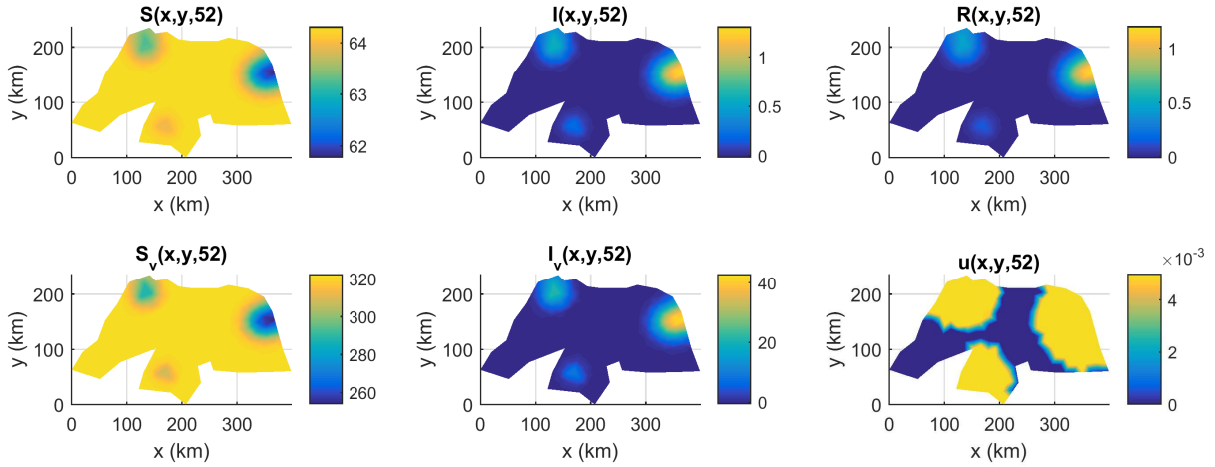

Figure 37 – Plots of solutions in space at $t = 52$ days, scenario with optimal control starting at $t = 52$ days. Each plot has a different scale.

In the time plots, Figure 31, it is possible to see differences in the numbers, as less control is being applied, but the overall behavior is also similar to the previous scenario. There are less immune and more susceptible humans, and consequently more infections, but still less than the scenario without control. The vaccination rate is higher than before, but it starts later and goes to zero approximately at the same time, which overall gives less vaccinated humans.

In Table 13, we can see that the number of new infections and cost $J(u^*)$ reduce to 69.32% and 82.58% from the case without control, respectively, which is a smaller reduction compared to the scenario with control starting at 35 days. The cost $J(u_{\max})$ from constant control corresponds to 105.83% of the cost without control and 116.33% of $J(u^*)$. Comparing the results of control starting at 52 days to the scenario in which it

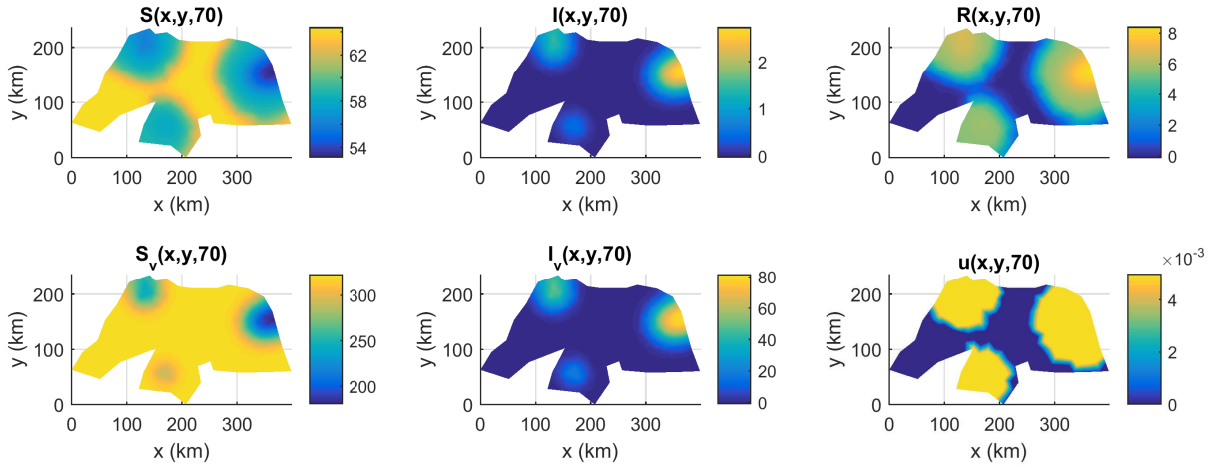

Figure 38 – Plots of solutions in space at $t = 70$ days, scenario with optimal control starting at $t = 52$ days. Each plot has a different scale.

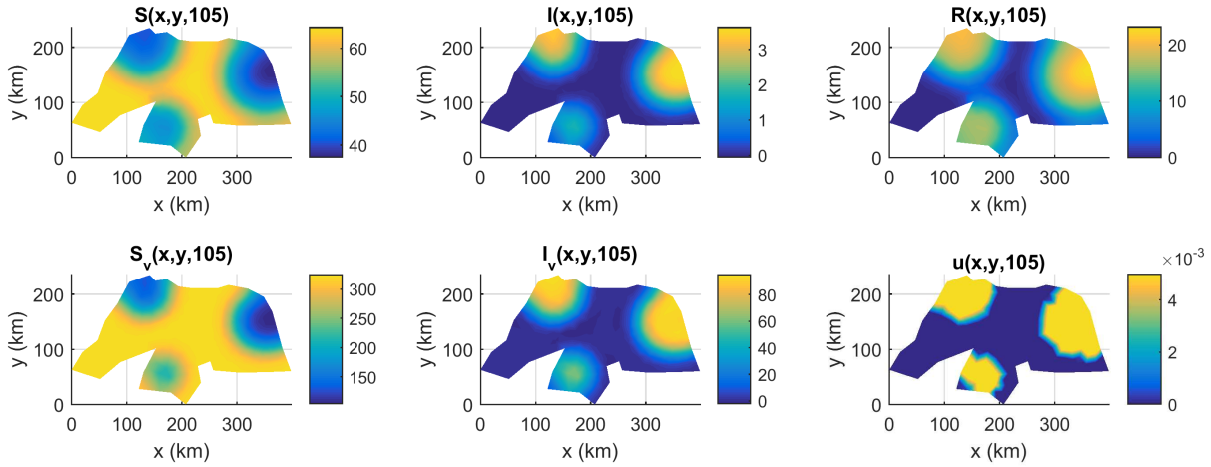

Figure 39 – Plots of solutions in space at $t = 105$ days, scenario with optimal control starting at $t = 52$ days. Each plot has a different scale.

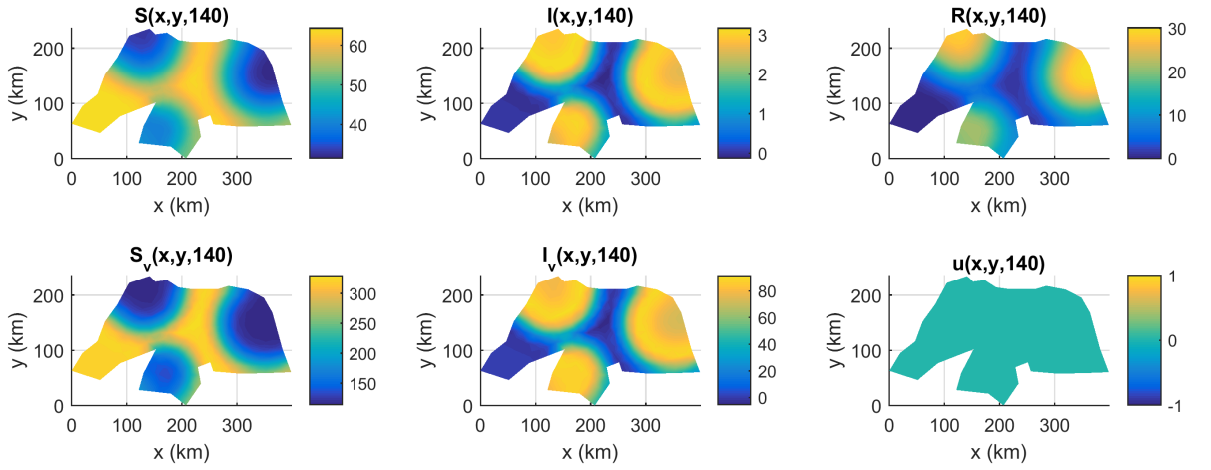

Figure 40 – Plots of solutions in space at $t = 140$ days, scenario with optimal control starting at $t = 52$ days. Each plot has a different scale.

starts at 35 days, we see that there is a small increase in the number of new infections and total cost, and the number of vaccinations is lightly reduced. Therefore, if the optimal control application starts later, it is less advantageous, but there is still improvement if compared to the application of no vaccination at all.

6.4 Simulation with optimal control starting at 70 days

In Figures 41 – 43 spatial results are shown for the scenario with control starting at $t = 70$ days. Again, the behavior is very similar if compared to the previous two with optimal control scenarios. The infected human solution, however, is closer to the scenario without control. Observing the total number of populations over time, in Figure 31, we see that all scenarios with control have similar behavior. The control variable also has the same behavior, starting high and decreasing over time until it reaches zero. This way it is possible to see that the delay in starting the vaccine application causes the control to be applied in a short time frame.

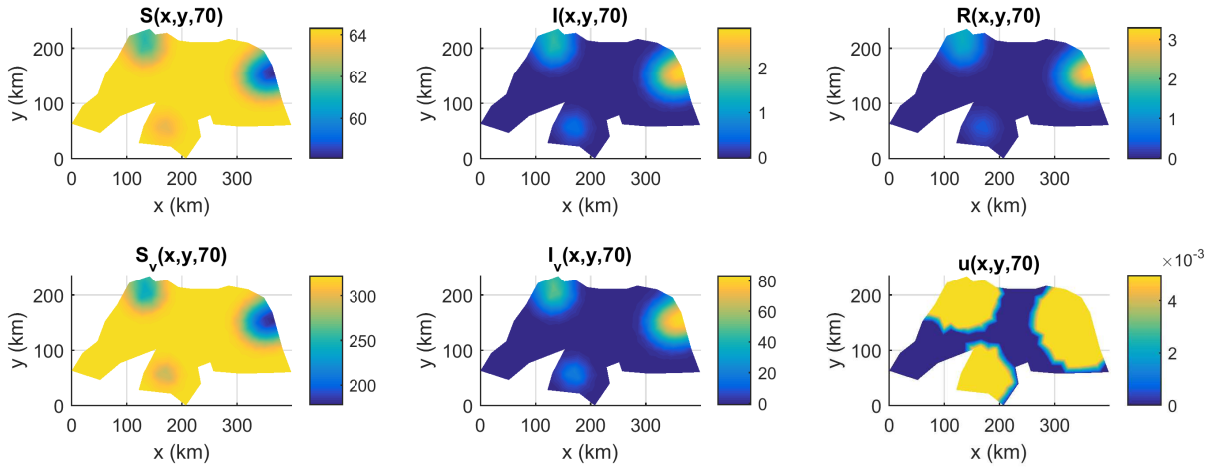

Figure 41 – Plots of solutions in space at $t = 70$ days, scenario with optimal control starting at $t = 70$ days. Each plot has a different scale.

From Table 13, the total incidence and cost $J(u^*)$ in this case reduce to 80.75% and 90.98% from the case without control, respectively, which is a small reduction. Comparing now the cost of applying a constant control after 70 days, we have that $J(u_{\max})$ corresponds to 90.56% of the cost without control and 126% of the optimal control cost. Although the results in terms of cost and new infections get worse as the starting optimal control is delayed, this scenario is still viable as a vaccination program, as there is still a significant reduction in the number of new cases.

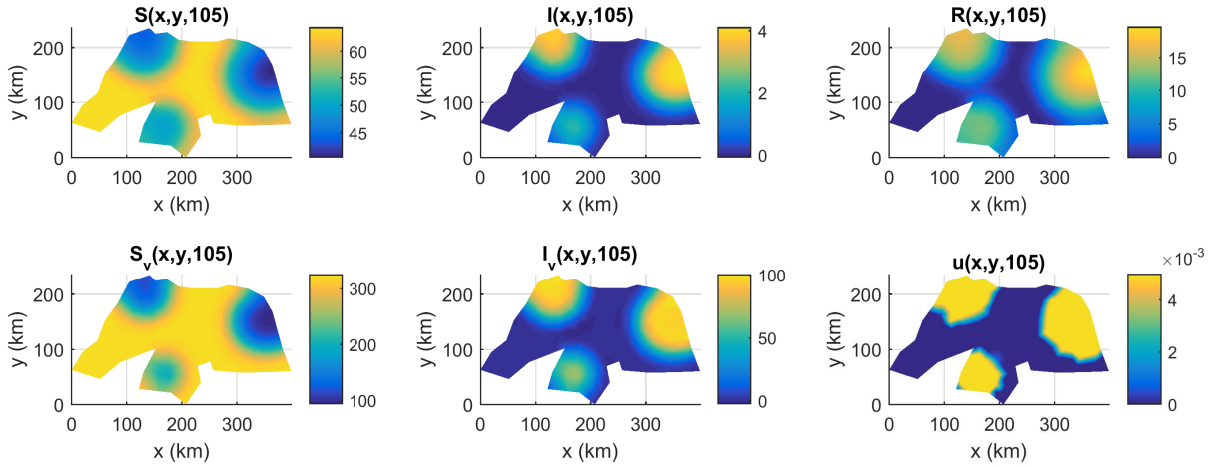

Figure 42 – Plots of solutions in space at $t = 105$ days, scenario with optimal control starting at $t = 70$ days. Each plot has a different scale.

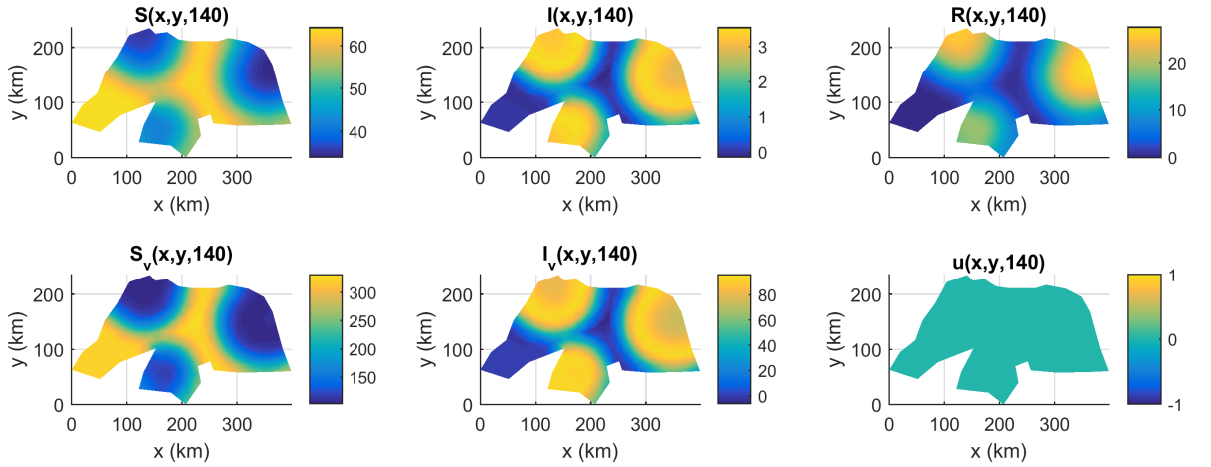

Figure 43 – Plots of solutions in space at $t = 140$ days, scenario with optimal control starting at $t = 70$ days. Each plot has a different scale.

6.5 Simulation with optimal control starting at 105 days

We do not show graphical solutions for the scenario with optimal control starting at $t = 105$ days, because its results had very small differences from the case without control. From Table 13, the number of new infections and the cost $J(u^*)$ in this scenario are 98% and 99.81% of the respective quantities from the scenario without control, so practically there is no improvement, even with almost $45,000$ vaccinations applied. Thus, starting the application of control too close to the final time of simulation is not a viable vaccination program.

Chapter 7
Conclusion and future perspectives

7.1 Concluding remarks

We proposed a spatiotemporal epidemic model for Zika virus with human and vector transmissions described by a system of partial differential equations, and vaccination as a control variable. Spatial movement is incorporated in the model through diffusion, and transmission is given by compartmental dynamics. Optimal control is applied to the model, in order to obtain a vaccination strategy over space and time that minimizes costs related to infections and vaccine application. We developed the optimality system using sensitivity and adjoint functions, and a directional derivative of the objective functional. The optimal control characterization is obtained in terms of the state and adjoint systems. Numerical methods were applied in order to obtain approximated solutions for both state and adjoint systems.

The finite element and implicit Euler methods were used in the discretization of the differential systems, a predictor-corrector method was used to iteratively treat the non linearities, and a forward-backward sweep was used in the optimal system resolution. A convergence analysis was carried out showing that the numerical methods produce errors consistent with the theoretical prediction, and therefore confirming that the solutions are trustworthy. Using available data for the initial Zika outbreak in the Rio Grande do Norte state in Brazil, we were able to estimate some parameters in the model, using a least squares approach coupled with the numerical solutions. Other parameter values were taken from available literature or assumed. The estimation methodology was tested with generated data in the presence of noise, showing that the methodology is able to retrieve results close to the data. In order to better represent the spatial spread of the disease in the data, we included immigration in the model due to infected humans coming from the outside. From the parameter estimation results we found that direct transmission of the Zika virus between humans is not relevant for the set of data used.

A global sensitivity analysis was carried out using PRCCs (partial rank correlation coefficients), which identify how the parameters in the model affects in the increase or decrease in an output of the model. We performed this analysis considering the overall cost of vaccination and the incidence (number of new infections) over time as outputs, in

two separated analyses. The cost is most sensitive to the transmission and recovery rates, carrying capacity and mortality rate of mosquitoes, and cost associated with infected humans. The incidence is also sensitive to the transmission and recovery rates, carrying capacity, and mortality rate of mosquitoes, in most of the simulated time.

Several scenarios were simulated in order to compare the results of optimal and constant controls, and without control. Different scenarios were analyzed by comparing the total cost, number of new infections, and number of people vaccinated, quantitatively. Optimal vaccination distributions were considered in several scenarios, varying the starting day of the control. From all of the scenarios showed, the lowest cost and number of new infections were obtained with the optimal control starting at 35 days, the earliest of all applications, from a simulation of 140 days. However, scenarios with control starting at 52 and 70 days also showed good results, with improvements if compared to the scenario without control. We also compared the optimal control scenarios to constant control cases, evaluating their respective costs and finding that optimal controls significantly reduce the cost if compared to constant controls, showing the successfulness of the optimal vaccination strategy. The results were obtained with assumed values for the cost coefficients c_1, c_2 and c_3 of the objective functional (3.1), but similar results would be obtained if other values with same ratios c_2/c_1 and c_3/c_1 were used.

In terms of novelty, to the best of our knowledge this work is the first to apply vaccination and optimal control to a partial differential model describing the dynamics of Zika virus in humans and mosquitoes. The connection between model and real life data in an epidemiological PDE with optimal control is also novel, regardless of the particular application. Furthermore, the sensitivity analysis performed is innovative, which considers the impact of parameters of a PDE model in the optimal functional cost.

The combination of different mathematical techniques served the purpose of quantitatively analyze a real life problem. We hope that the results of this thesis could help to provide a better understanding of a Zika outbreak and the planning of public health policies. Techniques used in this work could also be applied to other sets of data in order to assess the benefits of an optimal vaccination program, even to other diseases similar to Zika such as dengue, chikungunya, and malaria – also vector borne diseases. Small modifications in the model could be done to include particular features, with corresponding modifications in the optimality system and in the numerical methods. In this sense, the present work serves as a solid reference for possible future works.

Other types of modeling could also be considered as alternatives to the one we provided, and comparisons could be obtained to the results we have found. Depending on the different type of model to be used, the methods we used could be appropriate or not. As example, a metapopulation model could be considered, in patches of ODEs, representing different cities, and optimal control could also be applied as in [7, 54]. Stratified diffusion

is also a possibility [105, 111], considering non local diffusion to model immigration of infected humans, besides local diffusion.

Different types of controls could be included in the model, with a corresponding modified objective functional to be minimized. An optimal characterization can be obtained using the same techniques as before. In the following, we show an example of a model with multiple control measures, as a direct extension of the model proposed in this work.

7.2 Future work perspectives

Throughout this work we have considered only one control in model (2.1). It is possible to include multiple control variables, and obtain an optimal characterization for all of them at the same time. In this section we propose a first attempt modeling with multiple controls that could lead to a future, more complete, work. We decided to include four additional measures, plus vaccination, that could lower the number of infections in a Zika outbreak. The control variables $\boldsymbol{u} = (u_1, u_2, u_3, u_4, u_5)$ are defined as follows: u_1 is the vaccination rate, as in model (2.1); u_2 represents mosquito to human contact reduction through the use of repellents, window nets, public awareness; u_3 represents the use of larvicides and mechanical removal of larvae, eggs and pupae of immature mosquitoes, u_4 represents the use of insecticides and mosquito traps, aiming the elimination of adult mosquitoes; and u_5 represents human to human contact reduction through prophylaxis measures and public awareness, in cases such that human transmission is relevant.

As we are considering the removal of immature and adult mosquitoes, we need to consider them separately in the model. Thus, we include another compartment in the modified model, denoted by A_v, representing the aquatic phase of mosquitoes, in which they are still immature. This way, S_v now represents susceptible adult mosquitoes, and since only these mosquitoes bite humans and possibly contract the virus, I_v represents infected adult mosquitoes. A flow chart for the modified model can be seen in Figure 44, with parameters descriptions in Tables (1) and (14).

Table 14 – Description and units of some quantities from model (7.1). The others are shown in Table (1).

	Description	Unit
A_v	Immature mosq. density	immature mosq./km^2
$1/\gamma$	Immature phase duration	days
κ_v	Immature mosq. carrying capacity	immature mosq./km^2

The new system is then given by model (7.1) in $Q = \Omega \times (0, T)$. All populations S, I, R, A_v, S_v, I_v and the controls $\boldsymbol{u} = (u_1, u_2, u_3, u_4, u_5)$ are functions of space $\boldsymbol{x}$ and

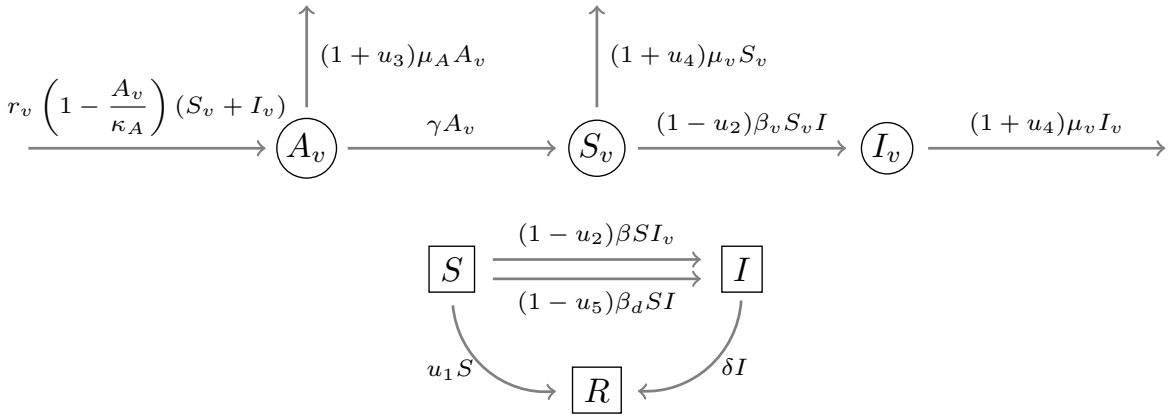

Figure 44 – Flow chart for model (7.1). Squares denote humans and circles mosquitoes. S, I, R denote susceptible, infected, and immune, respectively. A_v denotes mosquito immature phase.

time t, with spatial domain $\Omega \subset \mathbb{R}^2$ and smooth boundary $\partial\Omega$.

$$\begin{cases} \dfrac{\partial S}{\partial t} - \nabla\cdot(\alpha\nabla S) = -(1-u_2)\beta S I_v - (1-u_5)\beta_d SI - u_1 S, \\ \dfrac{\partial I}{\partial t} - \nabla\cdot(\alpha_I\nabla I) = (1-u_2)\beta S I_v + (1-u_5)\beta_d SI - \delta I, \\ \dfrac{\partial R}{\partial t} - \nabla\cdot(\alpha\nabla R) = u_1 S + \delta I, \\ \dfrac{\partial A_v}{\partial t} = r_v\left(S_v+I_v\right)\left(1-\dfrac{A_v}{\kappa_A}\right) - \left(1+u_3\right)\mu_A A_v - \gamma A_v, \\ \dfrac{\partial S_v}{\partial t} - \nabla\cdot(\alpha_v\nabla S_v) = -(1-u_2)\beta_v S_v I + \gamma A_v - (1+u_4)\mu_v S_v, \\ \dfrac{\partial I_v}{\partial t} - \nabla\cdot(\alpha_v\nabla I_v) = (1-u_2)\beta_v S_v I - (1+u_4)\mu_v I_v, \text{ in } Q. \end{cases} \tag{7.1}$$

Non flux boundary conditions (outward directional derivatives equal to zero) and appropriate initial conditions are also defined. Most of the parameters are the same than model (2.1) and can be found in Table 1. The new ones are κ_A, immature mosquitoes carrying capacity, and γ, the inverse of the number of days spent in the immature phase.

In this new model, both susceptible and infected mosquitoes are assumed to reproduce, with an intrinsic growth rate r_v with immature offspring given by A_v. For simplicity, this compartment is assumed to contain eggs, larvae, and pupae, which are phases of the mosquito life cycle that depend on water. Diffusion is not included in their equation, because there is no spatial movement. Logistic growth is also assumed here, with a carrying capacity of immature mosquitoes κ_A, representing limited resources in the aquatic phase. After a period of $1/\gamma$, the immature turn into adult susceptible mosquitoes, assuming there is no vertical transmission. Natural mortality is considered in all mosquito compartments.

The control of vaccination u_1 acts turning susceptible humans into immune,

in the same way as before. The mosquito contact reduction u_2 acts by reducing the transmission rates β and β_v, and could be thought of as a percentage reduction. In an analogous way, u_3 and u_4 acts by increasing the mortality of immature and adult mosquitoes, respectively, representing an effort in killing them. Lastly, u_5 is similar to u_2, reducing the direct transmission rate β_d. This control should be considered only in the case that Zika direct transmission in humans is relevant.

In order to obtain an optimal control solution, a new objective functional must be considered, extending the concept of (3.1) by assessing the multiple costs associated to all controls. As we are now concerned with eliminating mosquitoes, we should account for the cost of infected mosquitoes, in an analogous way that we considered the cost of infected humans in (3.1). The cost of application of u_2 and u_5 in the susceptible human population should also be taken into account, as well as the cost of u_3 applied to the immature mosquitoes and u_4 in both susceptible and infected adult mosquitoes. One alternative could be:

$$\begin{aligned} J(u_1,u_2,u_3,u_4,u_5) = \int_Q \Big(& A_1 I + A_2 I_v + (B_1 u_1 + B_2 u_2 + B_5 u_5) S \\ & + B_3 u_3 A_v + B_4 u_4 (S_v + I_v) + \sum_{i=1}^{5} C_i u_i^2 \Big) \mathrm{d}\boldsymbol{x}\mathrm{d}t. \end{aligned} \tag{7.2}$$

The right hand side of (7.2) contains several cost parameters. A_1 and A_2 are the costs associated to infected humans and mosquitoes, respectively. In particular, A_2 should account for the indirect costs that infected mosquitoes bring when transmitting the disease. B_1, B_2, B_3, B_4, B_5 are the costs involved in the application of each control variable u_1, u_2, u_3, u_4, u_5. Controls u_1, u_2, and u_5 are applied to susceptible humans, while u_3 to immatures mosquitoes and u_4 to adult ones. C_1, C_2, C_3, C_4, C_5 are nonlinear costs involved in controls u_1, u_2, u_3, u_4, u_5, respectively. These include logistics, production costs, propaganda, and public awareness efforts.

An optimal control characterization for this new problem would be completely analogous to the one solved in Chapter 3, following the same steps and leading to a corresponding optimal system consisting of state and adjoint equations, and the control characterizations. A numerical solution would also be similar, but a considerable attention should be given to the cost parameters in the objective functional (7.2), since their numerical values could potentially influence the convergence of the forward-backward sweep method.

The modified model (7.1) and the associated control measures showed are only examples of a more complete model for Zika virus. Clearly, a detailed study should be carried out, which could point out improvements in the model. Other modifications could also be considered in the state equations, control variables or objective functional. For example, non homogeneous initial conditions could be considered in order to obtain more

realistic simulations, as well as variable parameters such as diffusion and transmission coefficients. Both spatial and time dependence on the parameters could be considered. If time dependence were to be included, the final time of simulation could be extended, in order to evaluate the effects of infections throughout dry/wet and cold/hot seasons. Nevertheless, in any alternative model, the whole development of the present work could be used as a reference.

Bibliography

[1] Abboubakar, H., Kamgang, J. C., Nkamba, L. N., and Tieudjo, D. Bifurcation thresholds and optimal control in transmission dynamics of arboviral diseases. *Journal of Mathematical Biology* (2017), pp. 1–49 (cited on page 23).

[2] Agusto, F., Bewick, S., and Fagan, W. Mathematical model for Zika virus dynamics with sexual transmission route. *Ecological Complexity* 29 (2017), pp. 61–81 (cited on page 21).

[3] Althaus, C. L. and Low, N. How relevant is sexual transmission of Zika virus? *PLoS Medicine* 13.10 (2016) (cited on pages 19, 30, 66).

[4] An, G., Fitzpatrick, B., Christley, S., Federico, P., Kanarek, A., Neilan, R. M., Oremland, M., Salinas, R., Laubenbacher, R., and Lenhart, S. Optimization and control of agent-based models in biology: a perspective. *Bulletin of mathematical biology* 79.1 (2017), pp. 63–87 (cited on page 17).

[5] Anguelov, R., Dufourd, C., and Dumont, Y. Simulations and parameter estimation of a trap-insect model using a finite element approach. *Mathematics and Computers in Simulation* 133 (2017), pp. 47–75 (cited on pages 23, 66, 67).

[6] Arnold, D., Boffi, D., and Falk, R. Approximation by quadrilateral finite elements. *Mathematics of computation* 71.239 (2002), pp. 909–922 (cited on pages 51, 55).

[7] Asano, E., Gross, L. J., Lenhart, S., and Real, L. A. Optimal control of vaccine distribution in a rabies metapopulation model. *Mathematical biosciences and engineering* 5.2 (2008), pp. 219–238 (cited on pages 16, 23, 95).

[8] Axelsson, O. and Barker, V. A. *Finite element solution of boundary value problems: theory and computation*. Vol. 35. Siam, 1984 (cited on page 41).

[9] Bailey, N. T. *The mathematical theory of infectious diseases and its applications*. Griffin, 1975 (cited on page 16).

[10] Barrett, R., Berry, M., Chan, T. F., Demmel, J., Donato, J., Dongarra, J., Eijkhout, V., Pozo, R., Romine, C., and Van der Vorst, H. *Templates for the solution of linear systems: building blocks for iterative methods*. SIAM, 1994 (cited on pages 42, 52).

[11] Bartle, R. G. *The elements of integration and Lebesgue measure*. John Wiley & Sons, 2014 (cited on page 27).

[12] Besnard, M., Lastere, S., Teissier, A., Cao-Lormeau, V., and Musso, D. Evidence of perinatal transmission of Zika virus, French Polynesia, December 2013 and February 2014. *Eurosurveillance* 19.13 (2014), p. 20751 (cited on page 19).

[13] Birgin, E. and Martínez, J. *Practical augmented Lagrangian methods for constrained optimization*. SIAM, 2014 (cited on page 67).

[14] Bonyah, E., Khan, M. A., Okosun, K., and Islam, S. A theoretical model for Zika virus transmission. *PloS One* 12.10 (2017) (cited on page 21).

[15] Brezzi, F., Cockburn, B., Marini, L. D., and Süli, E. Stabilization mechanisms in discontinuous Galerkin finite element methods. *Computer Methods in Applied Mechanics and Engineering* 195.25 (2006), pp. 3293–3310 (cited on page 41).

[16] Brickley, E. B. and Rodrigues, L. C. Further pieces of evidence in the Zika virus and microcephaly puzzle. *The Lancet Child & Adolescent Health* 2.3 (2018), pp. 162–164 (cited on page 19).

[17] Brockmann, D., Hufnagel, L., and Geisel, T. The scaling laws of human travel. *Nature* 439.7075 (2006), p. 462 (cited on page 65).

[18] Brooks, A. N. and Hughes, T. J. Streamline upwind/Petrov-Galerkin formulations for convection dominated flows with particular emphasis on the incompressible Navier-Stokes equations. *Computer methods in applied mechanics and engineering* 32.1-3 (1982), pp. 199–259 (cited on page 41).

[19] Buchanan, J. L. and Turner, P. R. *Numerical methods and analysis*. McGraw-Hill, 1992 (cited on page 42).

[20] Burden, R. L. and Faires, J. D. *Numerical analysis*. Cengage Learning, 2015 (cited on pages 42, 50).

[21] Cantrell, R. S. and Cosner, C. *Spatial ecology via reaction-diffusion equations*. John Wiley & Sons, 2004 (cited on pages 16, 27).

[22] Carvalho, E. P., Martínez, J., Martínez, J. M., and Pisnitchenko, F. On optimization strategies for parameter estimation in models governed by partial differential equations. *Mathematics and Computers in Simulation* 114 (2015), pp. 14–24 (cited on pages 23, 66).

[23] CDC. *Centers for Disease Control and Prevention*. Access in: 06/16/2018. 2018. URL: http://www.cdc.gov/zika/index.html (cited on page 19).

[24] Christley, S., Neilan, R. M., Oremland, M., Salinas, R., and Lenhart, S. Optimal control of sugarscape agent-based model via a PDE approximation model. *Optimal Control Applications and Methods* 38.4 (2017), pp. 473–497 (cited on page 35).

[25] Ciarlet, P. G. *The finite element method for elliptic problems*. Elsevier, 1978 (cited on pages 17, 27, 41, 43).

[26] Cunha, M. C. C. *Métodos numéricos*. Editora da UNICAMP, 2000 (cited on pages 42, 50).

[27] D'Ortenzio, E., Matheron, S., Lamballerie, X. de, Hubert, B., Piorkowski, G., Maquart, M., Descamps, D., Damond, F., Yazdanpanah, Y., and Leparc-Goffart, I. Evidence of sexual transmission of Zika virus. *New England Journal of Medicine* 374.22 (2016), pp. 2195–2198 (cited on page 19).

[28] De Araujo, A. L., Boldrini, J. L., and Calsavara, B. M. An analysis of a mathematical model describing the geographic spread of dengue disease. *Journal of Mathematical Analysis and Applications* 444.1 (2016), pp. 298–325 (cited on page 22).

[29] De Silva, K. R., Phan, T. V., and Lenhart, S. Advection control in parabolic PDE systems for competitive populations. *Discrete & Continuous Dynamical Systems-Series B* 22.3 (2017) (cited on page 35).

[30] Ding, W. and Lenhart, S. "Introduction to Optimal Control for Discrete Time Models with an Application to Disease Modeling". *Modeling Paradigms and Analysis of Disease Trasmission Models*. 2010, pp. 109–120 (cited on page 17).

[31] Douglas Jr, J. and Dupont, T. Galerkin methods for parabolic equations. *SIAM Journal on Numerical Analysis* 7.4 (1970), pp. 575–626 (cited on pages 17, 49).

[32] Douglas Jr, J., Dupont, T., and Ewing, R. E. Incomplete iteration for time-stepping a Galerkin method for a quasilinear parabolic problem. *SIAM Journal on Numerical Analysis* 16.3 (1979), pp. 503–522 (cited on pages 17, 49).

[33] Edelstein-Keshet, L. *Mathematical models in biology*. Vol. 46. Siam, 1988 (cited on page 27).

[34] Edholm, C. J., Tenhumberg, B., Guiver, C., Jin, Y., Townley, S., and Rebarber, R. Management of invasive insect species using optimal control theory. *Ecological Modelling* 381 (2018), pp. 36–45 (cited on page 23).

[35] Eisenberg, M. C., Robertson, S. L., and Tien, J. H. Identifiability and estimation of multiple transmission pathways in cholera and waterborne disease. *Journal of theoretical biology* 324 (2013), pp. 84–102 (cited on page 17).

[36] Evans, L. C. *Partial differential equations*. American Mathematical Society, 1998 (cited on pages 17, 28, 41).

[37] Fister, R. Optimal control of harvesting in a predator-prey parabolic system. *Houston Journal of Mathematics* 23.2 (1997), pp. 341–355 (cited on pages 35, 41).

[38] Fitzgibbon, W., Morgan, J., and Webb, G. An outbreak vector-host epidemic model with spatial structure: the 2015–2016 Zika outbreak in Rio De Janeiro. *Theoretical Biology and Medical Modelling* 14.1 (2017), p. 7 (cited on pages 22, 23).

[39] Franca, L. P., Frey, S. L., and Hughes, T. J. Stabilized finite element methods: I. Application to the advective-diffusive model. *Computer Methods in Applied Mechanics and Engineering* 95.2 (1992), pp. 253–276 (cited on page 41).

[40] Fundação Oswaldo Cruz. Access in: 06/24/2018. 2018. URL: http://www.ioc.fiocruz.br/dengue (cited on page 20).

[41] Gao, D., Lou, Y., He, D., Porco, T. C., Kuang, Y., Chowell, G., and Ruan, S. Prevention and control of Zika as a mosquito-borne and sexually transmitted disease: a mathematical modeling analysis. *Scientific reports* 6 (2016) (cited on pages 21, 23, 24, 60, 64, 65, 69).

[42] Gardner, L. M., Bóta, A., Gangavarapu, K., Kraemer, M. U., and Grubaugh, N. D. Inferring the risk factors behind the geographical spread and transmission of Zika in the Americas. *PLoS Neglected Tropical Diseases* 12.1 (2018), e0006194 (cited on pages 22, 23).

[43] Golub, G. H. and Van Loan, C. F. *Matrix computations*. Vol. 3. JHU Press, 2012 (cited on page 42).

[44] Gomes, L. T. "Um estudo sobre o espalhamento de dengues usando equações diferenciais parciais e lógica fuzzy". Master's Dissertation. Campinas, SP: DMA, IMECC, UNICAMP, 2009 (cited on pages 17, 22).

[45] Google. *Google Earth Pro 7.3.1.4507 (64-bit)*. 2017. URL: https://www.google.com/earth/ (cited on page 61).

[46] Hackbusch, W. A numerical method for solving parabolic equations with opposite orientations. *Computing* 20.3 (1978), pp. 229–240 (cited on pages 17, 53).

[47] Hastings, W. K. Monte Carlo sampling methods using Markov chains and their applications (1970) (cited on page 76).

[48] Heines, B. "Assessing the Economic Tradeoffs Between Prevention and Suppression of Forest Fires". PhD. Thesis. Knoxville, TN: The University of Tennessee, Knoxville, 2017 (cited on page 77).

[49] Heines, B., Lenhart, S., and Sims, C. Assessing the economic trade-offs between prevention and suppression of forest fires. *Natural Resource Modeling* 31.1 (2018), e12159 (cited on pages 23, 24, 77).

[50] Honório, N. A., Castro, M. G., Barros, F. S. M. d., Magalhães, M. d. A. F. M., and Sabroza, P. C. The spatial distribution of Aedes aegypti and Aedes albopictus in a transition zone, Rio de Janeiro, Brazil. *Cadernos de Saúde Pública* 25.6 (2009), pp. 1203–1214 (cited on pages 60, 64, 65, 69).

[51] Hughes, T. J. *The finite element method: linear static and dynamic finite element analysis*. Courier Corporation, 2012 (cited on pages 41, 43, 50, 52).

[52] Johnson, C. *Numerical solution of partial differential equations by the finite element method*. Courier Dover Publications, 2012 (cited on pages 41, 52).

[53] Keeling, M. J. and Rohani, P. *Modeling infectious diseases in humans and animals*. Princeton University Press, 2008 (cited on pages 16, 27, 29).

[54] Kelly Jr, M. R., Tien, J. H., Eisenberg, M. C., and Lenhart, S. The impact of spatial arrangements on epidemic disease dynamics and intervention strategies. *Journal of biological dynamics* 10.1 (2016), pp. 222–249 (cited on pages 23, 95).

[55] Kermack, W. O. and McKendrick, A. G. "A contribution to the mathematical theory of epidemics". *Proceedings of the Royal Society of London A: mathematical, physical and engineering sciences*. Vol. 115. 772. The Royal Society. 1927, pp. 700–721 (cited on page 16).

[56] Kot, M. *Elements of mathematical ecology*. Cambridge University Press, 2001 (cited on pages 64, 65, 69).

[57] Kreyszig, E. *Introductory functional analysis with applications*. Vol. 1. wiley New York, 1978 (cited on page 28).

[58] Lenhart, S. and Workman, J. T. *Optimal control applied to biological models*. Crc Press, 2007 (cited on pages 17, 33, 53).

[59] LeVeque, R. J. *Finite difference methods for ordinary and partial differential equations: steady-state and time-dependent problems*. Vol. 98. Siam, 2007 (cited on pages 17, 42, 43, 55, 56).

[60] Levy, B., Edholm, C., Gaoue, O., Kaondera-Shava, R., Kgosimore, M., Lenhart, S., Lephodisa, B., Lungu, E., Marijani, T., and Nyabadza, F. Modeling the role of public health education in Ebola virus disease outbreaks in Sudan. *Infectious Disease Modelling* 2.3 (2017), pp. 323–340 (cited on pages 23, 24).

[61] Li, X. and Yong, J. *Optimal control theory for infinite dimensional systems*. Springer Science & Business Media, 2012 (cited on page 35).

[62] Lions, J. L. *Control of distributed singular systems*. Bordas Editions, 1985 (cited on page 33).

[63] Lions, J. L. *Optimal control of systems governed by partial differential equations*. Springer-Verlag, 1971 (cited on page 35).

[64] Malone, R. W., Homan, J., Callahan, M. V., Glasspool-Malone, J., Damodaran, L., Schneider, A. D. B., Zimler, R., Talton, J., Cobb, R. R., Ruzic, I., Smith-Gagen, J., Janies, D., and Wilson, J. Zika virus: medical countermeasure development challenges. *PLoS Neglected Tropical Diseases* 10.3 (2016) (cited on page 19).

[65] Manore, C. A., Ostfeld, R. S., Agusto, F. B., Gaff, H., and LaDeau, S. L. Defining the risk of Zika and chikungunya virus transmission in human population centers of the eastern United States. *PLoS Neglected Tropical Diseases* 11.1 (2017), e0005255 (cited on pages 21, 24).

[66] Marcondes, C. B. and Ximenes, M. d. F. F. d. Zika virus in Brazil and the danger of infestation by Aedes (Stegomyia) mosquitoes. *Revista da Sociedade Brasileira de Medicina Tropical* 49.1 (2016), pp. 4–10 (cited on page 19).

[67] Marino, S., Hogue, I. B., Ray, C. J., and Kirschner, D. E. A methodology for performing global uncertainty and sensitivity analysis in systems biology. *Journal of theoretical biology* 254.1 (2008), pp. 178–196 (cited on pages 18, 24, 76, 77).

[68] Matheson, T. S., Satterthwaite, B., and Callender Highlander, H. Modeling the Spread of the Zika Virus at the 2016 Olympics. *Spora: A Journal of Biomathematics* 3.1 (2017), p. 3 (cited on page 21).

[69] MathWorks. *Aerospace Toolbox: User's Guide (R2015a)*. 2015 (cited on page 61).

[70] MathWorks. *Matlab: User's Guide (R2015a)*. 2015 (cited on page 52).

[71] MathWorks. *Optimization Toolbox: User's Guide (R2015a)*. 2015 (cited on page 67).

[72] MathWorks. *Partial Differential Equation Toolbox: User's Guide (R2015a)*. 2015 (cited on page 62).

[73] McKay, M. D., Beckman, R. J., and Conover, W. J. Comparison of three methods for selecting values of input variables in the analysis of output from a computer code. *Technometrics* 21.2 (1979), pp. 239–245 (cited on page 76).

[74] Mier-y-Teran-Romero, L., Delorey, M. J., Sejvar, J. J., and Johansson, M. A. Guillain–Barré syndrome risk among individuals infected with Zika virus: a multi-country assessment. *BMC medicine* 16.1 (2018), p. 67 (cited on page 19).

[75] Ministério da Saúde. Access in: 06/16/2018. 2018. URL: http://portalms.saude.gov.br/saude-de-a-z/zika-virus (cited on pages 20, 60).

[76] Miyaoka, T. Y. "Impacto Ambiental e Populações que Interagem: Uma Modelagem Inovadora, Aproximação e Simulações Computacionais". Master's Dissertation. Campinas, SP: DMA, IMECC, UNICAMP, 2015 (cited on page 41).

[77] Miyaoka, T. Y., Meyer, J. F. C. A., and Souza, J. M. R. A General Boundary Condition with Linear Flux for Advection-Diffusion Models. *Trends in Applied and Computational Mathematics* 18.2 (2017), pp. 253–272 (cited on page 31).

[78] Mlakar, J., Korva, M., Tul, N., Popović, M., Poljšak-Prijatelj, M., Mraz, J., Kolenc, M., Resman Rus, K., Vesnaver Vipotnik, T., Fabjan Vodušek, V., Vizjak, A., Jože, P., Petrovec, M., and Avšič Županc, T. Zika virus associated with microcephaly. *New England Journal of Medicine* 2016.374 (2016), pp. 951–958 (cited on page 19).

[79] Mocenni, C., Madeo, D., and Sparacino, E. Linear least squares parameter estimation of nonlinear reaction diffusion equations. *Mathematics and Computers in Simulation* 81.10 (2011), pp. 2244–2257 (cited on pages 23, 67).

[80] Mordecai, E. A., Cohen, J. M., Evans, M. V., Gudapati, P., Johnson, L. R., Lippi, C. A., Miazgowicz, K., Murdock, C. C., Rohr, J. R., Ryan, S. J., et al. Detecting the impact of temperature on transmission of Zika, dengue, and chikungunya using mechanistic models. *PLoS Neglected Tropical Diseases* 11.4 (2017), e0005568 (cited on page 60).

[81] Motta, I. J., Spencer, B. R., Cordeiro da Silva, S. G., Arruda, M. B., Dobbin, J. A., Gonzaga, Y. B., Arcuri, I. P., Tavares, R. C., Atta, E. H., Fernandes, R. F., Costa, D. A., Ribeiro, L. J., Limonte, F., Higa, L. M., Voloch, C. M., Brindeiro, R. M., Tanuri, A., and Ferreira, O. C. Evidence for transmission of Zika virus by platelet transfusion. *New England Journal of Medicine* 375.11 (2016), pp. 1101–1103 (cited on page 19).

[82] Murray, J. D. *Mathematical Biology. Vol. 1: An Introduction*. Springer, 2002 (cited on page 27).

[83] Murray, J. D. *Mathematical Biology. Vol. 2: Spatial Models and Biomedical Applications*. Springer, 2002 (cited on page 27).

[84] Neilan, R. M. and Lenhart, S. Optimal vaccine distribution in a spatiotemporal epidemic model with an application to rabies and raccoons. *Journal of Mathematical Analysis and Applications* 378.2 (2011), pp. 603–619 (cited on pages 23, 35).

[85] NIAID. *National Institute of Allergy and Infectious Diseases*. Access in: 06/16/2018. 2018. URL: https://www.niaid.nih.gov/news-events/nih-begins-testing-investigational-zika-vaccine-humans (cited on page 20).

[86] NIH. *National Institutes of Health*. Access in: 05/30/2018. 2018. URL: https://www.nih.gov/news-events/news-releases/phase-2-zika-vaccine-trial-begins-us-central-south-america (cited on page 20).

[87] Oehler, E., Watrin, L., Larre, P., Leparc-Goffart, I., Lastere, S., Valour, F., Baudouin, L., Mallet, H., Musso, D., and Ghawche, F. Zika virus infection complicated by Guillain-Barré syndrome–case report, French Polynesia, December 2013. *Eurosurveillance* 19.9 (2014) (cited on page 19).

[88] Okubo, A. and Levin, S. A. *Diffusion and ecological problems: modern perspectives*. Vol. 14. Springer Science & Business Media, 2013 (cited on pages 16, 27).

[89] PAHO. *Pan American Health Organization*. Access in: 06/16/2018. 2017. URL: http://www.paho.org/zika (cited on pages 19, 20).

[90] Perez, L. and Dragicevic, S. An agent-based approach for modeling dynamics of contagious disease spread. *International journal of health geographics* 8.1 (2009), p. 50 (cited on page 16).

[91] Poletti, E. C. C. and Meyer, J. F. d. C. A. Numerical methods and fuzzy parameters: an environmental impact assessment in aquatic systems. *Computational and Applied Mathematics* 36.4 (2017), pp. 1517–1528 (cited on pages 17, 22).

[92] Powell, M. J. The BOBYQA algorithm for bound constrained optimization without derivatives. *Cambridge NA Report NA2009/06, University of Cambridge, Cambridge* (2009) (cited on page 67).

[93] Powell, M. A tolerant algorithm for linearly constrained optimization calculations. *Mathematical Programming* 45.1-3 (1989), pp. 547–566 (cited on page 67).

[94] Pulino, P. *Álgebra Linear e suas Aplicações – Notas de Aula*. Access in: 08/22/2018. 2004. URL: http://www.ime.unicamp.br/~pulino/ALESA/ (cited on page 52).

[95] Raimundo, S. M., Yang, H. M., and Massad, E. Modeling vaccine preventable vector-borne infections: yellow fever as a case study. *Journal of Biological Systems* 24.02n03 (2016), pp. 193–216 (cited on page 23).

[96] Ramírez Bernate, C. A. "Modelagem matemática e simulações computacionais de estratégias combinadas de combate a um inseto vetor: o caso do 'Aedes aegypti'". PhD. Thesis. Campinas, SP: DMA, IMECC, UNICAMP, 2017 (cited on pages 17, 22, 41).

[97] Ramsay, J. O., Hooker, G., Campbell, D., and Cao, J. Parameter estimation for differential equations: a generalized smoothing approach. *Journal of the Royal Statistical Society: Series B (Statistical Methodology)* 69.5 (2007), pp. 741–796 (cited on page 23).

[98] Rodrigues, H. S., Monteiro, M. T. T., and Torres, D. F. Vaccination models and optimal control strategies to dengue. *Mathematical biosciences* 247 (2014), pp. 1–12 (cited on page 23).

[99] Roques, L. and Bonnefon, O. Modelling Population Dynamics in Realistic Landscapes with Linear Elements: A Mechanistic-Statistical Reaction-Diffusion Approach. *PloS One* 11.3 (2016), e0151217 (cited on pages 22, 23).

[100] Ross, S. M. *Introduction to probability models*. Academic press, 2014 (cited on page 77).

[101] Rubianes Silva, J. C. "Modelagem matemática e simulação computacional da influência de poluentes e da velocidade de corrente na dinâmica populacional de macrófitas aquáticas". PhD. Thesis. Campinas, SP: DMA, IMECC, UNICAMP, 2015 (cited on pages 17, 22, 41).

[102] Saad-Roy, C., van den Driessche, P., and Ma, J. Estimation of Zika virus prevalence by appearance of microcephaly. *BMC infectious diseases* 16.1 (2016), p. 754 (cited on page 21).

[103] Saltelli, A., Chan, K., and Scott, E. M. *Sensitivity analysis*. Vol. 1. Wiley New York, 2000 (cited on pages 18, 77).

[104] Secretaria de Saúde. *Boletim epidemiológico do Rio Grande do Norte, 2016*. Access in: 08/16/2017. 2017. URL: http://www.saude.rn.gov.br (cited on pages 60, 61, 64, 65, 69).

[105] Shigesada, N., Kawasaki, K., and Takeda, Y. Modeling stratified diffusion in biological invasions. *The American Naturalist* 146.2 (1995), pp. 229–251 (cited on page 96).

[106] Shutt, D. P., Manore, C. A., Pankavich, S., Porter, A. T., and Del Valle, S. Y. Estimating the reproductive number, total outbreak size, and reporting rates for Zika epidemics in South and Central America. *Epidemics* 21 (2017), pp. 63–79 (cited on pages 21, 23).

[107] Silveira, G. P. and Barros, L. C. de. Analysis of the dengue risk by means of a Takagi–Sugeno-style model. *Fuzzy Sets and Systems* 277 (2015), pp. 122–137 (cited on page 22).

[108] Smith, R. C. *Uncertainty quantification: theory, implementation, and applications*. Vol. 12. Siam, 2013 (cited on page 18).

[109] Soubeyrand, S. and Roques, L. Parameter estimation for reaction-diffusion models of biological invasions. *Population ecology* 56.2 (2014), pp. 427–434 (cited on page 66).

[110] Stephenson, B., Lanzas, C., Lenhart, S., and Day, J. Optimal control of vaccination rate in an epidemiological model of Clostridium difficile transmission. *Journal of mathematical biology* 75.6-7 (2017), pp. 1693–1713 (cited on page 23).

[111] Strickland, C., Kristensen, N. P., and Miller, L. Inferring stratified parasitoid dispersal mechanisms and parameters from coarse data using mathematical and Bayesian methods. *Journal of The Royal Society Interface* 14.130 (2017), p. 20170005 (cited on pages 18, 23, 96).

[112] Torre, L., Tabares, P. C. C., Momo, F., Meyer, J. F., and Sahade, R. Climate change effects on Antarctic benthos: a spatially explicit model approach. *Climatic change* 141.4 (2017), pp. 733–746 (cited on pages 17, 22).

[113] Towers, S., Brauer, F., Castillo-Chavez, C., Falconar, A. K., Mubayi, A., and Romero-Vivas, C. M. Estimate of the reproduction number of the 2015 Zika virus outbreak in Barranquilla, Colombia, and estimation of the relative role of sexual transmission. *Epidemics* 17 (2016), pp. 50–55 (cited on pages 21, 23).

[114] Valega-Mackenzie, W. and Ríos-Soto, K. R. Can Vaccination Save a Zika Virus Epidemic? *Bulletin of mathematical biology* 80.3 (2018), pp. 598–625 (cited on page 22).

[115] Valtonen Örnhag, M. Classification of stiffness and oscillations in initial value problems. *Master's Theses in Mathematical Sciences* (2015) (cited on page 42).

[116] Wang, L., Zhao, H., Oliva, S. M., and Zhu, H. Modeling the transmission and control of Zika in Brazil. *Scientific Reports* 7 (2017) (cited on pages 21, 23, 24).

[117] Watkins, D. S. *Fundamentals of matrix computations*. Vol. 64. John Wiley & Sons, 2004 (cited on pages 42, 52).

[118] WHO. *World Health Organization*. Access in: 06/16/2018. 2018. URL: http://www.who.int/csr/disease/zika/en/ (cited on pages 19, 20, 61).

[119] Xue, H., Miao, H., and Wu, H. Sieve estimation of constant and time-varying coefficients in nonlinear ordinary differential equation models by considering both numerical error and measurement error. *Annals of statistics* 38.4 (2010), p. 2351 (cited on page 23).

[120] Yang, H. M., Boldrini, J. L., Fassoni, A. C., Freitas, L. F. S., Gomez, M. C., Lima, K. K. B. de, Andrade, V. R., and Freitas, A. R. R. Fitting the Incidence Data from the City of Campinas, Brazil, Based on Dengue Transmission Modellings Considering Time-Dependent Entomological Parameters. *PloS One* 11.3 (2016), e0152186 (cited on page 23).

[121] Zhang, Q., Sun, K., Chinazzi, M., Piontti, A. P. y, Dean, N. E., Rojas, D. P., Merler, S., Mistry, D., Poletti, P., Rossi, L., et al. Spread of Zika virus in the Americas. *Proceedings of the National Academy of Sciences* 114.22 (2017), E4334–E4343 (cited on pages 21, 23).

[122] Zheng, B., Tang, M., Yu, J., and Qiu, J. Wolbachia spreading dynamics in mosquitoes with imperfect maternal transmission. *Journal of Mathematical Biology* (2017), pp. 1–29 (cited on page 21).

[123] Zinszer, K., Morrison, K., Brownstein, J. S., Marinho, F., Santos, A. F., and Nsoesie, E. O. Reconstruction of Zika virus introduction in Brazil. *Emerging infectious diseases* 23.1 (2017), p. 91 (cited on page 21).